AD_____

AWARD NUMBER: W81XWH-14-1-0301

TITLE: Identifying Molecular Regulators of Neuronal Functions Affected in the Movement Disorder Dystonia

PRINCIPAL INVESTIGATOR: Nobutoshi Charles Harata, M.D., Ph.D.

CONTRACTING ORGANIZATION: University of Iowa
Iowa City, IA 52242

REPORT DATE: August 2015

TYPE OF REPORT: Annual Report

PREPARED FOR: U.S. Army Medical Research and Materiel Command
Fort Detrick, Maryland 21702-5012

REPORT DOCUMENTATION PAGE

Form Approved
OMB No. 0704-0188

1. REPORT DATE *(DD-MM-YYYY)*	**2. REPORT TYPE**	**3. DATES COVERED** *(From - To)*
August 2015	Annual	1 August 2014 - 31 July 2015

4. TITLE AND SUBTITLE

Identifying Molecular Regulators of Neuronal Functions Affected in the

Movement Disorder Dystonia

5a. CONTRACT NUMBER

5b. GRANT NUMBER
W81XWH-14-1-0301

5c. PROGRAM ELEMENT NUMBER

6. AUTHOR(S)

Nobutoshi Charles Harata
email: charles-harata@uiowa.edu

5d. PROJECT NUMBER

5e. TASK NUMBER

5f. WORK UNIT NUMBER

7. PERFORMING ORGANIZATION NAME(S) AND ADDRESS(ES)

University of Iowa
2 Gilmore Hall
Iowa City, Iowa 52242-1320

8. PERFORMING ORGANIZATION REPORT NUMBER

9. SPONSORING / MONITORING AGENCY NAME(S) AND ADDRESS(ES)

U.S. Army Medical Research and
Materiel Command
Fort Detrick, Maryland 21702-5012

10. SPONSOR/MONITOR'S ACRONYM(S)

11. SPONSOR/MONITOR'S REPORT NUMBER(S)

12. DISTRIBUTION / AVAILABILITY STATEMENT

Approved for Public Release; Distribution Unlimited

13. SUPPLEMENTARY NOTES

14. ABSTRACT

The movement disorder dystonia is characterized by involuntary muscle contractions in the limbs, hands, feet or neck. The aim of the research proposed here is to identify the functional changes that occur in brain neurons of a mouse model of DYT1 dystonia. The most significant finding during this period is that the intracellular Ca^{2+} dynamics in the axons and dendrites of cultured brain neurons were abnormal in the model mice. This result indicates that the pathophysiology of dystonia can involve dysregulation of Ca^{2+}-mediated events, such as synaptic transmission in the brain.

15. SUBJECT TERMS

DYT1 dystonia, torsinA, neuronal function, neurobiology, calcium, synapse, synaptic transmission

16. SECURITY CLASSIFICATION OF:			**17. LIMITATION OF ABSTRACT**	**18. NUMBER OF PAGES**	**19a. NAME OF RESPONSIBLE PERSON**
a. REPORT	**b. ABSTRACT**	**c. THIS PAGE**			USAMRMC
U	U	U	UU	65	**19b. TELEPHONE NUMBER** *(include area code)*

TABLE OF CONTENTS

TITLE

Identifying molecular regulators of neuronal functions affected in the movement disorder dystonia

INTRODUCTION

The hyperkinetic movement disorder dystonia is characterized by involuntary muscle contractions in the limbs, hands, feet or neck. The patients suffer from abnormal repetitive movements and postures. Clinical studies indicate that dystonia patients experience enhanced brain excitability in the absence of apparent neurodegeneration. Thus, one of the main pathophysiological features of dystonia appears to be abnormal control of neuronal excitability, e.g. an imbalance in excitatory glutamatergic and inhibitory GABAergic synaptic transmission. However, this functional abnormality is still not understood well, and this is holding back the development of effective treatments. The aim of this research is to identify the functional changes that occur in brain neurons under dystonia. We will test the hypothesis that an inability to control intracellular calcium ion (Ca^{2+}), an important regulator of neuronal excitability, leads to enhanced excitability of neurons and their network within the brain (**Fig. 1**). For this purpose, we will use brain neurons of a mouse model of DYT1 dystonia, which is the most common inherited form of dystonia. These mice bear a deletion in a glutamic-acid residue (ΔE) in one copy of the torsinA gene (ΔE-torsinA), and so mimic the heterozygous DYT1 carriers in humans.

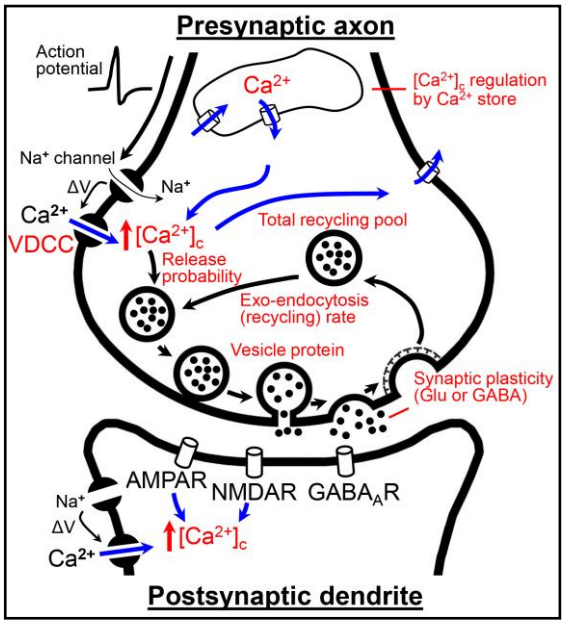

Fig. 1. Overview of the research. **Red** arrows show our hypothesis that cytoplasmic calcium concentration is dysregulated in DYT1 dystonia. **Blue** arrows and **red** fonts indicate mechanisms that are likely involved in DYT1 dystonia. **Abbreviations**: AMPAR, AMPA-subtype of glutamate receptor; $[Ca^{2+}]_c$, cytoplasmic Ca^{2+} concentration; GABA, γ-aminobutyric acid; $GABA_AR$, γ-aminobutyric acid A receptor; NMDAR, NMDA-subtype of glutamate receptor; VDCC, voltage-dependent Ca^{2+} channel; ΔV, membrane depolarization.

KEYWORDS

DYT1 dystonia, torsinA, neuronal function, neurobiology, calcium, synapse, synaptic transmission

ACCOMPLISHMENTS

Major goals of the project

Task 1. Define the mechanism whereby the cytoplasmic Ca^{2+} concentration ($[Ca^{2+}]_c$) is dysregulated by ΔE-torsinA (Months 1-18). In this annual report for Year 1 (Months 1-12), the percentage of completion is 66%.

Task 2. Determine how ΔE-torsinA causes aberrant neurotransmitter release at excitatory synapses (Months 12-30). The percentage of completion is 20%.

Task 3. Elucidate the neurophysiological and behavioral consequences of the dysregulated $[Ca^{2+}]_c$ and synaptic transmission in ΔE-torsinA mice (Months 18-36). This phase of the project has not been initiated yet.

Accomplishments under these goals

Institutional Animal Care and Use Committee (IACUC) approval (Task 1).
IACUC approval was obtained for all the experiments in the funded project on 04/10/2014, with the ACURF# 1403041.

Primary cultures of brain neurons (Task 1).
We have established the procedures for genotyping the neonatal mouse pups rapidly within a few hours, and for primary cultures of neurons obtained from the cerebral cortex, striatum and hippocampus of those pups. These procedures are easily applicable to the mouse model (heterozygous ΔE-torsinA knock-in mouse) that we use in the current study. They were published in a peer-reviewed journal (Koh et al, *J. Vis. Exp.* 2015; see the PRODUCTS / Journal Publication and APPENDICES sections). We have also published reviews about the DYT1 gene mutations and the properties of protein product torsinA (Harata, 2014a, 2014b; see the PRODUCTS / Journal Publication and APPENDICES sections).

Normal distribution of endoplasmic reticulum and mitochondria in neurons of DYT1 dystonia (Task 1).
One important regulator of $[Ca^{2+}]_c$ is the intracellular Ca^{2+} store that is composed of endoplasmic reticulum (ER) and mitochondria. The distribution and structure of ER and mitochondria have not been evaluated systematically in any cells of DYT1 dystonia. Considerable changes in them could indicate abnormal functions of the intracellular Ca^{2+} store. We evaluated them in the cultured neurons obtained from the hippocampus, cerebral cortex and striatum of the heterozygous ΔE-torsinA knock-in mice. By 14-16 days *in vitro*, the cultured neurons extended dendrites and axons, and developed extensive neuronal network. In order to visualize the ER and mitochondria, we stained the live neurons with specific fluorescent markers, ER-Tracker Green and MitoTracker Red CMXRos, respectively. The extent of cellular border was identified by staining the plasma membrane with the fluorescent marker, di-8-ANEPPS. The stained live neurons were observed with confocal fluorescence microscopy. The hippocampal data show that in either wild-type or heterozygous neurons, the plasma membrane was clear without breakages, the ER formed diffuse or trabecular network, and the mitochondria were thread-like without globular punctate staining (**Fig. 2**). This result was found in horizontal sections through the somata (**Fig. 2A**) and dendrites (**Fig. 2B**), and in vertical sections of somata (**Fig. 3**). The same result was also obtained in the cultures of cerebral cortical and striatal neurons (data not shown). These results show that the intracellular Ca^{2+} stores lack overt structural abnormalities, indicating that they might not serve as an appropriate diagnostic phenotype. However, these

structural results do not necessarily exclude a possibility that functional abnormalities are present in these intracellular Ca^{2+} stores.

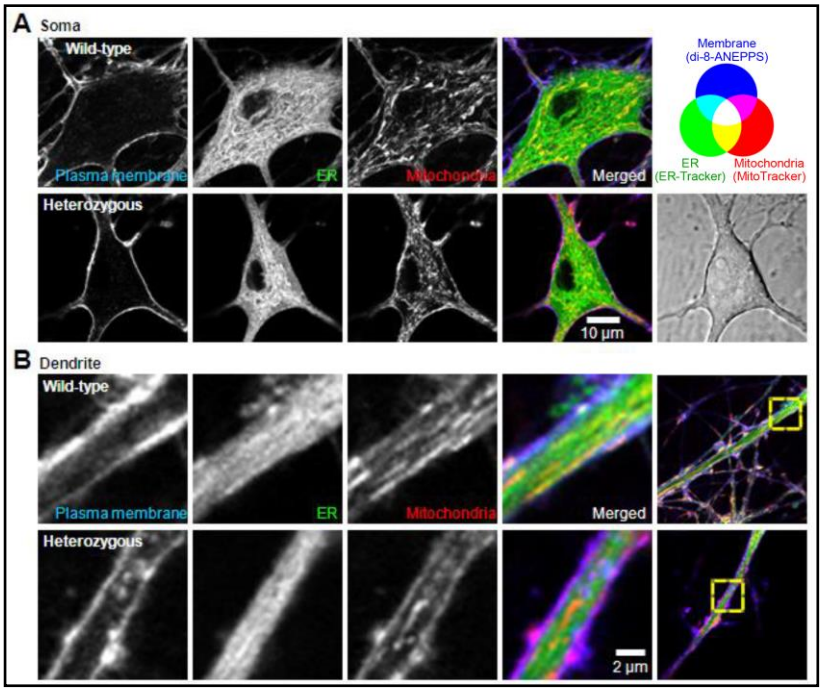

Fig. 2. Lack of structural abnormalities in ER and mitochondria of hippocampal neurons. The cultured neurons were stained with the ER marker ER-Tracker Green, the mitochondrial marker MitoTracker Red CMXRos, and the plasma membrane marker di-8-ANEPPS. The somatic (**A**) and dendritic regions (**B**) of the live neurons were imaged in the horizontal (x-y) plane, using confocal microscopy (single optical section). The dendritic regions in the four left panels were magnified from the dendritic regions indicated by yellow squares in the right-most panels. There were no marked differences between wild-type and heterozygous neurons. These neurons are representative of ~30 stained neurons.

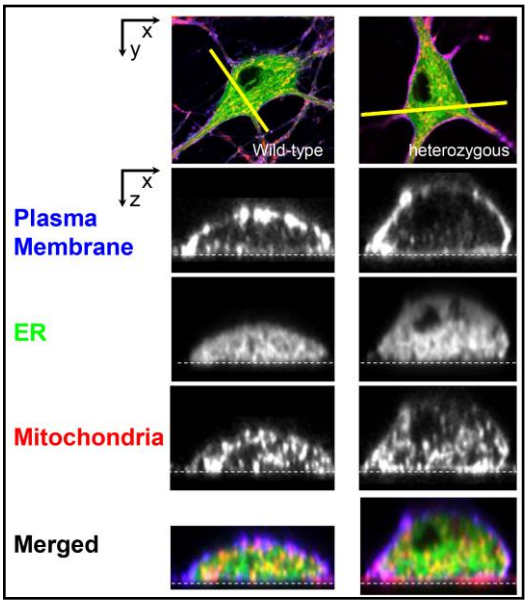

Fig. 3. Lack of structural abnormalities in ER and mitochondria of hippocampal neurons. The stained neurons in **Fig. 2** were imaged in the vertical (x-z) plane, using confocal microscopy (single optical section). The vertical plane was optically cut through the yellow line in the horizontal (x-y) plane. There were no marked differences between wild-type and heterozygous neurons.

Heterozygous neurons showed spontaneous Ca^{2+} activity more frequently than wild-type neurons (Task 1).

In order to evaluate the spontaneous excitability of neuronal network in the absence of any stimuli, the $[Ca^{2+}]_c$ was measured as the excitability readout from the dendrites of cultured hippocampal neurons. To date, we have only limited information about whether the excitability at the single-neuron level is affected, in the absence of experimental manipulation of glutamatergic and GABAergic synaptic transmission. Thus we have tested the net excitability of brain neurons of the DYT1 dystonia model without using antagonists of ionotropic glutamate and GABA receptors. $[Ca^{2+}]_c$ dynamics was imaged using a fluorescent Ca^{2+} indicator Fluo-5F-AM. The cultured hippocampal neurons of heterozygous ΔE-torsinA knock-in mice (HET) showed an increased frequency of spontaneous fluorescence increases, in comparison to wild-type neurons (WT) (**Fig. 4**). The fluorescence increase and its subsequent decay correspond to a temporary $[Ca^{2+}]_c$ rise and fall ($[Ca^{2+}]_c$ transient). Similar $[Ca^{2+}]_c$ transients were observed with cerebral cortical neurons, but not with the striatal neurons. In hippocampal and cerebral cortical cultures, the excitatory glutamatergic synapses made up 80-90% of all synapses and the inhibitory GABAergic synapses made up the remaining 10-20% (data not shown). In contrast, GABAergic synapses made up 99% of all synapses, and cholinergic synapses made up the remaining 1%, as we have published previously (Iwabuchi et al. PLoS ONE, 2013). Since the spontaneous Ca^{2+} activity was observed in hippocampal and cerebral cortical cultures but not in striatal cultures, our result indicates that the enhanced spontaneous Ca^{2+} activity is associated with enhanced glutamatergic synaptic transmission. In support of this notion, the frequency of spontaneous $[Ca^{2+}]_c$ transients was inhibited by blockers of AMPA and NMDA subtypes of ionotropic glutamate receptors (CNQX and AP5, respectively) (data not shown).

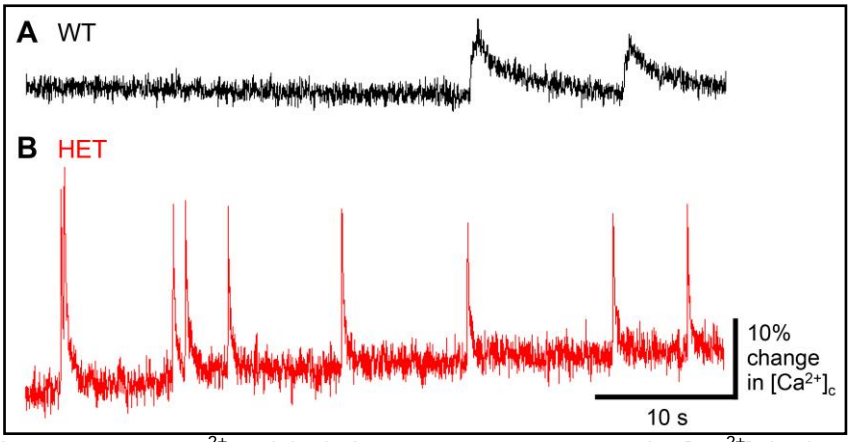

Fig. 4. Enhanced spontaneous Ca^{2+} activity in heterozygous neurons. The $[Ca^{2+}]_c$ in dendrites of cultured hippocampal neurons was imaged using a fluorescent Ca^{2+} indicator Fluo-5F-AM (1 μM). Wild-type (**A**) and heterozygous neurons (**B**). The changes in $[Ca^{2+}]_c$ were measured as the fold-changes in fluorescence intensity, normalized by the resting fluorescence intensity ($\Delta F/F_0$). These neurons are representative of ~10 neurons.

Heterozygous neurons showed higher resting level of $[Ca^{2+}]_c$ than wild-type neurons (Task 1). The previous result (**Fig. 4**) suggests that the resting (i.e. spontaneous) level of $[Ca^{2+}]_c$ might be higher in heterozygous neurons than wild-type neurons. In order to measure the absolute value of $[Ca^{2+}]_c$, we switched the Ca^{2+} indicator from Fluo-5F-AM to Fura-2-AM. Ratiometric measurement of Fura-2 with two excitation wavelengths allows the calculation of absolute value of $[Ca^{2+}]_c$, whereas a single-wavelength excitation of Fluo-5F allows visualizing only the relative changes in $[Ca^{2+}]_c$. In contrast to the advantage of Fluo-5F (capability to show rapid changes), Fura-2 does not allow rapid imaging (because of the need to change excitation wavelengths); however it did not pose a problem for measuring the resting $[Ca^{2+}]_c$ level. The measured $[Ca^{2+}]_c$ level was the same in the nuclei and somata of wild-type and heterozygous neurons of hippocampus ($p>0.05$, not significant, NS) (**Fig. 5, top**). In contrast, the $[Ca^{2+}]_c$ level in dendrites was higher in heterozygous neurons than wild-type neurons ($p<0.05$, *) (**Fig. 5, top**). Interestingly, this difference in resting $[Ca^{2+}]_c$ level was abolished by treating the cells with AMPA and NMDA receptor antagonists ("CNQX & AP5 (+)") (**Fig. 5, bottom**). These results are consistent with those in **Fig. 4**. These results show that the spontaneous neuronal activity was based on a glutamate receptor-mediated mechanism, supporting the hypothesis that dendritic $[Ca^{2+}]_c$ activity is abnormal due to enhanced glutamatergic synaptic transmission in heterozygous neurons.

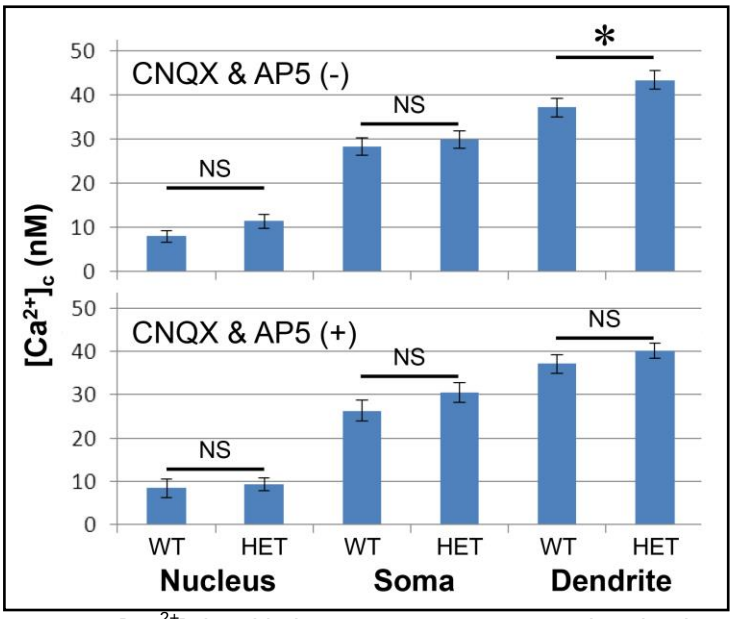

Fig. 5. Increased, spontaneous $[Ca^{2+}]_c$ level in heterozygous neurons. The absolute value of $[Ca^{2+}]_c$ was measured using a fluorescent Ca^{2+} indicator Fura-2-AM. Nuclear, somatic and dendritic levels were measured in the absence (**top**) and presence (**bottom**) of AMPA and NMDA receptor antagonists (CNQX & AP5). The data include 5-8 neurons per group.

Heterozygous neurons showed shorter latency of $[Ca^{2+}]_c$ transients in response to a single electrical stimulus (Task 1).

In addition to the spontaneous $[Ca^{2+}]_c$ transients (**Fig. 4**), we examined the $[Ca^{2+}]_c$ transients evoked by an electrical stimulation. A single 1-ms current pulse was applied to the cultured neurons (electric field stimulation), such that all neurons in the field are activated and fired an action potential. The $[Ca^{2+}]_c$ transients were induced similarly in dendrites of neurons cultured from the cerebral cortex, striatum and hippocampus (**Fig. 6**). However, a detailed analysis of the rising phase revealed a difference dependent on brain regions. In cerebral cortical cultures, the $[Ca^{2+}]_c$ transients in heterozygous neurons showed less time after stimulation until the $[Ca^{2+}]_c$ started increasing (shorter latency) than in wild-type neurons (red arrow in **left panel**). In striatal cultures, the latency in heterozygous neurons was indistinguishable from that in wild-type neurons (**middle panel**). In hippocampal cultures, the result was similar to the cerebral cortical cultures (red arrow in **right panel**). For better quantification, the imaging rate in hippocampus was raised to 1700 frames per second (fps), i.e. 0.59 ms per frame, from the 100 fps (10 ms per frame) in cerebral cortical and striatal cultures. The measured latency was shorter in heterozygous neurons ($p<0.05$, **bottom left**). These results demonstrate the enhanced $[Ca^{2+}]_c$ dynamics in heterozygous neurons of the cerebral cortex and hippocampus, in contrast to unchanged excitability in heterozygous neurons of the striatum. Notably, some heterozygous neurons in the hippocampus showed multiple $[Ca^{2+}]_c$ transients in response to a single stimulus (short red arrows in **bottom right panel**), also supporting the enhanced $[Ca^{2+}]_c$ dynamics in hippocampus (These second and third responses were not included in the latency analysis).

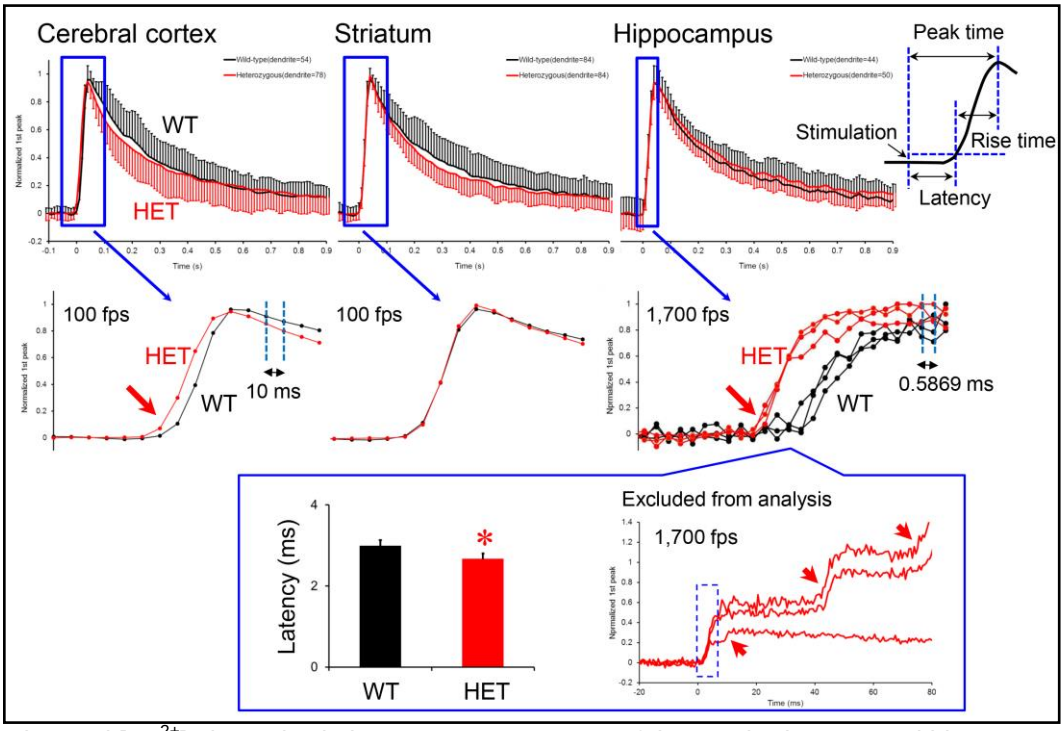

Fig. 6. Enhanced $[Ca^{2+}]_c$ dynamics in heterozygous neurons of the cerebral cortex and hippocampus, but not the striatum. We analyzed the latency of a $[Ca^{2+}]_c$ transient induced by a single 1-ms field stimulation in wild-type (**black traces**) and heterozygous neurons (**red traces**). The measured latency was shorter in heterozygous neurons than in wild-type counterparts ($p<0.05$, *). The $[Ca^{2+}]_c$ changes were imaged in dendrites of cultured neurons, using a fluorescent Ca^{2+} indicator Fluo-5F-AM. Long red arrows (**middle row**) indicate the early onsets of $[Ca^{2+}]_c$ transients in heterozygous neurons. Short red arrows (**bottom right**) indicate multiple $[Ca^{2+}]_c$ transients induced after the first one in heterozygous hippocampal neurons. The traces represent averages of all neurons. The data include 5-8 neurons per group.

Heterozygous neurons showed aberrant $[Ca^{2+}]_c$ rises in response to a train of action potentials (Task 1).

We further investigated the enhanced $[Ca^{2+}]_c$ dynamics in heterozygous neurons, by stimulating them with a train of electric stimuli. When all cultured neurons were stimulated by 10 pulses of electric field stimulation (1-ms duration at 1 Hz), the $[Ca^{2+}]_c$ increased transiently in the dendrites of both wild-type (**black**) and heterozygous (**red**) hippocampal neurons (**Fig. 7A**). However, in heterozygous neurons, additional $[Ca^{2+}]_c$ transients were out of synchrony with the stimuli (asynchronous; arrowheads). To quantify the $[Ca^{2+}]_c$ dynamics, we measured the area under the Ca^{2+} traces as the lump sum of $[Ca^{2+}]_c$ changes. It was significantly larger in heterozygous neurons than in wild-type neurons ($p<0.05$, t-test). Similar finding was obtained in the cerebral cortical neurons (**B**), but not in the striatal neurons ($p>0.05$) (**C**). The aberrant dynamics of dendritic $[Ca^{2+}]_c$ was abolished by combined application of CNQX + AP5, or by CNQX alone (data not shown), suggesting the involvement of AMPA receptor activation in the enhanced $[Ca^{2+}]_c$ dynamics.

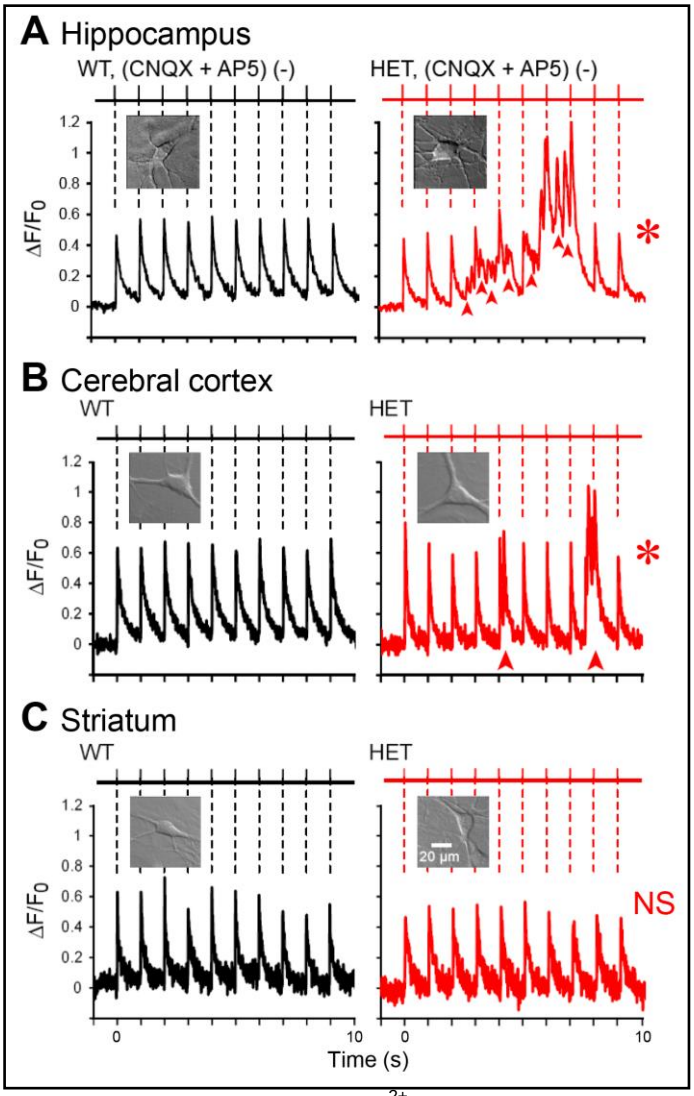

Fig. 7. A train of electrical stimuli induced aberrant $[Ca^{2+}]_c$ dynamics in the dendrites of cultured neurons from the hippocampus (**A**) and cerebral cortex (**B**), but not from the striatum (**C**), of heterozygous mutant mice. As in **Figs. 4, 6**, the changes in dendritic $[Ca^{2+}]_c$ were detected as changes in the fluorescence intensity of Fluo-5F-AM, and are expressed as fold-changes from baseline levels ($\Delta F/F_0$). The data include 30-50 neurons per group.

Asynchronous $[Ca^{2+}]_c$ dynamics in heterozygous neurons started at glutamatergic synapses (Task 1).

The results in **Figs. 4-7**, indicate that the enhanced dendritic $[Ca^{2+}]_c$ in heterozygous neurons is triggered by activation of postsynaptic glutamate receptors (**Fig. 1**). If this hypothesis is true, the abnormal dendritic $[Ca^{2+}]_c$ should start at glutamatergic synapses. To test this notion, we evaluated the asynchronous dendritic $[Ca^{2+}]_c$ dynamics during a train of stimuli, spatially located those asynchronous activities, and compared their position with the functional glutamatergic synapses (**Fig. 8**). During the live-cell imaging of heterozygous neurons, we located the positions of asynchronous dendritic $[Ca^{2+}]_c$ dynamics (arrows in top right panel of **Fig. 8B**), and the positions of functional synapses using a synaptic-vesicle endocytosis marker FM4-64 (arrows in bottom left panel of **Fig. 8B**). Thereafter, we chemically fixed the neurons for immunocytochemistry and located the positions of dendrites identified by a dendritic marker microtubule-associated protein 2 (MAP2) (right panel of **Fig. 8A**), and the positions of glutamatergic nerve terminals identified by vesicular glutamate transporter 1 (VGLUT1) (arrows in bottom right panel of **Fig. 8B**). All these spatial locations matched well. These results support the hypothesis linking the enhanced dendritic $[Ca^{2+}]_c$ dynamics to glutamate receptor activation (**Fig. 1**).

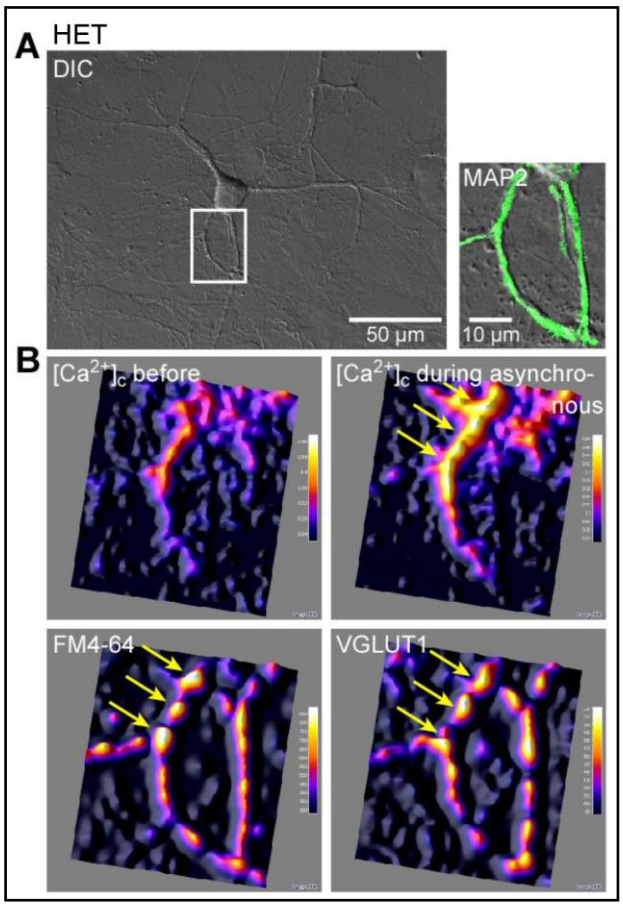

Fig. 8. Colocalization of aberrant $[Ca^{2+}]_c$ dynamics with the functional glutamatergic synapses. Cultured hippocampal neurons of heterozygous mice were stained with Fluo-5F-AM and stimulated (1 Hz, field stimulation). After Ca^{2+} imaging, the functional nerve terminals of the same neurons were labeled with 2.5 µM FM4-64. After the live-cell experiments, the neurons were fixed with paraformaldehyde, and immunocytochemically stained for a dendritic marker MAP2 and a glutamatergic nerve terminal marker VGLUT1. Arrows show colocalization of the aberrant $[Ca^{2+}]_c$ dynamics with the functional, glutamatergic nerve terminals. The data are representative of 5 reproducible experiments.

Asynchronous $[Ca^{2+}]_c$ dynamics was insensitive to a blockade of ryanodine receptors (Task 1). We next evaluated a potential involvement of intracellular Ca^{2+} stores in asynchronous $[Ca^{2+}]_c$ dynamics. The signal of Ca^{2+} influx into neuronal cytoplasm can be enhanced by the Ca^{2+} release from the ER, an intracellular Ca^{2+} store. This Ca^{2+}-induced Ca^{2+} release is mediated by ryanodine receptors, and can be blocked by high concentration of ryanodine (1 μM). This high concentration of ryanodine did not affect the asynchronous $[Ca^{2+}]_c$ dynamics in the dendrites of cultured hippocampal neurons during 1-Hz stimulation (**Fig. 9**). As a control, we confirmed that the same treatment abolished the responses of neurons to 10 mM caffeine that stimulates the Ca^{2+}-induced Ca^{2+} release. Also we found that depletion of ER Ca^{2+} by thapsigargin did not affect asynchronous $[Ca^{2+}]_c$ dynamics (data not shown). These data suggest that ER might not be involved in handling the abnormal $[Ca^{2+}]_c$ dynamics in heterozygous neurons.

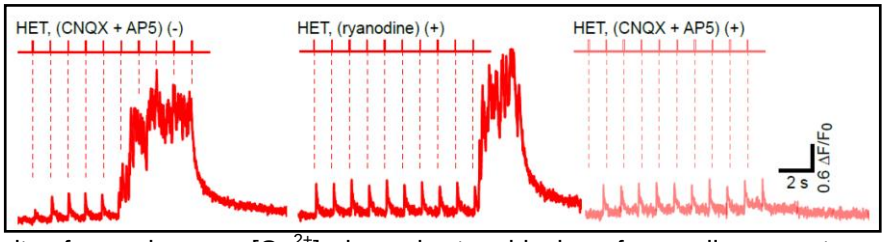

Fig. 9. Insensitivity of asynchronous $[Ca^{2+}]_c$ dynamics to a blocker of ryanodine receptors. Cultured hippocampal neurons of heterozygous mice were stained with Fluo-5F-AM and stimulated (1 Hz, field stimulation). These neurons experienced asynchronous $[Ca^{2+}]_c$ dynamics (**left**). In the presence of 1 μM ryanodine, the same stimulus train similarly induced asynchronous $[Ca^{2+}]_c$ dynamics in the same neurons (**middle**). The abnormal $[Ca^{2+}]_c$ dynamics were blocked by glutamate receptor antagonists CNQX and AP5 (**right**). The data are representative of 4 reproducible experiments.

Mitochondrial Ca^{2+} dynamics was abnormal in heterozygous neurons (Task 1).
In addition to the ER, the mitochondrion constitutes an intracellular Ca^{2+} store. To test its involvement in asynchronous $[Ca^{2+}]_c$ dynamics, we monitored the mitochondrial Ca^{2+} concentration ($[Ca^{2+}]_{MT}$). The cultured hippocampal neurons were transfected with a plasmid for the genetically encoded Ca^{2+} reporter, mitochondrial inverse pericam. When the neurons were stimulated with an electrical train (10 Hz, 3 s), the $[Ca^{2+}]_{MT}$ increased in somata and more so in dendrites (**Fig. 10**). However, the increase was significantly higher in heterozygous neurons than in wild-type neurons ($p<0.05$). Although it is still unclear whether the $[Ca^{2+}]_{MT}$ abnormality is the cause or result of asynchronous $[Ca^{2+}]_c$ dynamics under DYT1 dystonia mutation, the current result shows that mitochondria are involved in the abnormal Ca^{2+} activity of neurons.

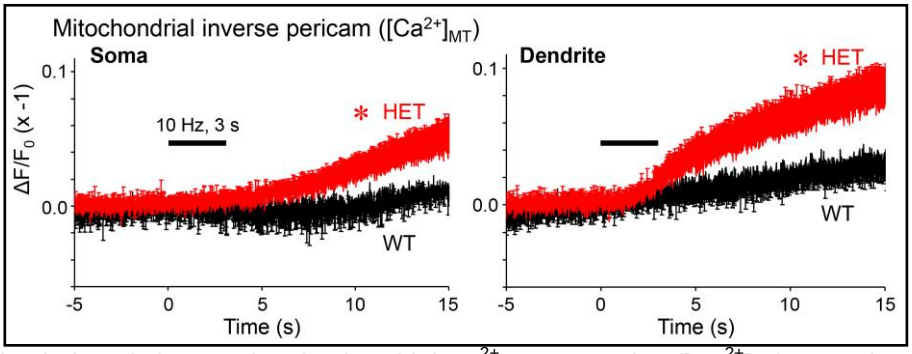

Fig. 10. Stimulus-induced changes in mitochondrial Ca^{2+} concentration ($[Ca^{2+}]_{MT}$) are enhanced in heterozygous neurons. Cultured hippocampal neurons were transfected with the Ca^{2+} indicator, mitochondrial inverse pericam. During and after stimulation with an electrical train (10 Hz, 3 s), $[Ca^{2+}]_{MT}$ increased in neurons of both genotypes. The amount of $[Ca^{2+}]_{MT}$ increase was larger in heterozygous neurons than in wild-type neurons ($p<0.05$). The traces represent averages of all neurons. The data were acquired from 4 and 6 neurons.

Electrical activity of cultured neurons can be visualized using a voltage-sensitive dye (Task 2). The above imaging results demonstrate that heterozygous neurons experience an enhanced dynamics of $[Ca^{2+}]_c$, which are an important regulator and indicator of neuronal excitability. In order to directly visualize the changes in neuronal excitability under DYT1 dystonia mutation, we introduced an imaging-based evaluation of neuronal membrane potentials. Imaging-based and electrophysiology-based evaluations will provide complementary information. The former has the capability of revealing spatial variations in membrane potentials, while the latter will allow the control of membrane potentials. This comment assumes that the sensitivity and time resolution of the imaging-based method are as high as those of electrophysiology. However, it has not been feasible to achieve the sensitive and fast imaging of membrane potentials. We optimized our imaging system and successfully achieved these aspects. The cultured hippocampal neurons of wild-type mice were treated with a voltage-sensitive fluorescent dye FluoVolt, and imaged by confocal microscopy (**Fig. 11A**). The dye cleanly stains the plasma membrane as expected. The cytoplasmic extent is demonstrated in the same neuron by co-staining the mitochondria with MitoTracker Red CMXRos. When these neurons were stimulated by a 1-ms field stimulation, the fluorescence intensity increased transiently (**Fig. 11B**). They represented action potentials because they were abolished by a Na^+ channel blocker tetrodotoxin (TTX). A small notch in the fluorescence trace remaining in the presence of TTX represents a small membrane potential change induced by field stimulation (stimulus artifact), indicating that our system is sensitive and fast enough to reveal small-amplitude and fast events. Various patterns of membrane-potential changes were observed in wild-type neurons after the stimulus-induced action potentials (**Fig. 11C**). They could be broadly categorized in the following three patterns: 1) no change in membrane potential (**Top**), 2) fast and slow depolarization (**Middle**), and 3) slow hyperpolarization lasting several 10's of ms (**Bottom**). Thus we were able to identify the individual action potentials, small depolarizations and small hyperpolarizations.

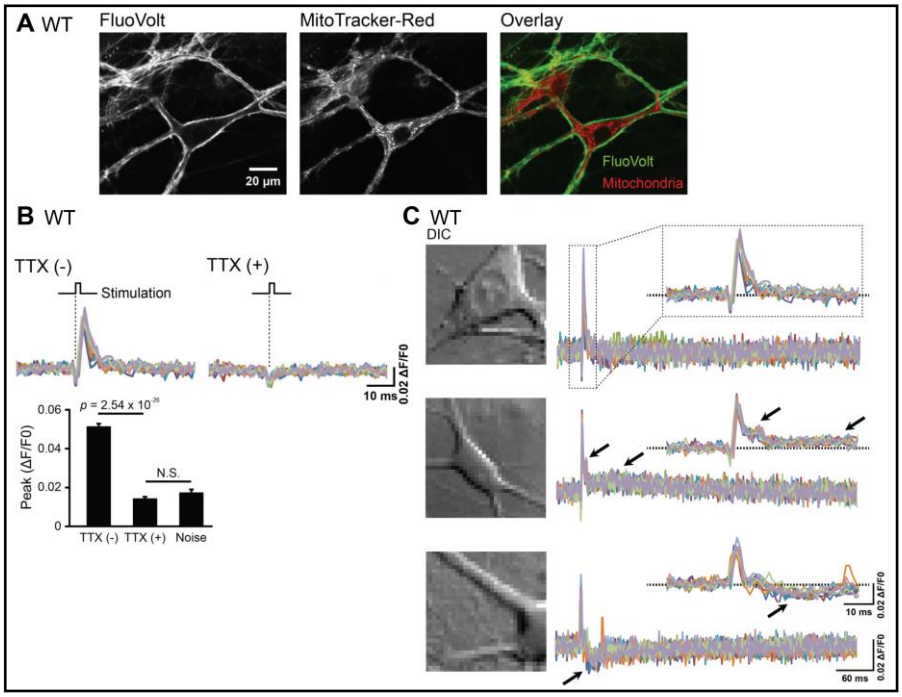

Fig. 11. Imaging membrane potentials with a voltage-sensitive fluorescent dye, FluoVolt. Cultured hippocampal neurons of wild-type mice were stained with FluoVolt (0.5 μM) and MitoTracker Red CMXRos (40 nM), and imaged while alive by confocal microscopy (**A**). Electric field stimulation transiently increased the fluorescence intensity of FluoVolt (**B**). The fluorescence change was abolished by tetrodotoxin (TTX, 1 μM), indicating that the fluorescence change represents an action potential.

Responses to 10 stimuli in a single neuron were overlaid, before and during treatment with tetrodotoxin. Tetrodotoxin significantly reduced the fluorescence responses (Student's paired t-test, n = 30 stimuli). Fluorescence imaging was achieved at 1000 fps (i.e. every 1 ms). Various patterns of membrane potential changes after action potentials (**C**). Shown are the three representative fluorescence responses after stimulus-induced action potentials. **Top**: no significant change. **Middle**: fast and slow depolarization (arrows). **Bottom**: slow hyperpolarization (arrows). Overlay of 10 traces from individual wild-type neurons.

Electrical activity of heterozygous neurons was enhanced, as assessed by imaging membrane potentials (Task 2).

When heterozygous neurons were stimulated by a single 1-ms field stimulation, they exhibited depolarizing responses following stimulation more frequently than their wild-type counterparts (**Fig. 12A**). These responses were blocked by tetrodotoxin (**Fig. 12A**) or AMPA receptor antagonist CNQX (**Fig. 12B**), suggesting that small-amplitude depolarizations (arrows in insets with expanded time scale) represent the excitatory postsynaptic potentials (EPSPs), and they trigger action potentials (arrows in main panels with slow time scale) when the EPSPs are of large amplitude. To quantify the overall change in neuronal excitability, we plotted the area under the curve during 10 sec of imaging (**Fig. 12C**). The final value of the area measured at the end of imaging was higher in heterozygous neurons than in wild-type neurons ($p<0.05$, Kolmogorov-Smirnov test). These results indicate that the overall excitability was increased in the mutant neurons, because they receive more glutamate as the neurotransmitter. Notably, these experiments (**Figs. 11, 12**) were performed without using antagonists of ionotropic glutamate and GABA receptors. Thus we have tested the net excitability of brain neurons of the DYT1 dystonia model in the absence of experimental manipulation of glutamatergic and GABAergic synaptic transmission.

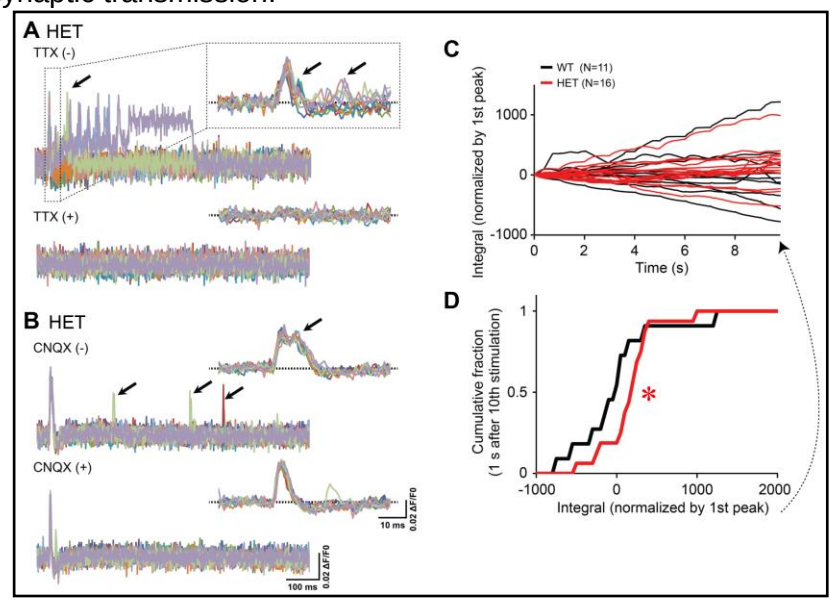

Fig. 12. Enhanced excitability of heterozygous neurons due to enhanced glutamatergic input. Overlay of 10 traces from a single mutant neuron, before and during treatment with tetrodotoxin (**A**). All responses were sensitive to tetrodotoxin, as in wild-type neurons. Overlay of 10 traces from a single mutant neuron, before and during treatment with AMPA receptor antagonist, CNQX (**B**). CNQX blocked small depolarizations, leaving action potentials intact. Thus, the small depolarizations were due to activation of AMPA receptors, and therefore represented EPSP. Arrows point to depolarizing responses: action potentials in panels with slow time scale (main panels), and EPSPs in panels with expanded time (insets). Area under the curve was plotted during stimulation with 10 pulses (**C**). Changes in single neurons were overlaid (each trace = each neuron). Black = wild-type neuron. Red = mutant neuron of heterozygous ΔE-torsinA knock-in mice. Cumulative changes after the 10^{th} pulse (**D**). Overall excitability was increased in mutant neurons.

Unmet goals so far.
The above results support our overall hypothesis that Ca^{2+} regulation becomes abnormal in dystonia, which enhances the neuronal excitability. In Task 1 (Months 1-18), we have not measured the axonal $[Ca^{2+}]_c$ and $[Ca^{2+}]_{MT}$ of the heterozygous and wild-type neurons. These will be achieved during the months 13-18. We have started only the initial phase of Task 2 (Months 12-30). We have not started Task 3 (Months 18-36). Thus, there are no unmet goals for these two Tasks yet.

Opportunities for training and professional development the project has provided
Dr. N. Charles Harata, M.D., Ph.D. (PI).
He was selected as a member of the Medical and Scientific Advisory Council of the Dystonia Medical Research Foundation (2014-2018). This professional development will help the team with knowledge and insights in dystonia.

Dr. Sadahiro Iwabuchi, Ph.D. (postdoctoral fellow).
He was trained by the PI for the data acquisition, quantitative data analyses, and internal laboratory progress report presentations. He was also trained by the PI for writing, revising and reviewing manuscripts in one-on-one sessions. He successfully presented a poster in an international meeting (Annual Meeting of the Society for Neuroscience, see the "Other publications, conference papers and presentations" section).

How results were disseminated to communities of interest
The PI has provided oral presentations in the following meetings specifically devoted to dystonia research:

- Medical and Scientific Advisory Council meeting of the Dystonia Medical Research Foundation in Scottsdale, Arizona (Feb 12-13, 2015).
- The Tyler's Hope for a Dystonia Cure Think Tank/Summit Meeting in Orlando, Florida (Mar 5-6, 2015).

Plan to do during the next reporting period to accomplish the goals
For Task 1 (Months 1-18), as stated above, we plan to evaluate the axonal $[Ca^{2+}]_c$ and $[Ca^{2+}]_{MT}$ in mutant and control neurons. For Task 2 (Months 12-30), we plan to examine how the DYT1 dystonia mutation causes aberrant neurotransmitter release at excitatory synapses in culture, which would be associated with the $[Ca^{2+}]_c$ abnormalities in postsynaptic dendrites that we have observed. For Task 3 (Months 18-36), we will initiate recording the excitatory glutamatergic transmission in brain slices.

IMPACT

Impact on the development of the principal discipline(s) of the project
We have provided the first evidence that the brain neurons of a dystonia mouse model suffer from abnormal regulation of the intracellular calcium ion concentration in an activity-dependent manner. Since calcium ion is an important regulator of neuronal activities, this finding strongly indicates that calcium dysregulation comprises one of the fundamental pathophysiological phenomena underlying dystonia. Identification of molecules responsible for this abnormality can lead to developments of novel treatments of dystonia.

Impact on other disciplines
We have developed procedures for rapid genotyping of newborn mouse pups, followed by primary culture of brain neurons (See the Journal Publication section and Appendix). Since the

genotyping is completed within a few hours after birth, this procedure enables neuronal cultures even from mice that could die several days after birth (which can happen in any genetically engineered mouse model). In addition, the neurons can be plated at very low density, enabling the imaging experiments at high spatial resolution without interference from neighboring cells. These procedures are easily applicable to neuronal cultures of any disease model. Thus they will have significant impacts on other disciplines of neurological and psychiatric disorders.

Impact on technology transfer
Nothing to report.

Impact on society beyond science and technology
Nothing to report.

CHANGES/PROBLEMS

Changes in approach and reasons for change
Nothing to report.

Actual or anticipated problems or delays and actions or plans to resolve them
Nothing to report.

Changes that had a significant impact on expenditures
There were personnel changes. Two personnel left the laboratories. They were:

- Dr. Sodikdjon Kodirov, Ph.D., Assistant Research Scientist in a collaborator's laboratory (Dr. Lee).
- Ms. Jin-Young Koh, research assistant.

We are actively recruiting personnel that have the similar expertise.

Significant changes in use or care of human subjects
Nothing to report.

Significant changes in use or care of vertebrate animals
Nothing to report.

Significant changes in use of biohazards and/or select agents
Nothing to report.

PRODUCTS

Journal publications
The following articles were published.

- **Harata NC**. Current gaps in the understanding of the subcellular distribution of exogenous and endogenous protein torsinA. *Tremor and Other Hyperkinetic Movements (N Y)* 4: 260, 2014a (DoD support was acknowledged).
- **Harata NC**. Addressing variant pathogenicity: the torsinA (*TOR1A*) gene as a model. *Hum Mutat*, 35(9): v, 2014b (DoD support was acknowledged only at the time of online submission).

- Koh JY, Iwabuchi S, Huang Z, **Harata NC**. Rapid genotyping of animals followed by establishing primary cultures of brain neurons. *J Vis Exp*, e51879, 2015 (DoD support was acknowledged).

Books or other non-periodical, one-time publications
The following article was submitted.

- **Harata NC**, Walker RH. TorsinA. *Neuroscience and Biobehavioral Psychology* (online), submitted (DoD support was acknowledged).

Other publications, conference papers and presentations
The following meeting abstracts were published.

- Iwabuchi S, Koh JY, **Harata NC**. Acetylcholine-induced calcium transients are sensitized in central neurons associated with DYT1 dystonia. Soc Neurosci Abstr. 40 (2014), Washington, DC, U.S.A.
- **Harata NC**, Iwabuchi S, Koh JY. Enhanced synaptic vesicle recycling in cultured striatal neurons of DYT1 dystonia mouse model. Soc Neurosci Abstr. 40 (2014), Washington, DC, U.S.A.

Website(s) or other Internet site(s)
Nothing to report.

Technologies or techniques
Nothing to report.

Inventions, patent applications, and/or licenses
Nothing to report.

Other Products
Nothing to report.

PARTICIPANTS & OTHER COLLABORATING ORGANIZATIONS

Individuals who have worked on the project

Name:	N. Charles Harata
Project Role:	PI
Nearest person month worked:	6
Contribution to Project:	Supervised the project, analyzed data, presented data in meetings and wrote manuscripts.
Funding Support:	University of Iowa (6 months).

Name:	Sadahiro Iwabuchi
Project Role:	Postdoctoral fellow
Nearest person month worked:	12
Contribution to Project:	Acquired and analyzed data.
Funding Support:	No other support.

Change in the active other support of the PD/PI(s) or senior/key personnel since the last reporting period
Nothing to report.

Partner organizations

Name:	Dr. Ruth H. Walker, MB, ChB, PhD
Location:	James J. Peters VA Medical Center, 130 West Kingsbridge Road, Bronx, NY 10468
Partner's contribution to the project:	collaboration through discussion of results and exchange of ideas.

SPECIAL REPORTING REQUIREMENTS

Not applicable.

APPENDICES

The reprints of the published manuscripts are attached as appendices in the following order:

- **Harata NC**. Current gaps in the understanding of the subcellular distribution of exogenous and endogenous protein torsinA. *Tremor and Other Hyperkinetic Movements (N Y)* 4: 260, 2014.
- **Harata NC**. Addressing variant pathogenicity: the torsinA (*TOR1A*) gene as a model. *Hum Mutat*, 35(9): v, 2014.
- Koh JY, Iwabuchi S, Huang Z, **Harata NC**. Rapid genotyping of animals followed by establishing primary cultures of brain neurons. *J Vis Exp*, e51879, 2015.

OPEN ACCESS Freely available online

Tremor and Other Hyperkinetic Movements

Viewpoints

Current Gaps in the Understanding of the Subcellular Distribution of Exogenous and Endogenous Protein TorsinA

N. Charles Harata*

Department of Molecular Physiology & Biophysics, University of Iowa Carver College of Medicine, Iowa City, IA, USA

Abstract

Background: An in-frame deletion leading to the loss of a single glutamic acid residue in the protein torsinA (ΔE-torsinA) results in an inherited movement disorder, DYT1 dystonia. This autosomal dominant disease affects the function of the brain without causing neurodegeneration, by a mechanism that remains unknown.

Methods: We evaluated the literature regarding the subcellular localization of torsinA.

Results: Efforts to elucidate the pathophysiological basis of DYT1 dystonia have relied partly on examining the subcellular distribution of the wild-type and mutated proteins. A typical approach is to introduce the human torsinA gene (*TOR1A*) into host cells and overexpress the protein therein. In both neurons and non-neuronal cells, exogenous wild-type torsinA introduced in this manner has been found to localize mainly to the endoplasmic reticulum, whereas exogenous ΔE-torsinA is predominantly in the nuclear envelope or cytoplasmic inclusions. Although these outcomes are relatively consistent, findings for the localization of endogenous torsinA have been variable, leaving its physiological distribution a matter of debate.

Discussion: As patients' cells do not overexpress torsinA proteins, it is important to understand why the reported distributions of the endogenous proteins are inconsistent. We propose that careful optimization of experimental methods will be critical in addressing the causes of the differences among the distributions of endogenous (non-overexpressed) vs. exogenously introduced (overexpressed) proteins.

Keywords: DYT1 dystonia, endogenous protein, localization, overexpression, torsinA

Citation: Harata NC. Current gaps in the understanding of the subcellular distribution of exogenous and endogenous protein torsinA. Tremor Other Hyperkinet Mov. 2014; 4. doi: 10.7916/D8JS9NR2

*To whom correspondence should be addressed. E-mail: charles-harata@uiowa.edu

Editor: Ruth Walker, Mount Sinai School of Medicine, USA

Received: June 22, 2014 **Accepted:** August 25, 2014 **Published:** September 23, 2014

Funding: Grants from the American Heart Association, Department of Defense (Peer Reviewed Medical Research Program award W81XWH-14-1-0301), Dystonia Medical Research Foundation, Edward Mallinckrodt, Jr. Foundation, National Science Foundation, and Whitehall Foundation to N.C.H.

Financial Disclosures: None.

Conflict of Interest: The author reports no conflict of interest.

Introduction

DYT1 dystonia is defined as "early-onset generalized isolated dystonia".[1] It is characterized by involuntary muscle contractions and abnormal postures, and caused by a mutation in the *TOR1A* gene (c.904_906delGAG/c.907_909delGAG; p.Glu302del/p.Glu303del) that results in deletion of a glutamic acid residue from the torsinA protein (ΔE-torsinA).[2–6] Patients with this autosomal dominant disorder are heterozygous for the mutation ($TOR1A^{+/\Delta E}$). TorsinA belongs to the AAA+ family (ATPases associated with various cellular activities).[7] Its ATPase activity is regulated by proteins in the endoplasmic reticulum (ER) and nuclear envelope,[8] and is thought to contribute to diverse cellular processes, including the unfolding of proteins during their degradation, the disassembly of protein aggregates, and the disassembly of protein complexes.[7] Although the biochemical properties of torsinA have been identified, how it contributes to neuronal function in the brain remains elusive. Because the first dystonia gene locus to be identified was for DYT1 dystonia, it serves as a paradigm for the pathogenesis and pathophysiology of this debilitating neurological disorder.

Knowledge of the subcellular distribution of torsinA is expected to provide insight into its function and the pathogenesis that occurs when it is mutated. According to a prevailing model for the localization and function of torsinA proteins, the wild-type form is present throughout the ER whereas the ΔE form is present in the nuclear envelope and

causes abnormalities in its ultrastructure (reviewed, e.g., in Granata et al.[9]). This proposed spatial redistribution of torsinA is thought to play a critical role in dystonia pathogenesis, because neuronal dysfunction can be caused by either a lack of wild-type torsinA or an accumulation of ΔE-torsinA in certain subcellular compartments. However, this model is based largely on studies in which expression of exogenous torsinA in host cells was forced (overexpression), and levels of the protein were much higher than in the endogenous state. As the total content of torsinA (wild-type plus ΔE-torsinA) in patient fibroblasts is similar to, or even slightly reduced from, that in normal subjects,[10–12] it is possible that the results from overexpression studies reflect a cellular state that is distinct from DYT1 dystonia.

The objective of this article is to compare imaging-based results obtained from exogenous overexpression in host cells with those for endogenous expression in a natural context, and to identify issues that will need to be resolved in order to settle the question of endogenous torsinA localization.

Search strategy and selection criteria

PubMED searches of articles were carried out using the terms "DYT1 dystonia," "torsinA," "TOR1A," "distribution," or "localization." No time limits were placed. The reference lists of the primary articles were also searched. Only mammalian studies reported in full-text articles written in English were analyzed.

Consistent localization results with overexpression systems

In overexpression systems, the human torsinA genes are exogenously introduced into model animals or cells. The distribution of overexpressed torsinA is typically evaluated by one of three methods: 1) torsinA is tagged with a fluorescent protein (fluorescence tag, e.g., green fluorescent protein [GFP], cyan fluorescent protein [CFP]) and its fluorescence is detected; 2) torsinA is tagged with a non-fluorescent peptide (epitope-tag, e.g., myc-tag, V5-tag, polyhistidine-tag) and is detected by immunocytochemistry using an anti-tag antibody; or 3) untagged torsinA is overexpressed and detected by immunocytochemistry using an anti-torsinA antibody. Western blotting was used to measure the fold increase in the level of protein overexpression. The value has been reported as ~1.3 to 1.5,[13] ~1.3 to 2.3,[14] ~2 to 6,[15] in transgenic mice, and as high as ~2 to ~20,[16] or ~10 to 50 in some cultured cells.[17,18] In studies where the Western blotting results were not quantified, the signals from endogenous protein were very weak or not detectable, in comparison to the overexpressed protein in cultured cells.[19–21]

Overexpression studies have provided relatively consistent results (Table 1). In Table 1, the reported data are entered according to the host cell types, and these are broadly classified into cultured non-neuronal cells, cultured tumor cells of neuronal origin, cultured neurons, and neurons *in situ*. All of the host cells had a wild-type background. For the sake of highlighting the potential variations among individual reports, the entries for a particular cell type are grouped together only where exactly the same result regarding either the subcellular distribution of torsinA or its colocalization with organellar markers was reported by the same group of researchers. In the case of wild-type torsinA, overexpressed protein was localized mainly in the ER, resulting in diffuse cytoplasmic—or where the resolution was high enough tubular or reticular—staining. At the level of light microscopy, the ER domain was almost equivalent to the cytoplasmic domain. A minor component of the signal emanated from the nuclear envelope (which is contiguous with the ER), in a perinuclear, ring-like pattern around the nucleoplasm. In the case of ΔE-torsinA, by contrast, the overexpressed protein was present mainly at the nuclear envelope and/or in cytoplasmic inclusion bodies. A minor component was present in the ER. Notably, the distributions of wild-type and ΔE forms of torsinA were not specific to the host cell types used, to whether the cells examined were cultured or in brain slices (*in situ*), or to the brain regions analyzed. Rather the distributions corresponded to whether it was wild-type or ΔE-torsinA that was overexpressed. Thus the general conclusion from these findings was that the signature feature of DYT1 dystonia is the mislocalization of ΔE-torsinA.

Advantages of overexpression systems

Overexpression systems are widely used, in part because they make it possible to introduce recombinant forms of torsinA with modifications. Other advantages of overexpression systems include the following: a fluorescence tag can be used to reveal torsinA localization, and the intensity of the tag is much stronger than background noise (autofluorescence); an epitope-tag can be used to reveal torsinA localization, and it can be detected with antibodies with high specificity for antigens not normally present in tissue; and, when an anti-torsinA antibody is used in this context, the signal of the overexpressed protein will be well above the background noise or endogenous signal, even though its affinity for torsinA may be lower than those of anti-tag antibodies for their respective tags. These overexpression systems have advantages in addition to their usefulness in analyzing the subcellular localization of torsinA. For example, they have been used to identify interacting partners of torsinA (reviewed, e.g., in Warner et al. [22]), to purify the torsinA protein,[8,19] to measure the rate of turnover of torsinA protein,[23] to evaluate the effects of torsinA in specific types of neurons,[24] and to establish what effects torsinA has on cell biological processes such as the ER- and oxidative-stress responses, and the chaperoning of proteins (reviewed, e.g., in Bragg et al.[6]).

Disadvantages of overexpression systems

Overexpression systems are associated with several general issues, including potentially violating balanced gene dosage, and affecting the folding of proteins, the assembly of protein complexes, and the regulation of downstream signaling.[25] In addition, overexpression systems have at least two disadvantages specific to the study of torsinA. One is that the distribution of torsinA is known to change depending on the expression level (Table 2). When ΔE-torsinA expression is low, it is present in the nuclear envelope (e.g. two- to 10-fold increase from the endogenous level), whereas when its expression is high, it is preferentially localized to cytoplasmic inclusions (e.g. ~20-fold

Table 1. Genotype-dependent Subcellular Distributions of Overexpressed Human TorsinA Proteins in Mammalian Systems

Cell Type/Name	WT-torsinA	ΔE-torsinA	References
Cultured non-neuronal cells			
Human astrocytes (brain region, not specified)	Diffuse cytoplasmic (colocalized with GFAP)	(–)	Armata et al.[76]
Human fibroblasts	Diffuse cytoplasmic (colocalized with PDI); no TEM abnormality of nuclear envelope	Inclusions; abnormal TEM of nuclear envelope	Hettich et al.[77]
Human glioma Gli36 cells	Diffuse cytoplasmic (colocalized with PDI); perinuclear staining	Inclusions; perinuclear	Bragg et al.[78]
Human glioma Gli36 cells	Diffuse cytoplasmic; perinuclear (colocalized with laminB, nucleoporin)	Perinuclear (colocalized with laminB, nucleoporin); with/without inclusions (not colocalized with laminB or nucleoporin), depending on expression levels	Bragg et al.[16]
Human osteosarcoma U2OS cells	Diffuse cytoplasmic; minimal inclusions (<5% of cells)	Inclusions (~90% of cells); not perinuclear	Kock et al.[79]
Human osteosarcoma U2OS cells	Diffuse cytoplasmic; minimal perinuclear	Diffuse cytoplasmic; perinuclear; no inclusions	Vander Heyden et al.[80]
Human osteosarcoma U2OS cells	Diffuse cytoplasmic	(–)	Naismith et al.[81]
Human osteosarcoma U2OS cells	Diffuse cytoplasmic (excluded from ER exit sites)	(–)	Vander Heyden et al.[82]
Human adenocarcinoma HeLa cells	Diffuse cytoplasmic (colocalized with KDEL)	Same as WT-torsinA overexpression	Giles et al.[26]
Human adenocarcinoma HeLa cells	Diffuse cytoplasmic; minimal perinuclear	Inclusions; minimal perinuclear	Zhu et al.[83]
Human embryonic kidney epithelial HEK293 cells	Diffuse cytoplasmic (colocalized with GRP78/BiP); perinuclear	Inclusions (not colocalized with GRP78/BiP); not perinuclear	Kustedjo et al.[19]
Human embryonic kidney epithelial HEK293 cells	Diffuse cytoplasmic (colocalized with PDI)	Inclusions (in>95% of cells)	O'Farrell et al.[21,84]
Human embryonic kidney epithelial HEK293 cells	Diffuse cytoplasmic	Inclusions; overexpressed ΔE-torsinA recruits overexpressed WT-torsinA to inclusions	Torres et al.[85]
Human embryonic kidney epithelial HEK293 cells	Diffuse cytoplasmic	Inclusions; these form whether or not torsinA has a carboxy-terminal V5-His-tag	Grundmann et al.[15]
Human embryonic kidney epithelial HEK293 cells	Diffuse cytoplasmic	(–)	Armata et al.[76]

Table 1. Continued

Cell Type/Name	WT-torsinA	ΔE-torsinA	References
Human embryonic kidney epithelial HEK293 cells	(–) (no light-microscopic data; normal TEM of nuclear envelope)	(–) (no light-microscopic data; abnormal TEM of nuclear envelope)	Zirn et al.[86]
Human embryonic kidney epithelial HEK293 cells	Diffuse cytoplasmic	Inclusions; overexpressed ΔE-torsinA recruits overexpressed WT-torsinA to inclusions	O'Farrell et al.[68]
Human embryonic kidney epithelial 293T cells	Diffuse cytoplasmic (colocalized with PDI)	Inclusions	Hettich et al.[77]
African green monkey kidney fibroblast-like COS-7 cells	Diffuse cytoplasmic (colocalized with GRP78/BiP); perinuclear; (N-terminus was modified to increase expression level in Kustedjo et al.[87])	Inclusions (not colocalized with GRP78/BiP); not perinuclear; (N-terminus was modified to increase expression level in Kustedjo et al.[87])	Kustedjo et al.[19,87]
African green monkey kidney fibroblast-like COS-7 cells	Diffuse cytoplasmic (colocalized with PDI)	Perinuclear; inclusions (not colocalized with PDI)	Naismith et al.[18]
African green monkey kidney fibroblast-like COS-7 cells	Diffuse cytoplasmic	Inclusions	Torres et al.[85]
African green monkey kidney fibroblast-like COS-7 cells	Diffuse cytoplasmic; minimal perinuclear	Inclusions; minimal perinuclear	Zhu et al.[83]
African green monkey kidney fibroblast-like COS-7 cells	Diffuse cytoplasmic (colocalized with PDI)	(–)	Nery et al.[88]
African green monkey kidney fibroblast-like COS-7 cells	Diffuse cytoplasmic (only partly colocalized with calreticulin, the soluble lumenal protein present throughout the ER, indicating that torsinA prefers ER flat sheet to ER tubules)	(–)	Vander Heyden et al.[82]
African green monkey kidney fibroblast-like COS-1 cells	Diffuse cytoplasmic	(–)	Shashidharan et al.[48]
African green monkey kidney epithelial Vero cells	Diffuse cytoplasmic (colocalized with KDEL); weak perinuclear	(–)	Maric et al.[89]
Mouse fibroblast NIH-3T3 cells	Diffuse cytoplasmic	Perinuclear	Jungwirth et al.[90]

Table 1. Continued

Cell Type/Name	WT-torsinA	ΔE-torsinA	References
Baby hamster kidney fibroblast BHK21 cells	Diffuse cytoplasmic (colocalized with KDEL); weak perinuclear (~20% of cells); no inclusions (~0%)	Perinuclear (~70% of cells); with/without inclusions (inclusions in ~70% of cells), depending on expression levels; overexpressed ΔE-torsinA recruits overexpressed WT-torsinA to perinuclear distribution	Goodchild and Dauer[10]
Baby hamster kidney fibroblast BHK21 cells	Diffuse cytoplasmic	Perinuclear; with/without diffuse cytoplasmic staining, depending on expression levels	Goodchild and Dauer[91]
Baby hamster kidney fibroblast BHK21 cells	Diffuse cytoplasmic (colocalized with KDEL in 100% of cells); inclusions (10% of cells); minimal perinuclear (colocalized with laminB1 in 6% of cells)	Inclusions (79% of cells; inclusions were smaller than those in overexpressed WT-torsinA); colocalized with laminB1 in 89%; colocalized with KDEL in 12%; not colocalized with lysosomal or autophagosomal markers	Calakos et al.[92]
Baby hamster kidney fibroblast BHK21 cells	Diffuse cytoplasmic (colocalized with PDI); perinuclear (not colocalized with PDI)	(–)	Jungwirth et al.[65]
Baby hamster kidney fibroblast BHK21 cells	Diffuse cytoplasmic	Perinuclear	Jungwirth et al.[90]
Chinese hamster ovary epithelial-like CHO cells	Diffuse cytoplasmic	Perinuclear; with/without inclusions, depending on expression levels	Naismith et al.[18]
Chinese hamster ovary epithelial-like CHO cells	Diffuse cytoplasmic (porcine torsinA)	Same as WT-torsinA overexpression (porcine torsinA)	Henriksen et al.[93]
Chinese hamster ovary epithelial-like CHO cells	Diffuse cytoplasmic (colocalized with GRP78/BiP)	(–)	Josse et al.[94]
Rat oligodendrocyte OLN cells	Punctate (porcine torsinA)	Same as WT-torsinA overexpression (porcine torsinA)	Henriksen et al.[93]
Cultured neuronal tumor cells			
Human neuroblastoma SH-SY5Y cells	Diffuse cytoplasmic (colocalized with PDI)	Inclusions (colocalized with VMAT2 but not with PDI); not perinuclear	Misbahuddin et al.[17]
Human neuroblastoma SH-SY5Y cells (differentiated)	Diffuse cytoplasmic	Perinuclear; inclusions	Hewett et al.[40]
Human neuroblastoma SH-SY5Y cells	Diffuse cytoplasmic (colocalized with PDI)	Perinuclear; inclusions (colocalized with snapin)	Granata et al.[37]

Table 1. Continued

Cell Type/Name	WT-torsinA	ΔE-torsinA	References
Human neuroblastoma SH-SY5Y cells	Diffuse cytoplasmic (colocalized with KDEL); perinuclear	Diffuse cytoplasmic (colocalized with KDEL); more preferential perinuclear staining than with WT-torsinA	Giles et al.[26,95]
Human neuroblastoma SH-SY5Y cells	Diffuse cytoplasmic (porcine torsinA)	Diffuse cytoplasmic; ring-like inclusions (porcine torsinA)	Henriksen et al.[93]
Human neuroblastoma SH-SY5Y cells	Diffuse cytoplasmic (excluding nucleoplasm)	Perinuclear; inclusions	Granata et al.[38]
Human neuroblastoma SH-SY5Y cells	Diffuse cytoplasmic (colocalized with PDI); no inclusions (found in ~4% of cells)	Inclusions (found in ~100% of cells); minimally colocalized with PDI	Vulinovic et al.[96]
Human neuroblastoma SK-N-AS cells	Diffuse cytoplasmic; minimal inclusions (~15% of cells); minimal perinuclear	Inclusions (~90% of cells); perinuclear	Cheng et al.[97]
Human neuroblastoma BE(2)-C cells (undifferentiated and differentiated)	Diffuse cytoplasmic (colocalized with PDI)	Inclusions	Hettich et al.[77]
Mouse neuroblastoma N2A cells	Diffuse cytoplasmic	(–)	Armata et al.[76]
Mouse neural line CAD cells (differentiated)	Punctate cytoplasmic in cell body and neurite (colocalized with PDI, partially with VAMP2); not perinuclear	Inclusions (colocalized with PDI, but not with VAMP2 or GM130); not perinuclear; TEM shows torsinA and PDI in inclusions	Hewett et al.[20]
Mouse neural line CAD cells	Diffuse cytoplasmic in cell body and process	Inclusions (colocalized with KLC in 57% of cells)	Kamm et al.[36]
Mouse neural line CAD cells	(–)	Perinuclear; inclusions	Naismith et al.[18]
Mouse neural line CAD cells	Diffuse cytoplasmic; minimal inclusions (<5% of cells)	Inclusions (~85% of cells); not perinuclear	Kock et al.[79]
Rat pheochromocytoma PC12 cells	Diffuse cytoplasmic (colocalized with PDI)	Perinuclear; inclusions (not colocalized with PDI)	Naismith et al.[18]
Rat pheochromocytoma PC12 cells	Diffuse cytoplasmic	Inclusions	Torres et al.[85]
Rat pheochromocytoma PC6-3 cells (differentiated)	Diffuse cytoplasmic (colocalized with GRP78/BiP, calnexin)	Perinuclear (colocalized with laminA); inclusions (colocalized with laminA/C, laminB, emerin, etc.)	Gonzalez-Alegre and Paulson[67]
Rat pheochromocytoma PC6-3 cells	Diffuse cytoplasmic	Inclusions; overexpressed ΔE-torsinA recruits overexpressed WT-torsinA to inclusions	Gonzalez-Alegre et al.[63]

Table 1. Continued

Cell Type/Name	WT-torsinA	ΔE-torsinA	References
Rat pheochromocytoma PC6-3 cells	Diffuse cytoplasmic	Perinuclear; inclusions	Gordon and Gonzalez-Alegre,[23] Gordon et al.,[73] Maric et al.,[89] Martin et al.[98]
Cultured neurons			
Mouse midbrain neurons (including substantia nigra, ventral tegmental area)	Diffuse cytoplasmic in soma and process; inclusions (~5% of all neurons, ~0% of TH-negative neurons, ~20% of TH-positive neurons)	Inclusions (54% of all neurons, 43% of TH-negative neurons, 84% of TH-positive neurons) (colocalized with TH, but not with PDI) (TH-positive neurons comprised 20–30% of all neurons)	O'Farrell et al.[68]
Mouse cerebral cortical neurons (7 DIV)	Diffuse cytoplasmic in soma and process	Perinuclear	Nery et al.[88]
Rat dorsal root ganglion neurons (3 DIV)	Diffuse cytoplasmic in soma; minimal perinuclear (4% of neurons); no inclusions (0% of neurons)	Diffuse cytoplasmic in soma; perinuclear (58%); inclusions (28%)	Kock et al.[99]
Neurons *in situ*			
Transgenic mouse, neurons in cerebral cortex	Diffuse cytoplasmic (colocalized with KDEL)	Perinuclear (colocalized with laminB1)	Goodchild and Dauer[10]
Transgenic mouse, neurons in striatum	Diffuse/punctate cytoplasmic; no inclusions; not perinuclear; ~twofold increase in torsinA protein level in comparison to non-transgenic control mice	Same as in transgenic mice overexpressing WT-torsinA or non-transgenic control; ~twofold increase in torsinA protein level in comparison to non-transgenic control mice	Sharma et al.[14]
Transgenic mouse, neurons in periaqueductal gray, pedunculopontine nucleus, pons	(–)	Inclusions (colocalized with lamin A/C, ubiquitin); these changes were absent in cerebral cortex, hippocampus, striatum, substantia nigra pars compacta, cerebellar cortex	Shashidharan et al.[100]

Table 1. Continued

Cell Type/Name	WT-torsinA	ΔE-torsinA	References
Transgenic mouse, neurons in substantia nigra, raphe nucleus, pedunculopontine nucleus, cerebellar cortex, deep cerebellar nuclei, gigantocellular reticular nucleus	Diffuse cytoplasmic in soma and dendrite; inclusions (colocalized with lamin A/C, ubiquitin-protein conjugates, but not with PDI) (inclusions not found in hippocampus, striatum, substantia nigra, cerebellar cortex); ~sixfold increase in human protein level from non-transgenic mice; high expression caused TEM abnormality of nuclear envelope (30% of neurons in striatum, 10–20% of brainstem neurons)	Similar to WT-torsinA overexpression; ~twofold increase in human protein level from non-transgenic mice; TEM nuclear envelope abnormality more frequent than in WT-torsinA overexpression (~50% of neurons in striatum, 30–40% of brainstem neurons)	Grundmann et al.[15]
Transgenic mouse, neurons in cerebral cortex, striatum, substantia nigra pars compacta, pontine nuclei	Diffuse cytoplasmic in soma and proximal dendrite; no perinuclear; no inclusions; human torsinA transcript was not increased in comparison to control human brains; no TEM abnormality of nuclear envelope in striatum, pontine nuclei, cerebellar cortex, spinal cord	Same as WT-torsinA overexpression and non-transgenic control; human torsinA transcript was four-to-fivefold higher than in control human brains; no TEM abnormality of nuclear envelope in striatum, pontine nuclei, cerebellar cortex, spinal cord	Zhao et al.[27] (same mice as reported in Sharma et al.[14])
Transgenic mouse, neurons in olfactory bulb	Diffuse cytoplasmic in soma and dendrite; inclusions in mitral cell; no staining in dentate gyrus of hippocampus or striatum	(–)	Regensburger et al.[101] (same mice as reported in Grundmann et al.[15])
Transgenic mouse, neurons in striatum (medium spiny neurons)	Diffuse/punctate cytoplasmic in soma and proximal dendrite; no staining in nucleoplasm, fibers	Diffuse/punctate cytoplasmic in soma and proximal dendrite; no staining in nucleoplasm or fibers.	Martella et al.[102] (same mice as reported in Sharma et al.[14])
Transgenic mouse, neurons in substantia nigra pars compacta (dopaminergic neurons; human torsinA was overexpressed only in dopaminergic neurons using TH promoter)	Diffuse cytoplasmic in soma and proximal dendrite	Perinuclear	Page et al.[24]
Transgenic mouse, neurons in striatum (cholinergic interneurons)	(–)	Same as in non-transgenic controls (diffuse cytoplasmic in soma and proximal dendrite)	Sciamanna et al.[75] (same mice as reported in Sharma et al.[14])

Table 1. Continued

Cell Type/Name	WT-torsinA	ΔE-torsinA	References
Transgenic rat, neurons in olfactory bulb, cerebral cortex, hippocampus, striatum, substantia nigra	Diffuse cytoplasmic in soma and proximal dendrite (not colocalized with lamin A/C that showed continuous curve); normal TEM of nuclear envelope; protein expression level was not specified for morphological studies	Perinuclear in a discontinuous pattern (colocalized with lamin A/C); abnormal TEM of nuclear envelope; not expressed in pons, cerebellum, brainstem; torsinA protein expression level was ~sevenfold higher than the lowest expressing line	Grundmann et al.[103]

In this article, "perinuclear" indicates ring-like staining of the nuclear envelope completely surrounding the nucleoplasm. "Inclusions" indicate intracellular, cytoplasmic inclusion bodies, except where intranuclear inclusion is specifically mentioned in Table 3. The cytoplasmic inclusions were often located near cellular nuclei. (–) indicates not tested.

Table 1 includes results with human torsinA, except for one study that analyzed porcine torsinA (mentioned as such).

Table 1 and Table 2 include both controlled and uncontrolled expression of the exogenous transgene.

In Tables 1–3, the results are limited to the distributions of wild-type and ΔE-torsinA. They do not include other naturally occurring mutations or genetically engineered proteins. Results from experimental manipulations that could affect the torsinA distribution were not included. Such manipulations are, e.g., the co-transfection with non-torsinA transgene constructs, the induction of cellular stress and ischemic insults, and the pharmacological regulation of biological processes.

Abbreviations and comments in Tables 1–3: calbindin D-28K (Purkinje neuron marker); calnexin (ER marker); ChAT, Choline Acetyltransferase (cholinergic neuron marker); CSN4, COP9 signalosome complex subunit 4; DIV, Days *In Vitro*; EM, Electron Microscopy; emerin (nuclear envelope marker); ER, Endoplasmic Reticulum; GABA, γ-Aminobutyric Acid (inhibitory neurotransmitter); GFAP, Glial Fibrillary Acidic Protein (astrocyte marker); GM130, Golgi Matrix protein of 130 kDa (Golgi apparatus marker); GRP78/BiP, Glucose-Regulated Protein of 78 kDa/Binding Immunoglobulin Protein, also known as heat shock 70 kDa protein 5 (HSPA5) (ER marker); KDEL, Lysine-Aspartic Acid-Glutamic Acid-Leucine Sequence (ER retention signal); KLC, Kinesin Light Chain (motor protein); lamins (nuclear envelope markers); NOS, Nitric Oxide Synthase (marker of a class of GABAergic neurons); NSE, Neuron-Specific Enolase (neuronal marker); nucleoporin (nuclear envelope marker); parvalbumin (marker of a class of GABAergic neurons); PDI, Protein Disulfide Isomerase (ER marker); SGI, Secretogranin I (secretory granule marker); snapin (SNAP25 [synaptosomal associated protein of 25 kDa]-binding protein); somatostatin (marker of a class of GABAergic neurons); TEM, Transmission Electron Microscopy; TH, Tyrosine Hydroxylase (dopaminergic/noradrenergic neuron marker); VAMP2, Vesicle-Associated Membrane Protein/Synaptobrevin 2 (synaptic vesicle/nerve terminal marker); VGAT, Vesicular GABA Transporter (GABAergic nerve terminal marker); VGLUT1 and 2, Vesicular Glutamate Transporters 1 and 2 (glutamatergic nerve terminal markers); VMAT2, Vesicular Monoamine Transporter 2 (monoaminergic marker); WT, wild type; ΔE, deletion of a single GAG codon in *TOR1A* or *Tor1a* gene (associated with DYT1 dystonia).

increase from the endogenous level).[16] The fact that the expression level is a strong determinant of at least the ΔE-torsinA distribution pattern indicates that the localization would have to be extrapolated to estimate the distribution of torsinA proteins at the low, endogenous level. However, it is unclear how such extrapolation can be achieved and, even if it is possible, to what extent the extrapolated properties would reflect those of the endogenous proteins. As a side note, some exceptions to the consistent overexpression results have been reported. For example, ΔE-torsinA was mislocalized in the neuroblastoma cell line SH-SY5Y but not in the non-neuronal HeLa cell line[26] or in the neurons of transgenic mice overexpressing human ΔE-torsinA[14,27] (Table 1). This phenomenon can be explained if the expression levels of wild-type and ΔE-torsinA were different in those studies.

Another disadvantage of the overexpression systems is their dependence on the properties of the promoters used to express the transgenes (promoters in transgenic animals have been reviewed in Tassone et al.,[28] Oleas et al.,[29] and Richter and Richter[30]). For instance, the commonly used human cytomegalovirus (CMV) major immediate–early promoter/enhancer is considered strong, but its effect is influenced by neuronal activity, with depolarization increasing its efficiency more than 90-fold.[31] Thus, expression will be low in neurons with weak spontaneous activity, and such activity may be masked by high expression in more active neurons. Moreover, different promoters demonstrate different tissue specificities and developmental expression profiles.[32]

In summary, the results obtained from overexpression systems are mostly clear and consistent, albeit with a few exceptions. However, caution is needed in interpreting them, especially with respect to the subcellular localization of torsinA proteins, until such outcomes are reliably replicated at endogenous levels of expression.

Inconsistent localization results for endogenous torsinA

Endogenous torsinA has been detected by indirect immunocytochemistry. The primary anti-torsinA antibody is detected using a secondary antibody conjugated with a fluorescent probe (fluorophore) or an enzyme that synthesizes colored or electron-dense product.[33] For a partial list of torsinA antibodies, see Xiao et al.[34] In sharp contrast to the outcomes for overexpression systems, the reported distribution of the endogenous torsinA protein is fairly inconsistent (Table 3).

In the case of *in vitro* studies, the cytoplasmic distribution of wild-type torsinA was typically diffuse, but it was punctate in a pattern consistent with vesicle staining in immature neurons and neuron-like tumor

Table 2. Subcellular Distributions of Human TorsinA Proteins at Different Overexpression Levels

Cell type/name	WT-torsinA	ΔE-torsinA	References
Human glioma Gli36 cells (expression level was actively controlled by tetracycline-regulated system)	Unchanged pattern (diffuse cytoplasmic; weak perinuclear), irrespective of expression levels	Perinuclear when expression level is low to moderate (two- to 10-fold increase from endogenous level); additional inclusions when the level is high (~20-fold increase from endogenous level)	Bragg et al.[16]
Baby hamster kidney fibroblast BHK21 cells (expression level was monitored)	Unchanged pattern (diffuse cytoplasmic; weak perinuclear), irrespective of expression levels	Perinuclear when expression level is low to moderate; additional inclusions when the level is high	Goodchild and Dauer[10]
Baby hamster kidney fibroblast BHK21 cells (expression level was monitored)	(–)	Perinuclear when the expression level is low; additional, diffuse cytoplasmic staining when the level is higher.	Goodchild and Dauer[91]
Chinese hamster ovary epithelial-like CHO cells (expression level was monitored)	(–)	Perinuclear and diffuse cytoplasmic when expression level is low; additional inclusions when the level is high (e.g.>fourfold higher than the low expression)	Naismith et al.[18]

cells.[35–38] In addition, wild-type torsinA was present in neurites and growth cones of immature cells,[35–38] whereas it was not detectable in axonal shafts or nerve terminals of more mature neurons.[39] In the fibroblasts of DYT1 dystonia patients, perinuclear staining was reported in one study[10] but was absent in others.[40,41] Notably, staining of cytoplasmic inclusions was absent in all cases, consistent with findings from studies in fibroblasts from control subjects.[10,40,41]

In the case of neurons *in situ*, the results were more variable than those described above. The majority of studies found that wild-type torsinA was distributed diffusely throughout the cytoplasm of the somata and proximal dendrites. However, the following patterns were also described: strong staining of axons and nerve terminals;[42–45] strong staining of the neuropil without staining of somata or dendrites;[46] staining of the proximal dendrites of some but not all neurons;[47] and staining of the nucleoplasm.[47,48] Of interest is the notion that the torsinA-positive domain of the neuron does not completely overlap with the ER.[49] Even after nucleoplasmic staining was excluded, the torsinA staining covered only a portion of the cytoplasm,[47,48] suggesting that a non-ER compartment could be stained. In the brains of DYT1 dystonia patients, the distribution of torsinA protein was the same as in those from control subjects, i.e., a lack of staining of inclusions or the nuclear envelope,[44,49] although cytoplasmic inclusions were found in brainstem regions.[50]

Approaches to filling the gap

The discrepancies in the distribution results for exogenous and endogenous torsinA proteins mainly arise from variation in the reported distribution of endogenous torsinA. It is difficult to interpret the results of overexpression studies, given that the pattern or determinant of endogenous localization is not yet clear. The latter could reflect genuine variations in the biology of this protein, reflecting subtle differences and changes in torsinA expression. It is also possible that the subcellular distribution of torsinA differs by cell type, by brain region, by species, and/or developmental stage, and there may even be intrinsic variation among individuals. Furthermore, in the case of human brains, the levels of protein expression may be affected by how, and for how long, the subjects had experienced pathological stresses before death, because torsinA expression at both the mRNA[51] and protein[52] levels is regulated by insults.

Before discussing these interesting variations of biological importance, however, it should be stated that the more likely causes of variation are technical issues concerning specificity and efficiency in detecting endogenous torsinA. Identifying the sources of any technical complications will help explain the discrepancies in the observed distributions for exogenous and endogenous torsinA.

One potentially important challenge in comparing the data for the two types of expression is that the lower level of expression for endogenous torsinA will make it difficult to distinguish positive signals from background noise. Importantly, any factor that negatively influences the immunocytochemical detection procedures may affect interpretation. Thus, it will be particularly important to test whether each step in the immunocytochemical procedure is working properly and is optimized, in both *in vitro* and *in situ* studies, and at both the light and the electron microscopy levels. The following are ways that future

Table 3. Subcellular Localization of Endogenous TorsinA Proteins in Mammalian Systems

Cell type/name	WT-torsinA	ΔE-torsinA	References
Cultured non-neuronal cells			
Human fibroblasts	Diffuse/punctate cytoplasmic; minimal perinuclear	Strong perinuclear; weaker cytoplasmic; no inclusions; patients' cells (*TOR1A*$^{+/\Delta E}$)	Goodchild and Dauer[10]
Human fibroblasts	Diffuse cytoplasmic; not perinuclear	Same as WT-torsinA; no inclusions; patients' cells (*TOR1A*$^{+/\Delta E}$)	Hewett et al.[40]
Human fibroblasts	Diffuse cytoplasmic; minimal perinuclear	Same as WT-torsinA; no inclusions; patients' cells (*TOR1A*$^{+/\Delta E}$)	Nery et al.[41]
Mouse embryonic fibroblasts	Diffuse cytoplasmic (partially colocalized with KDEL)	(–)	Giles et al.[26]
Cultured neuronal tumor cells			
Human neuroblastoma SH-SY5Y cells	Diffuse cytoplasmic in cell body; nucleoplasm	(–)	Hewett et al.[66]
Human neuroblastoma SH-SY5Y cells (differentiated)	Punctate cytoplasmic in cell body; punctate accumulation in neurite varicosity (colocalized with VAMP)	(–)	Ferrari-Toninelli et al.[35]
Human neuroblastoma SH-SY5Y cells	Diffuse cytoplasmic in cell body (colocalized with KDEL) (processes were not present)	(–)	Giles et al.[95]
Human neuroblastoma SH-SY5Y cells	Punctate cytoplasmic in cell body and process (colocalized with CSN4)	(–)	Granata et al.[38]
Human neuroglioma H4 cells	Diffuse cytoplasmic in cell body; no inclusions	(–)	McLean et al.[104]
Rat pheochromocytoma PC12 cells (differentiated)	Diffuse cytoplasmic in cell body and process (colocalized with PDI)	(–)	Hewett et al.[72]
Rat pheochromocytoma PC12 cells (differentiated)	Punctate accumulation in neurite tip (colocalized with snapin, SGI)	(–)	Granata et al.[37]
Cultured neurons			
Mouse cerebral cortical neurons	Diffuse cytoplasmic	(–)	Gonzalez-Alegre et al.[63]
Mouse cerebral cortical neurons (3–7 DIV)	Diffuse cytoplasmic (colocalized with KDEL); some perinuclear (more localized to nuclear envelope than in embryonic fibroblasts in the same study)	(–)	Giles et al.[26]
Mouse cerebral cortical neurons	Diffuse cytoplasmic	(–)	Kim et al.[105]

Table 3. Continued

Cell type/name	WT-torsinA	ΔE-torsinA	References
Mouse hippocampal neurons (4 DIV)	Punctate cytoplasmic in soma and process (colocalized with snapin)	(–)	Granata et al.[37]
Mouse cerebellar granule neurons (4–6 DIV)	Punctate cytoplasmic in soma and neurite (colocalized with CSN4)	(–)	Granata et al.[38]
Mouse neurons from cerebral cortex, hippocampus, striatum, ΔE-torsinA knock-in model (12–16 DIV)	Proximal dendrite; absent from axon and nerve terminal; soma was not evaluated	Same as in WT-torsinA; (*Tor1a*$^{+/\Delta E}$ and *Tor1a*$^{\Delta E/\Delta E}$)	Koh et al.[39]
Rat cerebral cortical neurons (8 DIV)	Punctate cytoplasmic in soma, neurite, growth cone (colocalized with KLC1)	(–)	Kamm et al.[36]
Neurons *in situ*			
Human neurons in cerebral cortex, hippocampus, substantia nigra pars compacta	Diffuse cytoplasmic in soma, proximal dendrite; nucleoplasm; no staining of white matter	(–)	Shashidharan et al.[48]
Human neurons in cerebral cortex, substantia nigra pars compacta (in Parkinson's disease)	Positive staining in intracellular Lewy bodies (that are positive for α-synuclein)	(–)	Shashidharan et al.[69]
Human neurons in cerebral cortex, hippocampus, caudate-putamen, thalamus, substantia nigra pars compacta, oculomotor nucleus, cerebellar cortex, spinal cord	Diffuse/punctate cytoplasmic in soma, proximal dendrite; fibers in white matter, brachium of superior colliculus, etc; no staining of nucleoplasm	(–)	Konakova et al.[42]
Human neurons in hippocampus, substantia nigra (in diffuse Lewy body disease)	No staining of soma or dendrite; positive staining in Lewy bodies (colocalized with α-synuclein and ubiquitin, but closely associated with only α-synuclein at <30-nm resolution).	(–)	Sharma et al.[106]
Human neurons in substantia nigra (in dementia with Lewy body disease)	No staining of soma or dendrite; positive staining in Lewy bodies (colocalized with α-synuclein which in turn is colocalized with heat shock proteins)	(–)	McLean et al.[104]
Human neurons in cerebral cortex, hippocampus, caudate-putamen, substantia nigra pars compacta, oculomotor nucleus, cerebellar cortex	Punctate cytoplasmic in soma (limited colocalization with PDI); proximal dendrite; nucleoplasm (sparing nucleoli); punctate neuropil (putative nerve terminals); no inclusions; not perinuclear	Same as in WT-torsinA; patient's brain (*TOR1A*$^{+/\Delta E}$)	Walker et al.[49]

Table 3. Continued

Cell type/name	WT-torsinA	ΔE-torsinA	References
Human neurons in cerebral cortex, hippocampus, oculomotor nucleus (in Huntington's disease, spinocerebellar ataxia type III, and Huntington's disease-like 2 which had previously been diagnosed as chorea-acanthocytosis[107])	Positive in intranuclear inclusion bodies (that are positive for ubiquitin, expanded polyglutamine repeats)	(–)	Walker et al.[108,109]
Human neurons in hippocampus, caudate-putamen, nucleus basalis of Meynert, substantia nigra pars compacta, cerebellar cortex	Punctate cytoplasmic in soma, proximal dendrite; some axons and "pencil bundle fibers" (axons of medium spiny neurons in caudate-putamen); punctate neuropil (putative nerve terminals)	Same as in WT-torsinA; no inclusions; only caudate-putamen and substantia nigra pars compacta were analyzed in patients' brains (*TOR1A*$^{+/\Delta E}$)	Rostasy et al.[44]
Human neurons in hippocampus, putamen, substantia nigra pars compacta, cerebellar cortex	No staining of soma or dendrite; punctate neuropil (putative axon, nerve terminals; vesicles in axons (immuno-EM).	(–)	Augood et al.[46]
Human neurons in periaqueductal gray, pedunculopontine nucleus, cuneiform nucleus	No inclusions	Inclusions (colocalized with laminA/C, ubiquitin-protein conjugates, ubiquitin, but weakly with PDI); these inclusions were absent in cerebral cortex, hippocampus, striatum, substantia nigra pars compacta; patients' brains (*TOR1A*$^{+/\Delta E}$)	McNaught et al.[50]
Human neurons in substantia nigra (in diffuse Lewy body disease)	Positive staining in Lewy bodies	(–)	O'Farrell et al.[84]
Human neurons in hippocampus, putamen, globus pallidus, substantia nigra pars compacta, oculomotor nucleus, superior colliculus, cerebellar cortex, dentate nucleus of deep cerebellar nuclei, during development	Diffuse/punctate cytoplasmic in soma, proximal dendrite; putative axon and nerve terminal; no nucleoplasm; no staining before postnatal 6 weeks	(–)	Siegert et al.[70]

Table 3. Continued

Cell type/name	WT-torsinA	ΔE-torsinA	References
Human neurons in pedunculopontine nucleus, cuneiform nucleus, pontine reticular formation (in normal subjects and patients with non-DYT1 dystonia)	No inclusions	(–)	Holton et al.[110]
Patus monkey neurons in hippocampus	Nucleoplasm, axon, nerve terminal (immuno-EM); no other compartments were analyzed	(–)	Walker et al.[43]
Macaque monkey neurons in putamen	No staining of soma or dendrite; staining in neuropil; vesicles in nerve terminals (immuno-EM).	(–)	Augood et al.[46]
Mouse neurons in cerebral cortex, hippocampus, caudate-putamen, thalamus, substantia nigra pars compacta, motor nucleus of trigeminal nerve, cerebellar cortex	Strong staining of fibers in cerebral cortical white matter, corpus callosum, internal capsule, anterior commissure, cerebral peduncle, etc; diffuse/punctate cytoplasmic in soma, proximal dendrite	(–)	Konakova and Pulst[45]
Mouse neurons in peri-aqueductal gray, pedunculopontine nucleus, pontine nuclei	Diffuse cytoplasmic in soma (colocalized with PDI, but not with lamin A/C or ubiquitin)	(–)	Shashidharan et al.[100]
Mouse neurons in cerebral cortex, substantia nigra pars compacta, pontine nuclei of ΔE-torsinA knock-in model	Diffuse cytoplasmic in soma; no inclusions in brains of male or female mice	Inclusions only in pontine nuclei of male mice (colocalized with ubiquitin) (not found in female mice) (*Tor1a*$^{+/\Delta E}$)	Dang et al.[111]
Mouse neurons in striatum (cholinergic interneurons)	Diffuse cytoplasmic in soma and proximal dendrite	(–)	Sciamanna et al.[75]
Mouse neurons in cerebellar cortex, deep cerebellar nuclei	Diffuse/punctate cytoplasmic in soma, dendrite, dendritic spine (partially colocalized with calbindin D-28K, parvalbumin), nerve terminal (partially colocalized with VGLUT1, VGLUT2, VGAT); nucleoplasm of neurons expressing high level of torsinA	(–)	Puglisi et al.[71]
Mouse neurons in red nucleus, interstitial nucleus of Cajal, of brain-restricted nestin-*Cre* *Tor1a*$^{flox/\Delta E}$ model ("nestin selective knock-in" mouse)	Diffuse cytoplasmic (expression level was ~60% of *Tor1a*$^{+/\Delta E}$ mice) (nestin-*Cre* control mouse)	Perinuclear (expression level was ~20% of *Tor1a*$^{+/\Delta E}$ mice) (*Tor1a*$^{-/\Delta E}$)	Liang et al.[61]

Table 3. Continued

Cell type/name	WT-torsinA	ΔE-torsinA	References
Rat neurons in hippocampus, substantia nigra pars compacta, cerebellar cortex, deep cerebellar nuclei	Nucleoplasm; diffuse cytoplasmic in soma, proximal dendrite (partially colocalized with TH)	(–)	Shashidharan et al.[48]
Rat neurons in cerebral cortex, hippocampus, striatum, cerebellar cortex	Nucleoplasm (sparing nucleoli); diffuse cytoplasmic in soma (partially colocalized with NSE, NOS, parvalbumin, GABA or ChAT), proximal dendrites of some but not all neurons; punctate neuropil (putative nerve terminals)	(–)	Walker et al.[47]
Rat neurons in cerebral cortex, hippocampus, striatum, substantia nigra pars compacta, cerebellar cortex	Diffuse cytoplasmic in soma, dendrite; not perinuclear or nucleoplasmic; punctate "pencil fiber bundle" axons in young striatum	(–)	Xiao et al.[34]
Rat neurons in cerebral cortex, hippocampus, striatum, thalamus, during development	Cytoplasm in soma, processes; increased staining intensity during postnatal 7 to 28 days	(–)	Oberlin et al.[112]
Rat neurons in striatum, globus pallidus, subthalamic nucleus	Nucleoplasm (sparing nucleoli); less strong in perikaryal cytoplasm and proximal dendrite	(–)	Yamada et al.[113]
Rat neurons in hippocampus	Diffuse cytoplasmic in soma, proximal dendrite of pyramidal neurons and parvalbumin- or somatostatin-positive interneurons	(–)	Zhao et al.[52]
Rat neurons in dorsal root ganglion	Diffuse cytoplasmic in soma; axon	(–)	Zhao et al.[52]

Note that the cells of DYT1 dystonia patients are listed under "ΔE-torsinA." However, they are heterozygous for the mutant allele (*TOR1A*$^{+/\Delta E}$), i.e., both wild-type and ΔE-torsinA proteins will be present. Similarly, heterozygous ΔE-torsinA knock-in mice (*Tor1a*$^{+/\Delta E}$) will express two types of full-length proteins. In contrast, the homozygous ΔE-torsinA knock-in mice (*Tor1a*$^{\Delta E/\Delta E}$) express only the ΔE-torsinA protein, and the brain-restricted nestin-*Cre Tor1a*$^{flox/\Delta E}$ mice express the ΔE-torsinA protein and exons 1 and 2 (out of exons 1–5) of wild-type protein (i.e., effectively *Tor1a*$^{-/\Delta E}$).

studies can achieve such optimization, as suggested for immunocytochemical reports more generally.[33,53–55]

Firstly, it will be important to test primary antibodies for their specificity in binding to the antigen. The literature suggests at least five controls for general immunocytochemical procedures.[53–55] The first control is to manipulate expression of the antigen. Suggested approaches are genetic deletion in knock-out animals or down-regulation by RNA interference. A variation of this test is to upregulate the antigen, for example, by overexpressing GFP-tagged antigen, and detecting this protein simultaneously by GFP fluorescence and immunocytochemistry using secondary antibody conjugated with a different fluorophore.[55] A drawback of this approach is that predominance of the overexpressed antigen can mask the specificity of a weak antibody. The second control is to preadsorb the antibody with the immunizing peptide. The third control is to compare the specificity of immunostaining at the cellular level to mRNA expression as assessed by *in situ* hybridization, taking into consideration that the two signals may be detected in different subcellular compartments. The fourth control is to test the antibody for overlap of its signal with that from other antibodies raised against non-overlapping epitopes of the same protein. The feasibility of this approach depends on the repertoire of available antibodies. The fifth control is to test the ability of the antibody to detect a single protein entity by Western blotting. However, in this case it needs to be born in mind that the proteins are

in different states with respect to their secondary, tertiary and quaternary structures when recognized by immunocytochemistry vs. Western blotting (denatured by sodium dodecyl sulfate, heat or reducing condition), and thus this test could produce irrelevant information. Controls of these types are especially important for polyclonal antibodies, given that they identify multiple epitopes in the antigen (torsinA), some of which could be shared with non-related proteins. Such non-specific binding is less likely to occur with monoclonal antibodies, for which the epitopes are specific peptide sequences that are not shared with other proteins.

Secondly, it will likewise be vital to control secondary antibodies for their specificity in binding to a primary antibody of interest. A typical method is to omit the primary antibody, and examine whether the signal is eliminated.[53,55] Omission of both the primary and secondary antibodies will establish to what extent the native tissue produces background noise, e.g., autofluorescence ("label control" in Burry[55]).

Thirdly, other aspects of immunocytochemical procedures will also require careful optimization. These include: the concentration of the primary antibody (e.g., too high a concentration leads to non-specific staining[33]); the type and duration of chemical fixation (e.g., one torsinA antibody was incompatible with procedures of cryo-immuno-electron microscopy[37]); and the type of embedding medium (e.g., paraffin embedding under heat can reduce the antigenicity). These aspects are especially important for *in situ* studies, because the procedures typically take longer than those required for *in vitro* studies and are therefore more susceptible to artifacts caused by non-ideal conditions. For example, animal tissues are chemically fixed for a prolonged period of time, first by trans-cardiac perfusion with a fixative (perfusion fixation) for ~30 min, and second by immersion of the tissue in the same fixative (immersion post-fixation) for one to two days. In contrast, cultured cells are typically fixed (immersion fixation) for ~30 min only. If torsinA antigenicity is affected by the duration of fixation, the results can be variable depending on the protocols used in individual experiments.

Lastly, not only the staining of samples, but also the imaging of signals can be affected by numerous factors. The first is optical resolution along the focal axis (in the z-direction). Resolution is limited to ~1 μm even when optical sectioning is carried out by confocal microscopy, and it is worse in the case of widefield microscopy.[56] Therefore, when paraffin sections (e.g., 3-μm thickness[57,58]) and floating sections (e.g., 50-μm thickness[59]) are used, the signal detected at any focal plane will be affected by stray signal from adjacent structures in other focal planes. Some forms of super-resolution fluorescence imaging will suffer from the same problem in thick sections. This issue is best resolved when ultrathin sectioning is achieved physically (e.g., 50–200 nm).[60] Second, the level of the focal plane is important because of the poor z-resolution of light microscopy. Even a non-diffuse signal can look diffuse and be mistaken as ER-like if the focal plane is outside the target structure. Third, it is essential to keep the imaging parameters at the same values (e.g., intensity setting and exposure time).[55] Otherwise, increasing the detection sensitivity could inappropriately lead to the inclusion of background noise as positive signal, and to an incorrect interpretation such as a diffuse ER-like pattern.

The influences of the technical aspects discussed above have not been extensively evaluated in the field of DYT1 dystonia, although considerable efforts have been made. These include using the torsinA knock-out tissue in immunostaining[61] or Western blotting,[61,62] using antisense knock-down in immunostaining[35,63,64] or Western blotting,[35,38,63,65] Western blotting using torsinA-overexpressing cells,[15,17,20,21,23,40,46,48,66–68] antigen preadsorption test in cellular staining[39,42,44,45,47,48,69–71] or Western blotting,[20,42,45,72] secondary antibody controls,[34,36,39,44,47,49,50,71] and the spatial range of signal spread in tissue.[71]

The key to definitive resolution of torsinA localization will be to evaluate these parameters for each antibody using each protocol, and using each tissue of interest in a given species. We understand that these efforts will be labor-intensive, and also that it will not be feasible to use such controls in studying human brains. However, systematic evaluation in at least the cellular and animal models will produce reliable immunocytochemical data that can be compared qualitatively to that produced in overexpression studies.

Of note, although species-specific antibodies are available,[23,73] one of the current challenges is that no antibody available can distinguish between the wild-type and ΔE-torsinA proteins.[11,13,39,74,75] The study of torsinA distribution will be significantly improved if antibodies or other tools capable of doing so are developed.

Conclusions

Knowledge of the subcellular distribution of torsinA will be critical for understanding how wild-type torsinA affects neuronal function, as well as how ΔE-torsinA leads to neuronal dysfunction. This information will help researchers narrow down the potential pathophysiological roles of torsinA in DYT1 dystonia. For this purpose, it will be important to reassess the prevailing model of torsinA distribution based on exogenous torsinA, after the endogenous distribution is reliably established. Such reassessments will be valuable regardless of the precise outcome. Should the endogenous and exogenous distributions match, torsinA mislocalization in the model will be reinforced as one of the key events in pathogenesis. Should they differ, it will indicate that ΔE-torsinA is mislocalized as a consequence of abnormally high expression. In this case the new results will be particularly important in providing novel insights into pathophysiological mechanisms. Even under such conditions, it should be emphasized that this article is not aimed at downplaying the value of overexpression studies. Such studies make it possible, for example, to modify the molecular structure of torsinA and to identify regulatory interacting partners. Nevertheless, at this point, it will be essential to establish whether overexpression studies truly reflect the roles of endogenous torsinA and the pathogenesis of DYT1 dystonia.

Acknowledgments

The author thanks the members of the Harata laboratory for helpful discussions throughout this work. The author apologizes to authors of

reports on non-mammalian models of DYT1 dystonia as well as to any authors whose work is not discussed here.

References

1. Albanese A, Bhatia K, Bressman SB, et al. Phenomenology and classification of dystonia: A consensus update. *Mov Disord* 2013;28:863–873.

2. Ozelius LJ, Hewett JW, Page CE, et al. The early-onset torsion dystonia gene (*DYT1*) encodes an ATP-binding protein. *Nat Genet* 1997;17:40–48.

3. Geyer HL, Bressman SB. The diagnosis of dystonia. *Lancet Neurol* 2006;5: 780–790.

4. Breakefield XO, Blood AJ, Li Y, Hallett M, Hanson PI, Standaert DG. The pathophysiological basis of dystonias. *Nat Rev Neurosci* 2008;9:222–234.

5. Tanabe LM, Kim CE, Alagem N, Dauer WT. Primary dystonia: Molecules and mechanisms. *Nat Rev Neurol* 2009;5:598–609.

6. Bragg DC, Armata IA, Nery FC, Breakefield XO, Sharma N. Molecular pathways in dystonia. *Neurobiol Dis* 2011;42:136–147.

7. Hanson PI, Whiteheart SW. AAA+ proteins: Have engine, will work. *Nat Rev Mol Cell Biol* 2005;6:519–529.

8. Zhao C, Brown RS, Chase AR, Eisele MR, Schlieker C. Regulation of Torsin ATPases by LAP1 and LULL1. *Proc Natl Acad Sci USA* 2013;110:E1545–1554.

9. Granata A, Schiavo G, Warner TT. TorsinA and dystonia: From nuclear envelope to synapse. *J Neurochem* 2009;109:1596–1609.

10. Goodchild RE, Dauer WT. Mislocalization to the nuclear envelope: An effect of the dystonia-causing torsinA mutation. *Proc Natl Acad Sci U S A* 2004;101: 847–852.

11. Goodchild RE, Kim CE, Dauer WT. Loss of the dystonia-associated protein torsinA selectively disrupts the neuronal nuclear envelope. *Neuron* 2005; 48:923–932.

12. Hewett JW, Nery FC, Niland B, et al. siRNA knock-down of mutant torsinA restores processing through secretory pathway in DYT1 dystonia cells. *Hum Mol Genet* 2008;17:1436–1445.

13. Napolitano F, Pasqualetti M, Usiello A, et al. Dopamine D2 receptor dysfunction is rescued by adenosine A2A receptor antagonism in a model of DYT1 dystonia. *Neurobiol Dis* 2010;38:434–445.

14. Sharma N, Baxter MG, Petravicz J, et al. Impaired motor learning in mice expressing torsinA with the DYT1 dystonia mutation. *J Neurosci* 2005;25: 5351–5355.

15. Grundmann K, Reischmann B, Vanhoutte G, et al. Overexpression of human wildtype torsinA and human ΔGAG torsinA in a transgenic mouse model causes phenotypic abnormalities. *Neurobiol Dis* 2007;27:190–206.

16. Bragg DC, Camp SM, Kaufman CA, et al. Perinuclear biogenesis of mutant torsin-A inclusions in cultured cells infected with tetracycline-regulated herpes simplex virus type 1 amplicon vectors. *Neuroscience* 2004;125:651–661.

17. Misbahuddin A, Placzek MR, Taanman JW, et al. Mutant torsinA, which causes early-onset primary torsion dystonia, is redistributed to membranous structures enriched in vesicular monoamine transporter in cultured human SH-SY5Y cells. *Mov Disord* 2005;20:432–440.

18. Naismith TV, Heuser JE, Breakefield XO, Hanson PI. TorsinA in the nuclear envelope. *Proc Natl Acad Sci U S A* 2004;101:7612–7617.

19. Kustedjo K, Bracey MH, Cravatt BF. Torsin A and its torsion dystonia-associated mutant forms are lumenal glycoproteins that exhibit distinct subcellular localizations. *J Biol Chem* 2000;275:27933–27939.

20. Hewett J, Gonzalez-Agosti C, Slater D, et al. Mutant torsinA, responsible for early-onset torsion dystonia, forms membrane inclusions in cultured neural cells. *Hum Mol Genet* 2000;9:1403–1413.

21. O'Farrell C, Hernandez DG, Evey C, Singleton AB, Cookson MR. Normal localization of ΔF323-Y328 mutant torsinA in transfected human cells. *Neurosci Lett* 2002;327:75–78.

22. Warner TT, Granata A, Schiavo G. TorsinA and DYT1 dystonia: A synaptopathy? *Biochem Soc Trans* 2010;38:452–456.

23. Gordon KL, Gonzalez-Alegre P. Consequences of the DYT1 mutation on torsinA oligomerization and degradation. *Neuroscience* 2008;157:588–595.

24. Page ME, Bao L, Andre P, et al. Cell-autonomous alteration of dopaminergic transmission by wild type and mutant (ΔE) TorsinA in transgenic mice. *Neurobiol Dis* 2010;39:318–326.

25. Gibson TJ, Seiler M, Veitia RA. The transience of transient over-expression. *Nat Methods* 2013;10:715–721.

26. Giles LM, Chen J, Li L, Chin LS. Dystonia-associated mutations cause premature degradation of torsinA protein and cell-type-specific mislocalization to the nuclear envelope. *Hum Mol Genet* 2008;17:2712–2722.

27. Zhao Y, DeCuypere M, LeDoux MS. Abnormal motor function and dopamine neurotransmission in DYT1 ΔGAG transgenic mice. *Exp Neurol* 2008;210:719–730.

28. Tassone A, Sciamanna G, Bonsi P, Martella G, Pisani A. Experimental models of dystonia. *Int Rev Neurobiol* 2011;98:551–572.

29. Oleas J, Yokoi F, Deandrade MP, Pisani A, Li Y. Engineering animal models of dystonia. *Mov Disord* 2013;28:990–1000.

30. Richter F, Richter A. Genetic animal models of dystonia: Common features and diversities. *Prog Neurobiol* 2014; in press. doi: http://dx.doi.org/10.1016/j.pneurobio.2014.07.002.

31. Wheeler DG, Cooper E. Depolarization strongly induces human cytomegalovirus major immediate-early promoter/enhancer activity in neurons. *J Biol Chem* 2001;276:31978–31985.

32. Maskri L, Zhu X, Fritzen S, et al. Influence of different promoters on the expression pattern of mutated human α-synuclein in transgenic mice. *Neurodegener Dis* 2004;1:255–265.

33. Hoffman GE, Le WW, Sita LV. The importance of titrating antibodies for immunocytochemical methods. *Curr Protoc Neurosci* 2008;Chapter 2:Unit 2 12.

34. Xiao J, Gong S, Zhao Y, LeDoux MS. Developmental expression of rat torsinA transcript and protein. *Brain Res Dev Brain Res* 2004;152:47–60.

35. Ferrari-Toninelli G, Paccioretti S, Francisconi S, Uberti D, Memo M. TorsinA negatively controls neurite outgrowth of SH-SY5Y human neuronal cell line. *Brain Res* 2004;1012:75–81.

36. Kamm C, Boston H, Hewett J, et al. The early onset dystonia protein torsinA interacts with kinesin light chain 1. *J Biol Chem* 2004;279:19882–19892.

37. Granata A, Watson R, Collinson LM, Schiavo G, Warner TT. The dystonia-associated protein torsinA modulates synaptic vesicle recycling. *J Biol Chem* 2008;283:7568–7579.

38. Granata A, Koo SJ, Haucke V, Schiavo G, Warner TT. CSN complex controls the stability of selected synaptic proteins via a torsinA-dependent process. *EMBO J* 2011;30:181–193.

39. Koh JY, Iwabuchi S, Harata NC. Dystonia-associated protein torsinA is not detectable at the nerve terminals of central neurons. *Neuroscience* 2013;253C: 316–329.

40. Hewett JW, Zeng J, Niland BP, Bragg DC, Breakefield XO. Dystonia-causing mutant torsinA inhibits cell adhesion and neurite extension through interference with cytoskeletal dynamics. *Neurobiol Dis* 2006;22:98–111.

41. Nery FC, Zeng J, Niland BP, et al. TorsinA binds the KASH domain of nesprins and participates in linkage between nuclear envelope and cytoskeleton. *J Cell Sci* 2008;121:3476–3486.

42. Konakova M, Huynh DP, Yong W, Pulst SM. Cellular distribution of torsin A and torsin B in normal human brain. *Arch Neurol* 2001;58:921–927.

43. Walker RH, Good PF, Brin MF, Sandu D, Shashidharan P. TorsinA immunoreactivity in normal and DYT1 brain: Light microscopic studies in DYT1 human and electron microscopic studies in non-human primate brain. In: Nicholson LFB, Faull RLM, editors. The basal ganglia VII. New York: Kluwer Academic/Plenum Publishers; 2002. p 511–520 (Advances in behavioral biology; vol. 52).

44. Rostasy K, Augood SJ, Hewett JW, et al. TorsinA protein and neuropathology in early onset generalized dystonia with GAG deletion. *Neurobiol Dis* 2003;12:11–24.

45. Konakova M, Pulst SM. Immunocytochemical characterization of torsin proteins in mouse brain. *Brain Res* 2001;922:1–8.

46. Augood SJ, Keller-McGandy CE, Siriani A, et al. Distribution and ultrastructural localization of torsinA immunoreactivity in the human brain. *Brain Res* 2003;986:12–21.

47. Walker RH, Brin MF, Sandu D, et al. Distribution and immunohistochemical characterization of torsinA immunoreactivity in rat brain. *Brain Res* 2001;900:348–354.

48. Shashidharan P, Kramer BC, Walker RH, Olanow CW, Brin MF. Immunohistochemical localization and distribution of torsinA in normal human and rat brain. *Brain Res* 2000;853:197–206.

49. Walker RH, Brin MF, Sandu D, Good PF, Shashidharan P. TorsinA immunoreactivity in brains of patients with *DYT1* and non-*DYT1* dystonia. *Neurology* 2002;58:120–124.

50. McNaught KS, Kapustin A, Jackson T, et al. Brainstem pathology in DYT1 primary torsion dystonia. *Ann Neurol* 2004;56:540–547.

51. Augood SJ, Penney JB, Jr., Friberg IK, et al. Expression of the early-onset torsion dystonia gene (DYT1) in human brain. *Ann Neurol* 1998;43:669–673.

52. Zhao Y, Xiao J, Ueda M, et al. Glial elements contribute to stress-induced torsinA expression in the CNS and peripheral nervous system. *Neuroscience* 2008;155:439–453.

53. Saper CB. An open letter to our readers on the use of antibodies. *J Comp Neurol* 2005;493:477–478.

54. Rhodes KJ, Trimmer JS. Antibodies as valuable neuroscience research tools versus reagents of mass distraction. *J Neurosci* 2006;26:8017–8020.

55. Burry RW. Controls for immunocytochemistry: An update. *J Histochem Cytochem* 2011;59:6–12.

56. Egner A, Hell SW. Aberrations in confocal and multi-photon fluorescence microscopy induced by refractive index mismatch. In: Pawley JB, editor. Handbook of biological confocal microscopy. New York: Springer; 2006. p 404–413.

57. Harata N, Iwasaki Y. Evidence for early blood-brain barrier breakdown in experimental thiamine deficiency in the mouse. *Metab Brain Dis* 1995;10:159–174.

58. Masuda T, Kawaguchi J, Oikawa H, et al. How thick are the paraffin-embedded tissue sections routinely prepared in laboratory? A morphometric study using a confocal laser scanning microscope. *Pathol Int* 1998;48:179–183.

59. Konno H, Yamamoto T, Suzuki H, et al. Targeting of adoptively transferred experimental allergic encephalitis lesion at the sites of Wallerian degeneration. *Acta Neuropathol* 1990;80:521–526.

60. Micheva KD, Smith SJ. Array tomography: A new tool for imaging the molecular architecture and ultrastructure of neural circuits. *Neuron* 2007;55:25–36.

61. Liang CC, Tanabe LM, Jou S, Chi F, Dauer WT. TorsinA hypofunction causes abnormal twisting movements and sensorimotor circuit neurodegeneration. *J Clin Invest* 2014;124:3080–3092.

62. Yokoi F, Yang G, Li J, DeAndrade MP, Zhou T, Li Y. Earlier onset of motor deficits in mice with double mutations in *Dyt1* and *Sgce*. *J Biochem* 2010; 148:459–466.

63. Gonzalez-Alegre P, Bode N, Davidson BL, Paulson HL. Silencing primary dystonia: Lentiviral-mediated RNA interference therapy for DYT1 dystonia. *J Neurosci* 2005;25:10502–10509.

64. Yokoi F, Dang MT, Mitsui S, Li J, Li Y. Motor deficits and hyperactivity in cerebral cortex-specific *Dyt1* conditional knockout mice. *J Biochem* 2008;143: 39–47.

65. Jungwirth M, Dear ML, Brown P, Holbrook K, Goodchild R. Relative tissue expression of homologous torsinB correlates with the neuronal specific importance of DYT1 dystonia-associated torsinA. *Hum Mol Genet* 2010;19:888–900.

66. Hewett JW, Kamm C, Boston H, et al. TorsinB - perinuclear location and association with torsinA. *J Neurochem* 2004;89:1186–1194.

67. Gonzalez-Alegre P, Paulson HL. Aberrant cellular behavior of mutant torsinA implicates nuclear envelope dysfunction in DYT1 dystonia. *J Neurosci* 2004;24:2593–2601.

68. O'Farrell CA, Martin KL, Hutton M, Delatycki MB, Cookson MR, Lockhart PJ. Mutant torsinA interacts with tyrosine hydroxylase in cultured cells. *Neuroscience* 2009;164:1127–1137.

69. Shashidharan P, Good PF, Hsu A, Perl DP, Brin MF, Olanow CW. TorsinA accumulation in Lewy bodies in sporadic Parkinson's disease. *Brain Res* 2000;877:379–381.

70. Siegert S, Bahn E, Kramer ML, et al. TorsinA expression is detectable in human infants as young as 4 weeks old. *Brain Res Dev Brain Res* 2005;157:19–26.

71. Puglisi F, Vanni V, Ponterio G, et al. Torsin A localization in the mouse cerebellar synaptic circuitry. *PLoS One* 2013;8:e68063.

72. Hewett J, Ziefer P, Bergeron D, et al. TorsinA in PC12 cells: Localization in the endoplasmic reticulum and response to stress. *J Neurosci Res* 2003;72:158–168.

73. Gordon KL, Glenn KA, Gonzalez-Alegre P. Exploring the influence of torsinA expression on protein quality control. *Neurochem Res* 2011;36:452–459.

74. Cao S, Hewett JW, Yokoi F, et al. Chemical enhancement of torsinA function in cell and animal models of torsion dystonia. *Dis Model Mech* 2010;3: 386–396.

75. Sciamanna G, Tassone A, Martella G, et al. Developmental profile of the aberrant dopamine D2 receptor response in striatal cholinergic interneurons in DYT1 dystonia. *PLoS One* 2011;6:e24261.

76. Armata IA, Ananthanarayanan M, Balasubramaniyan N, Shashidharan P. Regulation of *DYT1* gene expression by the Ets family of transcription factors. *J Neurochem* 2008;106:1052–1065.

77. Hettich J, Ryan SD, de Souza ON, et al. Biochemical and cellular analysis of human variants of the DYT1 dystonia protein, TorsinA/TOR1A. *Hum Mutat* 2014;35:1101–1113. doi: http://dx.doi.org/10.1002/humu.22602.

78. Bragg DC, Kaufman CA, Kock N, Breakefield XO. Inhibition of N-linked glycosylation prevents inclusion formation by the dystonia-related mutant form of torsinA. *Mol Cell Neurosci* 2004;27:417–426.

79. Kock N, Naismith TV, Boston HE, et al. Effects of genetic variations in the dystonia protein torsinA: Identification of polymorphism at residue 216 as protein modifier. *Hum Mol Genet* 2006;15:1355–1364.

80. Vander Heyden AB, Naismith TV, Snapp EL, Hodzic D, Hanson PI. LULL1 retargets TorsinA to the nuclear envelope revealing an activity that is impaired by the DYT1 dystonia mutation. *Mol Biol Cell* 2009;20:2661–2672.

81. Naismith TV, Dalal S, Hanson PI. Interaction of torsinA with its major binding partners is impaired by the dystonia-associated *Δ*GAG deletion. *J Biol Chem* 2009;284:27866–27874.

82. Vander Heyden AB, Naismith TV, Snapp EL, Hanson PI. Static retention of the lumenal monotopic membrane protein torsinA in the endoplasmic reticulum. *EMBO J* 2011;30:3217–3231.

83. Zhu L, Millen L, Mendoza JL, Thomas PJ. A unique redox-sensing sensor II motif in TorsinA plays a critical role in nucleotide and partner binding. *J Biol Chem* 2010;285:37271–37280.

84. O'Farrell C, Lockhart PJ, Lincoln S, et al. Biochemical characterization of torsinB. *Brain Res Mol Brain Res* 2004;127:1–9.

85. Torres GE, Sweeney AL, Beaulieu JM, Shashidharan P, Caron MG. Effect of torsinA on membrane proteins reveals a loss of function and a dominant-negative phenotype of the dystonia-associated ΔE-torsinA mutant. *Proc Natl Acad Sci U S A* 2004;101:15650–15655.

86. Zirn B, Grundmann K, Huppke P, et al. Novel *TOR1A* mutation p.Arg288Gln in early-onset dystonia (DYT1). *J Neurol Neurosurg Psychiatry* 2008; 79:1327–1330.

87. Kustedjo K, Deechongkit S, Kelly JW, Cravatt BF. Recombinant expression, purification, and comparative characterization of torsinA and its torsion dystonia-associated variant ΔE-torsinA. *Biochemistry* 2003;42:15333–15341.

88. Nery FC, Armata IA, Farley JE, et al. TorsinA participates in endoplasmic reticulum-associated degradation. *Nat Commun* 2011;2:393.

89. Maric M, Shao J, Ryan RJ, Wong CS, Gonzalez-Alegre P, Roller RJ. A functional role for torsinA in herpes simplex virus 1 nuclear egress. *J Virol* 2011; 85:9667–9679.

90. Jungwirth MT, Kumar D, Jeong DY, Goodchild RE. The nuclear envelope localization of DYT1 dystonia torsinA-ΔE requires the SUN1 LINC complex component. *BMC Cell Biol* 2011;12:24.

91. Goodchild RE, Dauer WT. The AAA+ protein torsinA interacts with a conserved domain present in LAP1 and a novel ER protein. *J Cell Biol* 2005; 168:855–862.

92. Calakos N, Patel VD, Gottron M, et al. Functional evidence implicating a novel *TOR1A* mutation in idiopathic, late-onset focal dystonia. *J Med Genet* 2010;47:646–650.

93. Henriksen C, Madsen LB, Bendixen C, Larsen K. Characterization of the porcine *TOR1A* gene: The first step towards generation of a pig model for dystonia. *Gene* 2009;430:105–115.

94. Josse L, Smales CM, Tuite MF. Transient expression of human TorsinA enhances secretion of two functionally distinct proteins in cultured Chinese hamster ovary (CHO) cells. *Biotechnol Bioeng* 2010;105:556–566.

95. Giles LM, Li L, Chin LS. Printor, a novel torsinA-interacting protein implicated in dystonia pathogenesis. *J Biol Chem* 2009;284:21765–21775.

96. Vulinovic F, Lohmann K, Rakovic A, et al. Unraveling cellular phenotypes of novel *TorsinA/TOR1A* mutations. *Hum Mutat* 2014;35:1114–1122. doi: http://dx.doi.org/10.1002/humu.22604.

97. Cheng FB, Feng JC, Ma LY, et al. Combined occurrence of a novel *TOR1A* and a *THAP1* mutation in primary dystonia. *Mov Disord* 2014;29:1079–1083.

98. Martin JN, Bair TB, Bode N, Dauer WT, Gonzalez-Alegre P. Transcriptional and proteomic profiling in a cellular model of DYT1 dystonia. *Neuroscience* 2009;164:563–572.

99. Kock N, Allchorne AJ, Sena-Esteves M, Woolf CJ, Breakefield XO. RNAi blocks DYT1 mutant torsinA inclusions in neurons. *Neurosci Lett* 2006; 395:201–205.

100. Shashidharan P, Sandu D, Potla U, et al. Transgenic mouse model of early-onset DYT1 dystonia. *Hum Mol Genet* 2005;14:125–133.

101. Regensburger M, Kohl Z, Grundmann K, Winner B, Riess O, Winkler J. Adult neural precursor cells unaffected in animal models of DYT1 dystonia. *Neuroreport* 2009;20:1529–1533.

102. Martella G, Tassone A, Sciamanna G, et al. Impairment of bidirectional synaptic plasticity in the striatum of a mouse model of DYT1 dystonia: Role of endogenous acetylcholine. *Brain* 2009;132:2336–2349.

103. Grundmann K, Glockle N, Martella G, et al. Generation of a novel rodent model for DYT1 dystonia. *Neurobiol Dis* 2012;47:61–74.

104. McLean PJ, Kawamata H, Shariff S, et al. TorsinA and heat shock proteins act as molecular chaperones: suppression of α-synuclein aggregation. *J Neurochem* 2002;83:846–854.

105. Kim CE, Perez A, Perkins G, Ellisman MH, Dauer WT. A molecular mechanism underlying the neural-specific defect in torsinA mutant mice. *Proc Natl Acad Sci U S A* 2010;107:9861–9866.

106. Sharma N, Hewett J, Ozelius LJ, et al. A close association of torsinA and α-synuclein in Lewy bodies: A fluorescence resonance energy transfer study. *Am J Pathol* 2001;159:339–344.

107. Walker RH, Rasmussen A, Rudnicki D, et al. Huntington's disease-like 2 can present as chorea-acanthocytosis. *Neurology* 2003;61:1002–1004.

108. Walker RH, Morgello S, Davidoff-Feldman B, et al. Autosomal dominant chorea-acanthocytosis with polyglutamine-containing neuronal inclusions. *Neurology* 2002;58:1031–1037.

109. Walker RH, Good PF, Shashidharan P. TorsinA immunoreactivity in inclusion bodies in trinucleotide repeat diseases. *Mov Disord* 2003;18:1041–1044.

110. Holton JL, Schneider SA, Ganesharajah T, et al. Neuropathology of primary adult-onset dystonia. *Neurology* 2008;70:695–699.

111. Dang MT, Yokoi F, McNaught KS, et al. Generation and characterization of Dyt1 ΔGAG knock-in mouse as a model for early-onset dystonia. *Exp Neurol* 2005;196:452–463.

112. Oberlin SR, Konakova M, Pulst S, Chesselet MF. Development and anatomic localization of torsinA. *Adv Neurol* 2004;94:61–65.

113. Yamada K, Goto S, Kaji R, Kuratsu J. Modulation of torsinA expression in the globus pallidus internus is associated with levodopa-induced dyskinesia in hemiparkinsonian rats. *Neurosci Lett* 2006;396:62–66.

Human Mutation

OFFICIAL JOURNAL
HGVS
HUMAN GENOME VARIATION SOCIETY
www.hgvs.org

■ Addressing Variant Pathogenicity: The TorsinA (*TOR1A*) Gene as a Model

Recent advances in high-throughput sequencing have brought renewed attention to the challenges of addressing pathogenicity of genetic variants (*MacArthur et al., Nature 508: 469–476, 2014*; *Kassahn et al., Hum Mutat 35: 413–423, 2014*). With an accelerating pace of variant discovery, this will be an important problem involving any gene. An in-frame deletion of a glutamic acid codon from the *TOR1A* gene (c.904_906delGAG/c.907_909delGAG; p.Glu302del/p.Glu303del, or p.ΔE) leads to DYT1 dystonia, an inherited movement disorder characterized by involuntary muscle contractions. This is the first form of dystonia for which the affected gene locus was identified and it serves as one of the leading models in studying molecular mechanisms of dystonia. Although other variants in the coding region of *TOR1A* have been reported, they are rare and their pathogenicity has not been examined in-depth, until now.

In this issue, Hettich et al. (*Hum Mutat 35:1101-1113, 2014*) and Vulinovic et al. (*Hum Mutat 35:1114-1122, 2014*) evaluate the pathogenic properties of multiple *TOR1A* variants, comparing the properties of the encoded proteins to those of wild-type and p.ΔE counterparts. Hettich et al. focus on the known variants p.R288Q and p.F205I, while Vulinovic et al. examine p.R288Q, as well as p.A14_P15del and p.E121K, which they had newly identified in dystonia patients.

These reports share two types of standard analyses in *TOR1A* studies: the assessment of subcellular distribution and dimerization potential of overexpressed variant proteins. In addition, they employ complementary approaches from a repertoire of molecular and cell biological methods currently available in the dystonia field. Hettich et al. compare the structural features of variant proteins by homology modeling and molecular dynamics simulations, and assessed the impact of the variant proteins on cellular properties, including structural integrity of nuclear envelope and endoplasmic reticulum, amount and time course of chaperone/secretory activity, and cellular shape. Vulinovic et al. test the results of *in silico* pathogenicity prediction tools, the time course of variant protein degradation, and the degradation mechanisms through autophagy-lysosome and proteasome pathways. In both studies, the properties of the variants differ from those of wild-type proteins in certain respects, consistent with their pathogenicity. Interestingly, their properties fall between those of wild-type and p.ΔE. Although how these variable changes relate to different clinical symptoms remains an open question, the knowledge gained will provide critical information about *TOR1A* function.

We now know nine naturally occurring amino acid sequence variations of *TOR1A*, including one reported recently (*Cheng et al., Mov Disord 29:1079–83, 2014*). As additional variants are found, the two studies described here—in particular, their systematic use of a wide array of approaches—will serve as excellent models for analysis of pathogenicity in general.

N. Charles Harata

University of Iowa Carver College of Medicine, Iowa City, Iowa

DOI: 10.1002/humu.22413

Video Article

Rapid Genotyping of Animals Followed by Establishing Primary Cultures of Brain Neurons

Jin-Young Koh*[1,2], Sadahiro Iwabuchi*[1], Zhengmin Huang[3], N. Charles Harata[1]

[1]Department of Molecular Physiology & Biophysics, University of Iowa Carver College of Medicine

[2]Department of Psychiatry, University of Iowa Carver College of Medicine

[3]EZ BioResearch LLC

*These authors contributed equally

Correspondence to: N. Charles Harata at charles-harata@uiowa.edu

URL: http://www.jove.com/video/51879
DOI: doi:10.3791/51879

Keywords: Neuroscience, Issue 95, AP2, genotyping, glial feeder layer, mouse tail, neuronal culture, nucleic-acid extraction, PCR, tattoo, torsinA

Date Published: 1/29/2015

Citation: Koh, J.Y., Iwabuchi, S., Huang, Z., Harata, N.C. Rapid Genotyping of Animals Followed by Establishing Primary Cultures of Brain Neurons. *J. Vis. Exp.* (95), e51879, doi:10.3791/51879 (2015).

Abstract

High-resolution analysis of the morphology and function of mammalian neurons often requires the genotyping of individual animals followed by the analysis of primary cultures of neurons. We describe a set of procedures for: labeling newborn mice to be genotyped, rapid genotyping, and establishing low-density cultures of brain neurons from these mice. Individual mice are labeled by tattooing, which allows for long-term identification lasting into adulthood. Genotyping by the described protocol is fast and efficient, and allows for automated extraction of nucleic acid with good reliability. This is useful under circumstances where sufficient time for conventional genotyping is not available, *e.g.,* in mice that suffer from neonatal lethality. Primary neuronal cultures are generated at low density, which enables imaging experiments at high spatial resolution. This culture method requires the preparation of glial feeder layers prior to neuronal plating. The protocol is applied in its entirety to a mouse model of the movement disorder DYT1 dystonia (ΔE-torsinA knock-in mice), and neuronal cultures are prepared from the hippocampus, cerebral cortex and striatum of these mice. This protocol can be applied to mice with other genetic mutations, as well as to animals of other species. Furthermore, individual components of the protocol can be used for isolated sub-projects. Thus this protocol will have wide applications, not only in neuroscience but also in other fields of biological and medical sciences.

Video Link

The video component of this article can be found at http://www.jove.com/video/51879/

Introduction

Rodent models of genetic diseases have proven useful in establishing the physiological functions of normal proteins and nucleic acids, as well as the pathophysiological consequences of defects in these. Examples include mice deficient for proteins involved in key cellular functions, as well as mouse models of disorders such as Alzheimer's disease. However, certain genetic manipulations can lead to neonatal lethality shortly or a few days after birth. In these cases, primary cell cultures are an important tool because live cells can be obtained from the embryonic or neonatal pups before death, they can be maintained for at least a few weeks *in vitro*, and during this time early neuronal development can be followed by biochemical, functional and morphological experiments. For the primary cultures, it can be beneficial to plate the neurons at low density; this makes it possible to visualize the individual somata, dendrites, axonal shafts and nerve terminals at high spatial resolution. However, the survival and differentiation of neurons at low density typically requires that they are plated on a glial feeder layer, co-cultured with glial cells in the absence of physical contact with them, or cultured in medium conditioned by glia [1].

The establishment of low-density neuronal cultures on glial feeder layers can be dependent on fast and reliable genotyping beforehand – within a few hr in contrast to a few days. Speed is especially important when the neuronal genotype needs to be matched to that of a glial feeder layer prepared beforehand. As a more practical example, it may be necessary to decide which pups of which genotype to use in generating cultures, to optimize the efficiency of an experiment.

Here we demonstrate the working protocol that has been used for fast, simplified and reliable mouse genotyping in previous publications [2-6]. Mouse tails and a commercially available kit are used. This protocol includes single-step extraction of nucleic acids from the tissue, and requires neither a nucleic-acid purification step nor use of a termination buffer ('stop solution'). The reliability of this genotyping method is illustrated by presenting the results of a series of tests when differences are introduced with respect to the starting amount of the specimens, the age of the animals and the length of the PCR amplicons. This kit offers the advantages of automated extraction and reliability.

For the sake of being comprehensive, the use of tattooing for long-term identification of the genotyped mice is also demonstrated. Tattooing is achieved by applying tattooing ink to the dermis of the skin (under the epidermis) [7]. A procedure is described for tattooing the paw pads of newborn or 1 day old mice, although tattoos can be applied to other parts of the body, such as tails and toes, and to animals of all ages. In

addition, procedures will be demonstrated for plating and culturing mouse neurons at a low density, based on optimized preparation of different types of glial feeder layers [2,8].

We use a genetic mouse model of the inherited neurological disorder DYT1 dystonia – an autosomal-dominant movement disorder caused by a mutation in the gene *TOR1A* (c.904_906delGAG/c.907_909delGAG; p.Glu302del/p.Glu303del) [9]. The encoded protein, torsinA, belongs to the "ATPases associated with diverse cellular activities" (AAA+) family of proteins, whose members generally perform chaperone-like functions, assisting in: protein unfolding, protein-complex disassembly, membrane trafficking, and vesicle fusion [10-13]. The mutation results in an in-frame deletion of a codon for glutamic acid, and can lead to manifestation of 'early-onset generalized isolated dystonia' [14,15]. However, the pathophysiological mechanisms responsible for this disorder remain poorly understood. In a knock-in mouse model, the mutant allele is *Tor1a*^{tm2Wtd}, mentioned hereafter as *Tor1a*$^{\Delta E}$. Heterozygous ΔE-torsinA knock-in mice are viable and genetically mimic human patients with DYT1 dystonia, whereas homozygous knock-in mice die after birth [16,17], with the latency to postnatal death affected by genetic background [18]. The early death of homozygous knock-in mice necessitates that both the genotyping of animals and the establishment of neuronal cultures are completed rapidly. As another example of genotyping, *Tfap2a* (transcription factor AP-2α, activating enhancer binding protein 2α) will be used. The protein encoded by this gene is important in regulating multiple cellular processes, such as proliferation, differentiation, survival and apoptosis [19].

Protocol

NOTE: All animal procedures performed in this study were approved by the Institutional Animal Care and Use Committee of the University of Iowa.

1. Long-term Identification of Mice Using Tattooing the Paw Pads

1. Immobilize a paw with the paw pad (plantar surface) facing the experimenter. Hold the paw with the thumb and the index finger. Be careful not to pinch the paw.
   NOTE: Stable immobilization is important to ensure that the tattoo pigment is placed into the dermis of the paw pad, and thus is permanent [7].
2. Swab the paw pad with 70% ethanol on a gauze sponge or swab.
3. Apply skin oil to a cotton-tipped applicator, and gently press the tip against the surface of the paw pad several times. Use only a small amount of skin oil; when present in large amounts, it will prevent the tattoo pigment from reaching the skin.
4. Dip the tips of the tattoo needles into the tattooing ink just prior to tattooing. Use clean, aseptic and sharp tattooing needles, to decrease the pain and the possibility of infection, and also to increase the tattooing efficiency.
5. While the paw pad surface is covered with the skin oil, press the tattoo needle tips vertically and lightly against the skin in the center of the paw pad, and inject the ink multiple times. See Table of Materials/Equipment for information about electric tattooing system.
6. Spray 70% ethanol on a gauze sponge, gently press it against the paw to remove extra tattoo pigment on the skin surface, and inspect the quality of tattoo. Check that the middle of paw pad has a dark, round spot that differs from normal skin pigmentation. If the tattoo is not dark or large enough for easy viewing, repeat the prior tattooing steps.

2. Genotyping Newborn Mice Using a Fast PCR Genotyping Kit

1. Disinfect the distal end of a mouse tail with 70% ethanol, cut 5 mm or less of the tail tip and transfer it to a tube of an 8-tube strip of the type used for PCR. Use an un-used razor blade for each pup to avoid cross contamination between specimens. Alternatively, use a pair of scissors, but in this case, carefully and thoroughly remove the remaining tissue on the blades using 70% ethanol. Check for bleeding. If bleeding occurs, apply pressure to the cut portion of the tail with a gauze sponge until bleeding has stopped.
2. Add 200 µl of DNA Extraction Solution to each PCR tube containing a specimen. See Table of Materials/Equipment for its composition and information about the kit.
3. Place the tube strip into a PCR thermal cycler, and start the DNA extraction using the following program: 1 cycle at 55 °C for 10 min, 1 cycle at 95 °C for 10 min, and holding at 4 °C.
   NOTE: This is the same PCR thermal cycler that is later used for PCR.
4. After the DNA extraction is finished, remove the tube strip from the thermal cycler and invert 5 times.
5. Transfer 4 µl of the solution (DNA extract) of each specimen to an un-used tube of an 8-tube strip, and mix with: 10 µl of 2X PCR Ready Mix II, 2 µl of mixed forward & reverse primers (recommended at 0.5 µM; see **Table of Materials/Equipment** for sequences), and 4 µl of nuclease-free H_2O, for each specimen. Spin briefly (*e.g.,* 3 sec) using a table-top centrifuge. Keep the tubes on ice at all times except when handling.
6. Perform thermal cycling. See Table of Materials/Equipment for the thermal program.
7. Detect the amplified DNA products. Load the total reaction solution from the PCR (20 µl) directly into a well of an agarose gel. Load the molecular weight markers into a separate well. Apply an electric field.
8. Acquire fluorescence images of the bands under ultraviolet light.

3. Primary Culture of Mouse Brain Neurons on Glial Feeder Layer

NOTE: The procedures for brain dissection and cell dissociation (3.1) are common to all the subsequent procedures. The procedures for mouse glial cultures (3.2), rat glial cultures (3.3), and mouse neuronal cultures (3.4) are described separately afterwards.

1. Brain Dissection and Cellular Dissocaiation
   1. Sacrifice one mouse or rat pup by decapitation, rapidly remove the brain, and place it into Hanks' solution (see **Table 1** for composition) + 20% fetal bovine serum (FBS) in a 35 mm dish (kept on ice).

2. Cut the brain through the midline into two hemispheres. Remove the region of interest(*e.g.,* cerebral cortex, striatum and hippocampus) from each hemisphere of the brain. Remove the meninges and major blood vessels from the surface. Cut the brain region into 4-10 thin slices using a surgical blade.
3. Rinse the brain slices in a 15 ml centrifugation tube, once with Hanks' solution + 20% FBS, then 3 times with the Hanks' solution (*i.e.*, without serum) (all at 4 °C). To rinse, add 5-10 ml solution, let the brain slices settle at the bottom of the tube, aspirate the solution from the top, and add a fresh solution. Finish the rinsing procedure by aspirating the solution.
4. Filter 2 ml of the trypsin-containing digestion solution (see **Table 1** for composition) using a 3 ml syringe and a 0.2 µm syringe filter, and add the filtrate directly into the tube containing the brain slices. Let the trypsinization proceed for 13 min at RT.
5. Neutralize the trypsin solution first by aspirating most of it and then by adding 7-10 ml of Hanks' solution + 20% FBS (4 °C).
6. Rinse the brain slices, twice with Hanks' solution + 20% FBS, and then three times with the Hanks' solution (*i.e.* without serum) (all at 4 °C). Finish the rinsing procedure by aspirating the solution.
7. Filter 2 ml of the dissociation solution (see **Table 1** for composition) using a 3 ml syringe and a 0.2 µm syringe filter, and add the filtrate directly to the tube with the brain slices.
8. Mechanically dissociate the cells by gently triturating 10-20 times, until visible tissue pieces disappear. Use a cotton-plugged, fire-polished Pasteur pipette and avoid making bubbles during trituration.
9. Wait 3 min for small pieces to settle down.
10. Transfer the majority of the solution (~1.5 ml, leaving some solution at the bottom) to a 15 ml centrifugation tube that contains 3 ml Hanks' solution + 20% FBS solution (4 °C), using the cotton-plugged, fire-polished Pasteur pipette. Do not transfer all the solution because the inclusion of any sediment at the bottom typically results in deterioration of the culture.
11. Centrifuge for 13 min at ~185 g (~1,100 rpm) at 4 °C.
12. Aspirate the supernatant gently, add 1 ml of pre-warmed plating medium (37 °C) to the pellet, and resuspend it by gently pipetting several times using the cotton-plugged, fire-polished Pasteur pipette.
    NOTE: Three different types of plating media are used for different culture purposes: plating medium-1 for mouse glial cells, plating medium-2 for mouse neurons, and plating medium-3 for rat neurons and glial cells (see **Table 1** for compositions).
13. Take out 10 µl of the cell suspension, mix it with 10 µl of 0.4% trypan blue solution, and measure the density of live cells, using either a hemocytometer or an automated cell counter.

2. Mouse Glial Cultures
    1. Wash the coverslips to help establish healthy cultures of mouse cells.
        1. Immerse glass coverslips (round, 12 mm diameter) in 70% nitric acid in a glass Petri dish. Protect from light using aluminum foil, and place it on an orbital shaker O/N.
        2. Rinse the glass coverslips in the Petri dish at least three times with distilled water. Immerse them in distilled water. Place the dish on an orbital shaker O/N.
        3. Dry the coverslips on a Whatman 150 mm filter paper in the biological safety cabinet.
        4. Autoclave the coverslips.
        5. Place the coverslips into 24-well culture dish.

    2. Label and genotype newborn mice according to steps 1 and 2.
    3. Obtain the brain cells from the mouse pups, according to step 3.1.
        NOTE: Use of the cerebral cortex is typical for preparing the mouse glial feeder layer. However, other brain regions, such as hippocampus and striatum, will work after proper adjustment of cell density due to different numbers and yields of cells from different regions.
    4. Add ~4 ml of pre-warmed plating medium-1 to the final cell suspension (~1 ml). For pre-warming culture media, place the solution in the culture incubator (5% CO_2-95% O_2, 37 °C) O/N, to allow the temperature and pH values to stabilize.
    5. Transfer the cell suspension to an uncoated T25 culture flask, using the cotton-plugged, fire-polished Pasteur pipette. Place the flask in the culture incubator.
    6. At 1 day *in vitro* (DIV), rinse the cultured cells in the T25 flask twice with plating medium-1 (4 °C). Place the flask back into the incubator. Perform rinsing by aspirating the medium inside the flask completely with a Pasteur pipette, adding ~5 ml of fresh medium and gently tilting the flask several times in a swirling motion.
    7. At 6-9 DIV, (*i.e.,* one day before trypsinization and plating on coverslips, in steps 3.2.8-3.2.13), place 100 µl of the coating material with extracellular matrix proteins (see Table of Materials/Equipment for comments about the coating material) on the glass coverslips in a culture dish, and place the culture dish in the culture incubator.
    8. At 7-10 DIV, when the cells are 20-40% confluent (spatially continuous), trypsinize them.
        1. Rinse the flask once, by aspirating all the solution within the flask and adding ~13 ml of Hanks' solution (4 °C), gently tilt the flask several times in a swirling motion, and aspirate the solution completely.
        2. Add 40 µl of DNase solution (final concentration, 750 units/ml) to 4 ml Trypsin-EDTA solution, pass the solution through a 0.2 µm syringe filter, and add the filtrate directly to the cells in the flask.
        3. Let the trypsinization proceed for 13 min at 37 °C in the incubator.
        4. Neutralize the trypsin solution by adding 2 ml of 100% FBS (4 °C) to the flask.
        5. Transfer the trypsinized cells to a 15 ml centrifugation tube using a 5- to 10-ml pipette, add ~4 ml of Hanks' solution + 20% FBS (4 °C), centrifuge at ~185 g and 4 °C for 13 min, and aspirate the supernatant.

    9. Resuspend the pellet in 1 ml of pre-warmed plating medium-1.
    10. Measure the density of the cells according to step 3.1.13.
    11. Aspirate the coating material completely from the glass coverslips, and plate ~50 µl of the resuspended glial cells on coverslips.
        NOTE: These cells will establish the glial feeder layer.
    12. Place the culture dish with coverslips in the incubator.
    13. 20-60 min later, add 1 ml of pre-warmed plating medium-1 to each well, and place the dish back in the incubator. Note: While the plating medium is added, it will be helpful to use another pipette to press down the periphery of the coverslip (where there are no plated cells), so that the coverslip will not float in the medium.

14. At 1 DIV of the glial feeder layer (*i.e.,* on the glass coverslip), replace the medium with 1 ml of pre-warmed plating medium-1, by aspirating all of the solution in a well and then filling it with fresh medium.
15. At 2-3 DIV of the glial feeder layer when the cells are 80-100% confluent, add mitotic inhibitor (10 µl of a mixture of 5-fluoro-2'-deoxyuridine + uridine; final concentrations of 81.2 and 204.8 µM, respectively) to each well, to inhibit DNA replication and therefore to suppress glial-cell proliferation.
16. At 7-9 DIV, when the cells are 90-100% confluent (1-2 hr before plating neurons on the glial feeder layer), replace the culture medium with pre-warmed plating medium-2 (37 °C).
    NOTE: Neurons will be plated on the same day, using step 3.4.

3. Rat Glial Cultures
    1. Coat a T25 culture flask with the same coating material.
       NOTE: This is necessary for later removal of non-adherent cells in step 3.3.5.
        1. Add 2.0 ml of the coating material to the flask, and place the flask in the culture incubator.
        2. After 2-3 hr, aspirate the coating material completely, such that the floor of the flask becomes dry.
    2. Obtain the cells from the rat pups, according to step 3.1.
       NOTE: The CA3-CA1 region of the hippocampus is used for preparing the rat glial feeder layer. However, other brain regions, such as the cerebral cortex and striatum, will work after adjusting for differences in cell density due to different numbers and yields of cells from different regions.
    3. Add ~4 ml of pre-warmed plating medium-3 to the final cell suspension (~1 ml).
    4. Transfer the cell suspension into the coated T25 culture flask, using the cotton-plugged, fire-polished Pasteur pipette. Place the flask in the culture incubator (5% CO_2-95% O_2, 37°C).
    5. At 2-3 DIV, when cells are 20-40% confluent, remove non-adherent or weakly adherent cells, by closing the lid tightly, shaking the flask vigorously ~10 times, aspirating the solution, and adding 4-5 ml of plating medium-3 (at 4 °C). Repeat this procedure once. Examine the cultured cells across the entire flask floor (*e.g.,* using phase-contrast microscope) to confirm that those that appear neuronal (*i.e.*, those for which the outer rim of the cell body appears phase-bright) are completely removed. Repeat the procedure as often as necessary to remove these cells, and then return the flask to the incubator.
       NOTE: The strength and the total number of 'shakes' required may differ among individual experimenters. The important thing is not to keep the total number of shakes to a set number, but to confirm that neuron-like cells are eliminated.
    6. At 6-8 DIV, when cells are 90-100% confluent, passage the glial cells by trypsinizing them as in step 3.2.8.
    7. After centrifugation, resuspend the pellet in 1 ml of plating medium-3 (4 °C), add 10 ml of plating medium-3 (4 °C), transfer the trypsinized cells to an un-coated T75 flask, and culture them in the incubator.
       NOTE: Rat glial cells will be passaged twice; in contrast the mouse glial cells are passaged only once because they become unhealthy after multiple passages. Rat glial cells will be passaged in T75 flasks that are not coated with any coating material. The coating allows rat glial cells to grow too quickly and yield many ciliated cells (putative ependymal cells), which will deteriorate the neuronal culture condition later.
    8. At 17-19 DIV of glial culture in a flask (*i.e.,* 11 days after passaging and one day before trypsinization and plating onto coverslips by steps 3.3.9-3.3.14), place 100 µl of the coating material on unwashed glass coverslips (round, 12 mm diameter) in a culture dish, and place the culture dish in the culture incubator.
       NOTE: For rat glial cultures, a difference was not noticed in the culture results with or without washing the coverslips.
    9. At 18-20 DIV of glial culture in a flask (*i.e.,* 12 days after passaging), prepare the glial feeder layer by trypsinizing the cultured cells, according to step 3.2.8.
    10. During centrifugation, aspirate the coating material completely from the glass coverslips.
    11. After centrifugation, resuspend the pellet in 1 ml of plating medium-3 (4 °C), and measure the cell density, according to step 3.1.13.
    12. Adjust the glial density to 10^4 live cells/ml, and plate 100 µl of the glial cell suspension on the coated glass coverslips.
        NOTE: These cells will establish the glial feeder layer.
    13. Place the culture dish with coverslips into the incubator for 20-60 min.
    14. Add 1 ml of plating medium-3 (4 °C) to each well, and place the dish back in the incubator.
    15. At 3-4 DIV of the glial feeder layer, when the cells on the coverslip are 40-80% confluent, add 1 ml of the pre-warmed growth medium (see **Table 1** for composition) that contains cytosine β-D-arabinofuranoside (AraC, final concentration of 4 µM) to stop glial-cell proliferation. Plate neurons at 7-9 DIV of the glial feeder layer when the cells are 60-80% confluent, using step 3.4.

4. Mouse Neuronal Cultures
    1. Label and genotype newborn mice according to steps 1 and 2.
    2. Use the mouse pups for step 3.1.
    3. Adjust the density of live-cell suspension to ~2.0 x 10^5 cells/ml using pre-warmed plating medium-2 for plating on mouse glial cells, or using plating medium-3 for plating on rat glial cells.
    4. Plate the cells on the glial feeder layer, by gently adding the cell suspension to the culture medium of each well. Note: The volume of the cell suspension to be added will be determined by the target number of cells in a culture well. For example, plate ~60 µl of cell suspension to achieve 12,000 cells/well.
    5. Note that no solution changes are necessary after the neurons are plated. Be careful to avoid evaporation of the solution from the wells over the course of culture, by humidifying the inside of the culture incubator.

Representative Results

As an example of the application of this protocol, representative results are shown for labeling mice by tattooing, reliable genotyping under various experimental conditions, and establishing primary neuronal cultures on glial feeder layers.

Tattooing

Newborn pups were labeled on the paw pads using a tattooing system ('Newborn' in **Figure 1**). The labels remained clearly visible at 3 weeks ('3-week-old') and 32 weeks of age ('32-week-old'). The individual mice can be uniquely identified by a combination of tattoos on the four paws (numbers 1-16) and by the information about the animal cage, or more complex numbering schemes (not shown).

Genotyping

One representative example of genotyping is shown (**Figure 2**). The *Tor1a* gene of wild-type (*Tor1a*$^{+/+}$), heterozygous (*Tor1a*$^{+/\Delta E}$) and homozygous (*Tor1a*$^{\Delta E/\Delta E}$) ΔE-torsinA knock-in mice was amplified from the genomic DNA isolated from tail clips of newborn pups. Genotyping in this specific example is based on the presence of a single 34-base-pair loxP site in the mutant *Tor1a* allele after successful Cre recombination and deletion of a neomycin resistance cassette [16,18].

Genomic DNA was extracted with minimal hands-on time, and many samples were processed simultaneously. The extraction volumes were kept constant, and therefore no adjustment of the volume was necessary to accommodate the changes in conditions tested. The reliability of genotyping was tested under four conditions, as detailed below.

First, the effect of differences in the amount of starting tissue was examined (**Figure 3**). Tails of different lengths were prepared from the heterozygous ΔE-torsinA knock-in mice (*Tor1a*$^{+/\Delta E}$) at weaning age (~3 weeks). Tail lengths of 2 to 5 mm, the range typically recommended in genotyping protocols, gave the same genotyping result of high quality. The two bands correspond to the wild-type and mutated alleles (*Tor1a*$^{+}$ and *Tor1a*$^{\Delta E}$, respectively).

Second, the effects of variability in animal age were examined (**Figure 4**). Tails were obtained from newborn, 3-week-old and ~24-week-old heterozygous ΔE-torsinA knock-in mice (*Tor1a*$^{+/\Delta E}$). Homozygotes were not used because they die several days after birth [16-18]. The two expected bands for wild-type and mutated *Tor1a* genes were visible regardless of animal age (**Figure 4A**). The general applicability of this result was tested using a second gene, *Tfap2a*[19] in wild-type mice (*Tfap2a*$^{+/+}$) (**Figure 4B**).

Third, the effects of differences in length of the PCR amplicons were tested (**Figure 5**). For this purpose, different primer pairs were synthesized for a given gene, such that the amplified DNAs are of different base pair lengths. The *Tfap2a* gene was consistently detected with different amplicon lengths.

Fourth, two DNA extraction methods were compared (**Figure 6**). In one method, PCR strip tubes and the PCR thermal cycler were used (described in step 2). This is an automated, parallel multi-tube extraction method ('Auto' in **Figure 6**). Because multiple tubes can be handled simultaneously in strip format, and a PCR machine is used with a program to operate in four temperature steps, there is no need to transfer the tubes, manually change the temperature during the extraction or use multiple pieces of equipment. Thus it is easy to process many specimens. This was compared with the second method based on manual, single-tube extraction ('Manual' in **Figure 6**). This uses individual PCR tubes and separate non-PCR machines (heat blocks and water baths) to control temperature during DNA extraction. In this case, multiple, single tubes were moved to a new temperature after each step, requiring multiple temperature-controlling apparatuses. In both cases, the *Tor1a* gene was analyzed in wild-type, heterozygous and homozygous ΔE-torsinA knock-in mice (**Figure 6A**), and the *Tfap2a* gene was analyzed in wild-type mice (**Figure 6B**). The two extraction protocols yielded equivalent genotyping results.

In summary, the results presented in **Figures 3** to **6** demonstrate that the genotyping method is robust, achieving reliable and reproducible results in spite of variations in tissue amount, animal age, amplicon length, and the extraction protocol used.

Neuronal cultures

For culturing mouse neurons on the mouse glial feeder layer, the order of the procedures is: (tattooing newborn mice → genotyping for glial culture →) glial culture → tattooing newborn mice → genotyping for neuronal culture → neuronal culture. For cultures established on the rat glial feeder layer, the procedures in parentheses are skipped.

We examined the supportive effect of the pre-seeded glial feeder layer on neuronal survival and growth. Neurons were obtained from the CA3-CA1 region of hippocampus, the motor region of cerebral cortex, and the striatum of newborn wild-type mice. They were plated at low density on rat glial feeder layer that had been obtained from the CA3-CA1 region of hippocampus and seeded prior to neuronal plating, according to the scheme illustrated in **Figure 7** (simplified summary of the procedures). Low-density cultures are optimal for the imaging of individual dendrites, somata [4,6], nerve terminals [2,3,5,8] and axonal shafts [5] at high spatial resolution. The hippocampal cells (containing both neurons and glial cells) were plated on coated glass coverslips, either with (**Figure 8A**) or without a pre-established glial feeder layer (**Figure 8B**, **C**) and observed with phase-contrast optics. In the presence of a nearly confluent glial feeder layer, the neurons (in each panel, an arrowhead indicates one representative neuron) were relatively dispersed 3 and 7 days after plating (days *in vitro*, DIV) (**Figure 8A**). They also showed signs of good health, such as a clear margin of neuronal somata, extended dendrites, a lack of clustered somata, and a lack of bundled neurites (high-magnification images in insets). At 14 DIV, these neurons formed a dense network characterized by long neurites (dendrites and axons). Note that glial proliferation was inhibited before neurons were plated, by adding growth medium containing the mitotic inhibitor AraC (step 3.3.15).

In contrast, in the absence of the glial feeder layer at the time of plating hippocampal neurons, the growth of the cultured hippocampal neurons was impaired, even in the absence of AraC. At 3 DIV, glial cells (included in the newly plated hippocampal cells) have not formed a confluent sheet (asterisk in top panel of **Figure 8B**). The cultures showed several signs that are not appropriate for high-resolution imaging studies, such as wide areas without underlying glial cells (asterisk), the presence of clustered somata and the presence of bundled neurites in some areas (data not shown). By 7 DIV, glial cells formed a confluent sheet (middle panel of **Figure 8C**). However, neurons were fewer in number than when the neurons were plated on a pre-established glial feeder layer. The surviving neurons also lacked long, network-forming neurites (inset). The glial cells were more heterogeneous in curvature and thickness than those in the feeder layer culture, thus appearing phase-bright. In order to test the effects of suppressing glial proliferation on neurons, we applied AraC-containing growth medium. When AraC was added on 3 or 7 DIV and the cells were cultured until 14 DIV and observed on this day (**Figure 8B** and **C**, bottom panels), the glial cells covered most of the coverslip surface. However, the neurons were still few in number, especially when AraC was applied at 7 DIV. The surviving neurons had only

short processes and were not extensively connected. Thus, the late addition of AraC allowed a uniform glial layer to form but did not promote neuronal viability or neurite extension; rather the uncontrolled glial growth had deleterious effects on neurons.

These data show that the glial feeder layer is critical for the survival and growth of neurons plated at low density, and that the glial layer must be present at the time of neuronal plating rather than later during neuronal culture. Similar results were obtained using cultures of cerebral cortical (**Figure 9**) and striatal neurons (**Figure 10**).

The qualitative observation about neuronal survival was confirmed by quantitative analysis. Specifically, the number of surviving neurons at 14 DIV was counted, based on phase-contrast images of the cultures (**Figure 11**). The number was greatest for neurons cultured on a glial feeder layer (*i.e.*, plated on the glial feeder layer). The number was lower in the case of neurons cultured in the absence of a glial feeder layer. The number was reduced even further when the cells were treated with AraC at a later time. These differences were statistically significant, and were noted in cultures of neurons obtained from all three brain regions.

The types of surviving cells were identified at 14 DIV in the mouse hippocampal cultures plated on the rat hippocampal feeder layer. Double-immunocytochemistry was performed using antibodies against the neuronal marker, microtubule-associated protein 2 (MAP2), and the astrocytic glial cell marker, glial fibrillary acidic protein (GFAP). The cells with extended processes were positive for MAP2, whereas the cells in the underlying glial feeder layer were positive for GFAP (two representative image fields, **Figure 12A**). This staining was not an artifact of a specific combination of primary and secondary antibodies, because the same pattern was obtained when a different set of secondary antibodies was used (**Figure 12B**).

In contrast, when the same staining was performed on the cultures consisting of only a glial feeder layer, *i.e.,* in the absence of added mouse cells (two representative image fields, **Figure 13A**), no cells were positive for MAP2. The cells of the feeder layer were consistently positive for GFAP. For a negative control, both primary antibodies were omitted from the immunocytochemical procedure (**Figure 13B**). No staining was detected in these samples, although cells were present, as evident from the transmitted light optics (differential interference contrast, DIC) and nuclear staining with Hoechst dye. Thus, non-specific staining in the MAP2 and GFAP channels was very weak.

These immunocytochemical data were also analyzed quantitatively (**Figure 14**). In each 8-bit image, intensity was measured and plotted along a line. Overlaid plots reveal MAP2 staining when mouse cells (samples containing neurons) were cultured on a glial feeder layer (Neuron +, glia +, primary antibody (1° Ab) +), whereas such staining was absent in cultures of glial feeder cells alone (Neuron −, glia +, 1° Ab +). In a negative control without primary antibodies, staining was negligible in cultures of glial feeder cells alone (Neuron −, glia +, 1° Ab −). GFAP staining was apparent in the glial feeder layer, regardless of whether mouse cells were plated (Neuron +, glia +, 1° Ab +) or not (Neuron −, glia +, 1° Ab +). Again, staining in the negative control was negligible (Neuron −, glia +, 1° Ab −). These results show that the rat glial feeder layer was composed mostly of astrocytes, and that the neurons were present only when mouse cells were added. They also indicate that the neurons present in these cultures originated solely from mouse.

The Results Section of the online video also shows the DIC and MAP2 images of cultured neurons plated on a glial feeder layer, both prepared from the CA3-CA1 hippocampal region of wild-type mice.

For detailed control of cell culture, it is recommended to measure the density of live cells, both for assessing the general quality of the brain dissection and cellular dissociation steps, and for plating the cells at the pre-determined density. Listed below are four sets of typical density measurements. Note, however, that these numbers can vary depending on culture conditions and reagents. For example, even different lots of serum from the same vendor can affect the results. Thus, these numbers should be considered a general indicator, rather than an absolute guideline.

For cellular dissociation (step 3.1.13), typical values for the live-cell density obtained from one pup are: ~2 x 10^5 cells/ml (mouse motor cortex and mouse CA3-CA1 hippocampus), ~5 x 10^5 cells/ml (mouse cerebral cortex and rat CA3-CA1 hippocampus), and ~1 x 10^6 cells/ml (mouse striatum). In all these cases, the fractions of live cells were >90% (viability, defined as the ratio of the number of live cells to that of the total number of cells). The motor cortex is loosely defined as the region of the cerebral cortex that lies immediately dorsal to the striatum [20]. For hippocampal cultures, the CA3 and CA1 regions of the hippocampus proper are preferred. The whole hippocampus additionally includes the dentate gyrus, the inclusion of which leads to formation of large nerve terminals of granule cells and introduces heterogeneity in synaptic properties [21]. The striatal culture includes the caudate-putamen and globus pallidus, but does not include the nucleus accumbens, or medial or lateral septal nuclei in the nearby structures.

For mouse glial culture (step 3.2.11), the plating density is ~10,000 glial cells on each 12-mm round coverslip, using ~50 µl of cell suspension at a density of ~2 x 10^5 cells/ml. Usually the density measured in the supernatant is relatively constant and does not require adjustment. To convert the density over different areas, the useful information is that the coverslip has a diameter of 1.20 cm and an area of 1.13 cm^2. Thus, ~10,000 cells / coverslip = ~8,800 cells / cm^2 on a coverslip.

For rat glial culture (step 3.3.12), the plating density is ~1,000 glial cells on each 12-mm round coverslip, using ~100 µl of cell suspension at a density of ~1x10^4 cells/ml. Thus, 1,000 cells/coverslip = ~900 cells/cm^2 on a coverslip.

For low-density mouse neuronal culture (step 3.4.4), the plating density ranges between 2,000 and 48,000 cells per well of a 24-well plate. Typical values when plating neurons on rat glial cells are: 10,000-24,000 cells/well for cerebral cortical neurons, 12,000-24,000 cells/well for CA3-CA1 hippocampal neurons and 24,000-48,000 cells/well for striatal neurons. When plating on mouse glial cells, the number is reduced, *e.g.*, 2,000 cells/well for CA3-CA1 hippocampal neurons. As a side note, for plating rat CA3-CA1 hippocampal neurons on a rat glial feeder layer, the plating density is 1,000-6,000 cells/well. For converting the density in a well to the density on a coverslip, the useful information is that the internal well diameter at the bottom is 1.56 cm and its area is 1.91 cm^2. Thus, for example, 12,000 cells/well = 7,100 cells / coverslip = 6,300 cells/cm^2 on a coverslip. These densities were chosen with the aim of culturing relatively sparse neurons for high-resolution cellular imaging. Researchers should choose their numbers that best suit their experimental aims.

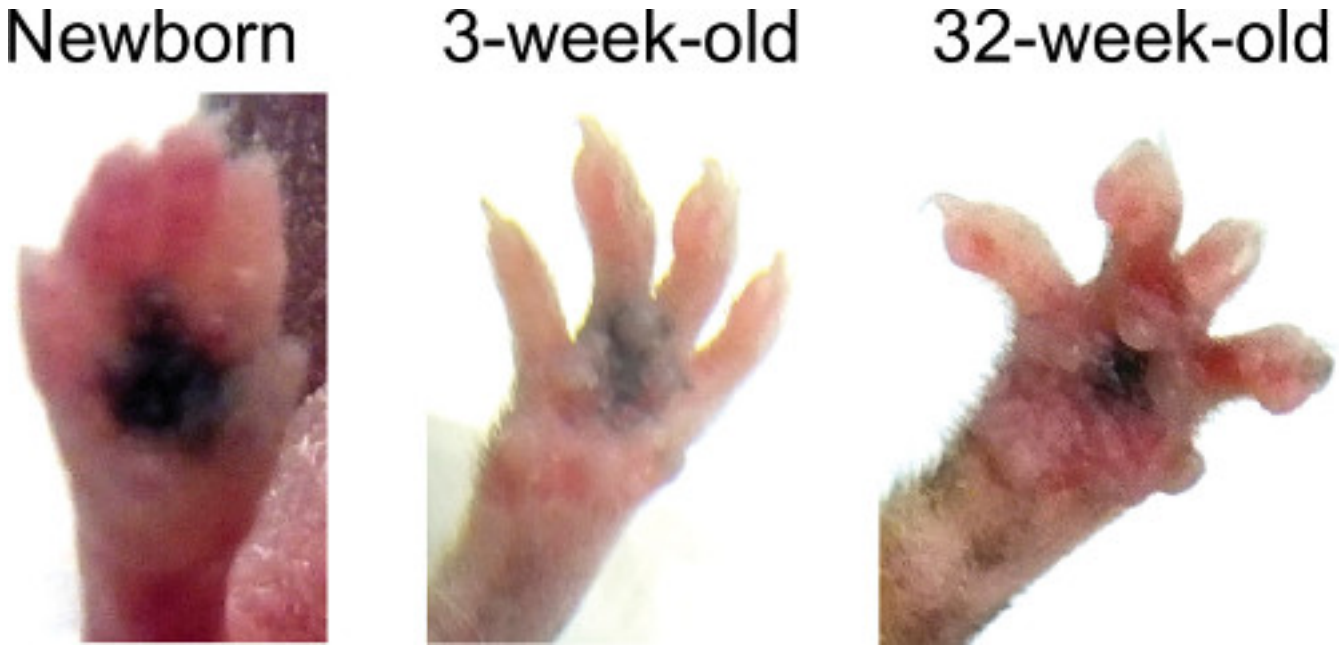

Figure 1. Tattooed paw pads of mice. Newborn mice were labeled by tattooing the paw pads. They were photographed immediately after tattooing (newborn), at 3 weeks of age (3-week-old) and at 32 weeks of age (32-week-old). The labels remained easily visible throughout adulthood. Images were taken from different animals. They are not shown at the same scale. Please click here to view a larger version of this figure.

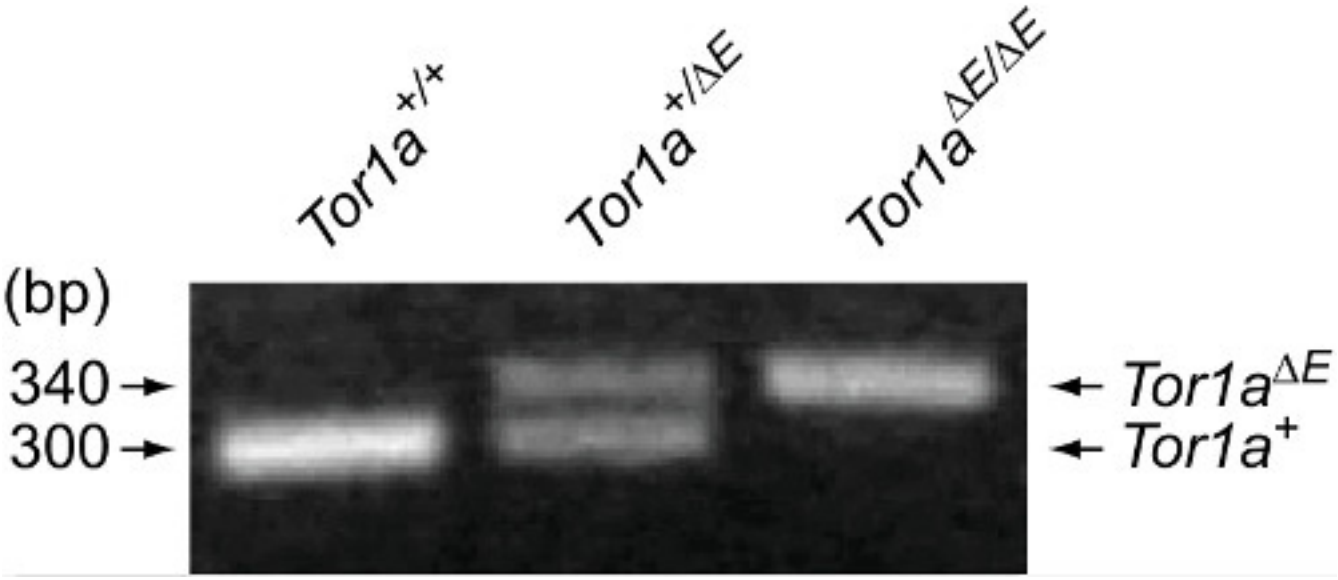

Figure 2. Genotyping of wild-type (*Tor1a*$^{+/+}$), heterozygous (*Tor1a*$^{+/\Delta E}$) and homozygous (*Tor1a*$^{\Delta E/\Delta E}$) ΔE-torsinA knock-in mice. The *Tor1a* gene alleles were analyzed in wild-type and mutant forms, using DNA extracted from the tails of newborn pups. Tail tips were ~4 mm in length. DNA was stained using SYBR Safe DNA Gel Stain. See the Table of Materials/Equipment for the information about the primers and thermal cycling program for *Tor1a* gene. Please click here to view a larger version of this figure.

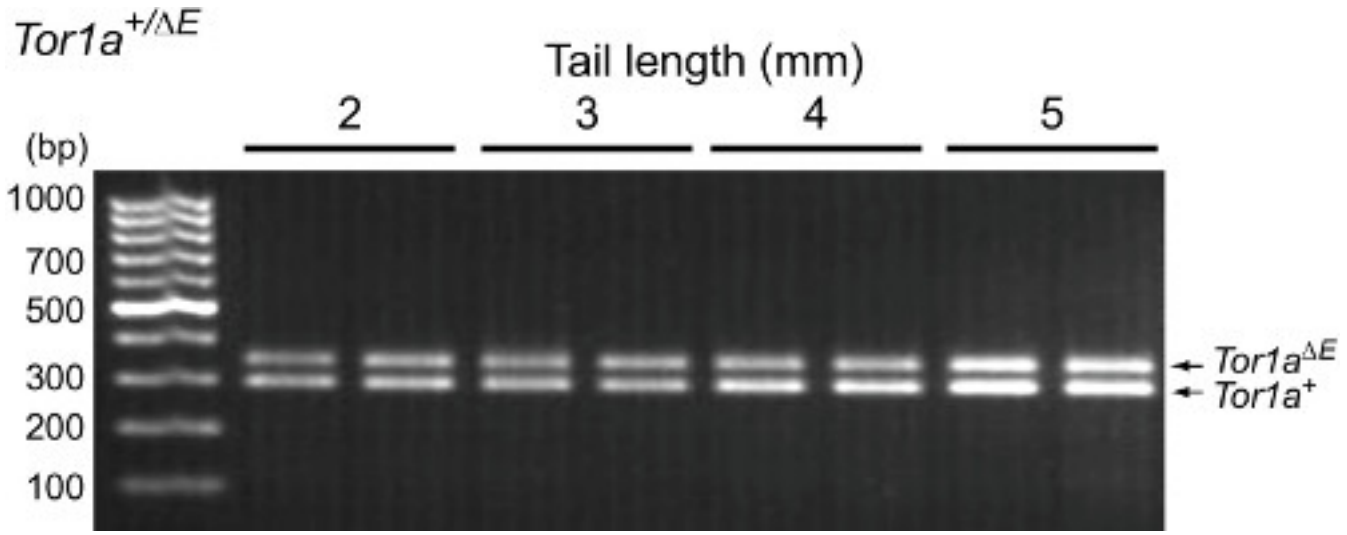

Figure 3. Detection of genomic DNA in the context of variation in the amount of starting material. Tail tips of different lengths were used. Tested animals were 3-week-old, heterozygous ΔE-torsinA knock-in mice (*Tor1a*$^{+/\Delta E}$). Lanes represent the tail lengths of 2, 3, 4 and 5 mm, in duplicate (from left). The tail tips were obtained from different mice. Molecular-weight size markers in the leftmost lane represent DNA lengths in steps of 100 base pairs. Please click here to view a larger version of this figure.

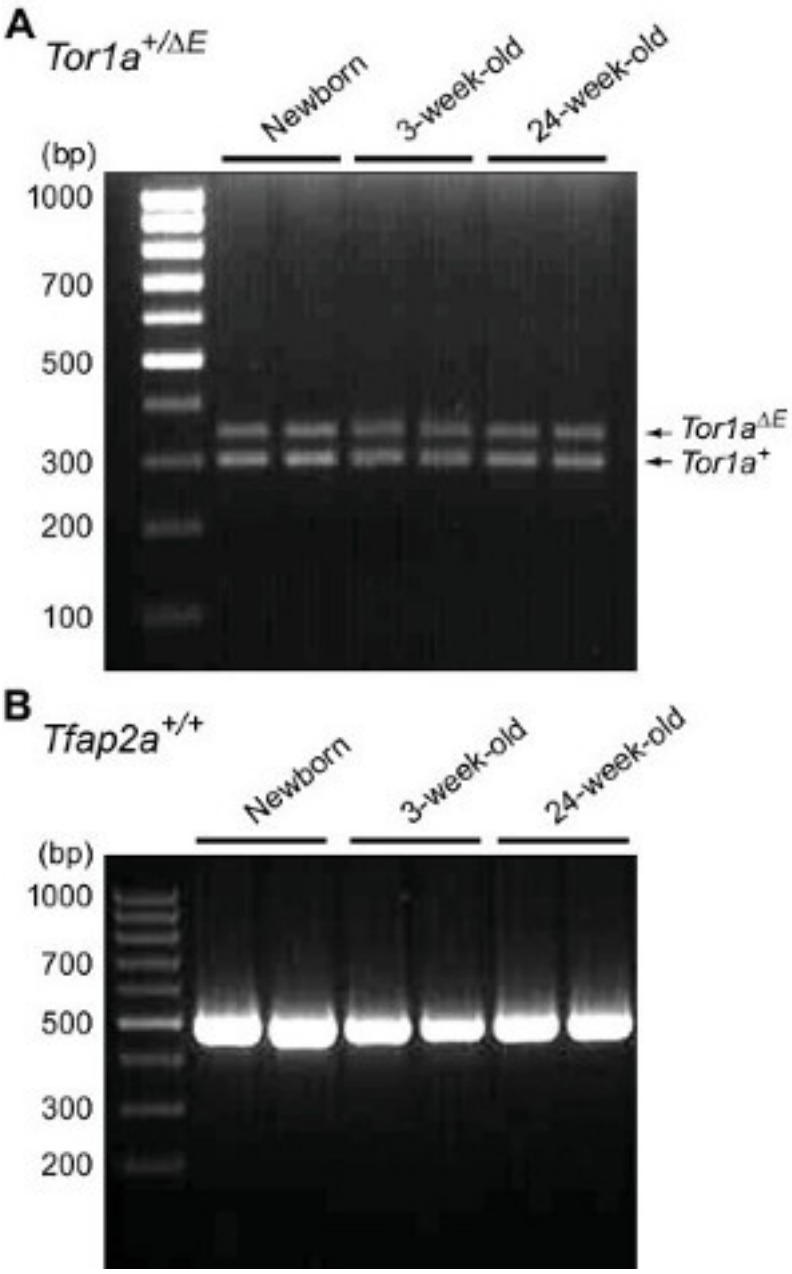

Figure 4. Detection of genomic DNA in the context of variation in animal age. (A) *Tor1a* gene. Lanes represent tail tips obtained from heterozygous ΔE-torsinA knock-in mice (*Tor1a*$^{+/\Delta E}$) at the following stages: newborn, 3-week-old, and ~24-week-old (in duplicates from left). **(B)** *Tfap2a* gene. Lanes represent tail tips obtained from wild-type (*Tfap2a*$^{+/+}$) mice at the following stages: newborn, 3-week-old, and ~24-week-old (in duplicates from left). Both genes were amplified from tails ~4 mm in length. The expected PCR fragment is 498 bp. The PCR program was the same as that used for *Tor1a* gene. Please click here to view a larger version of this figure.

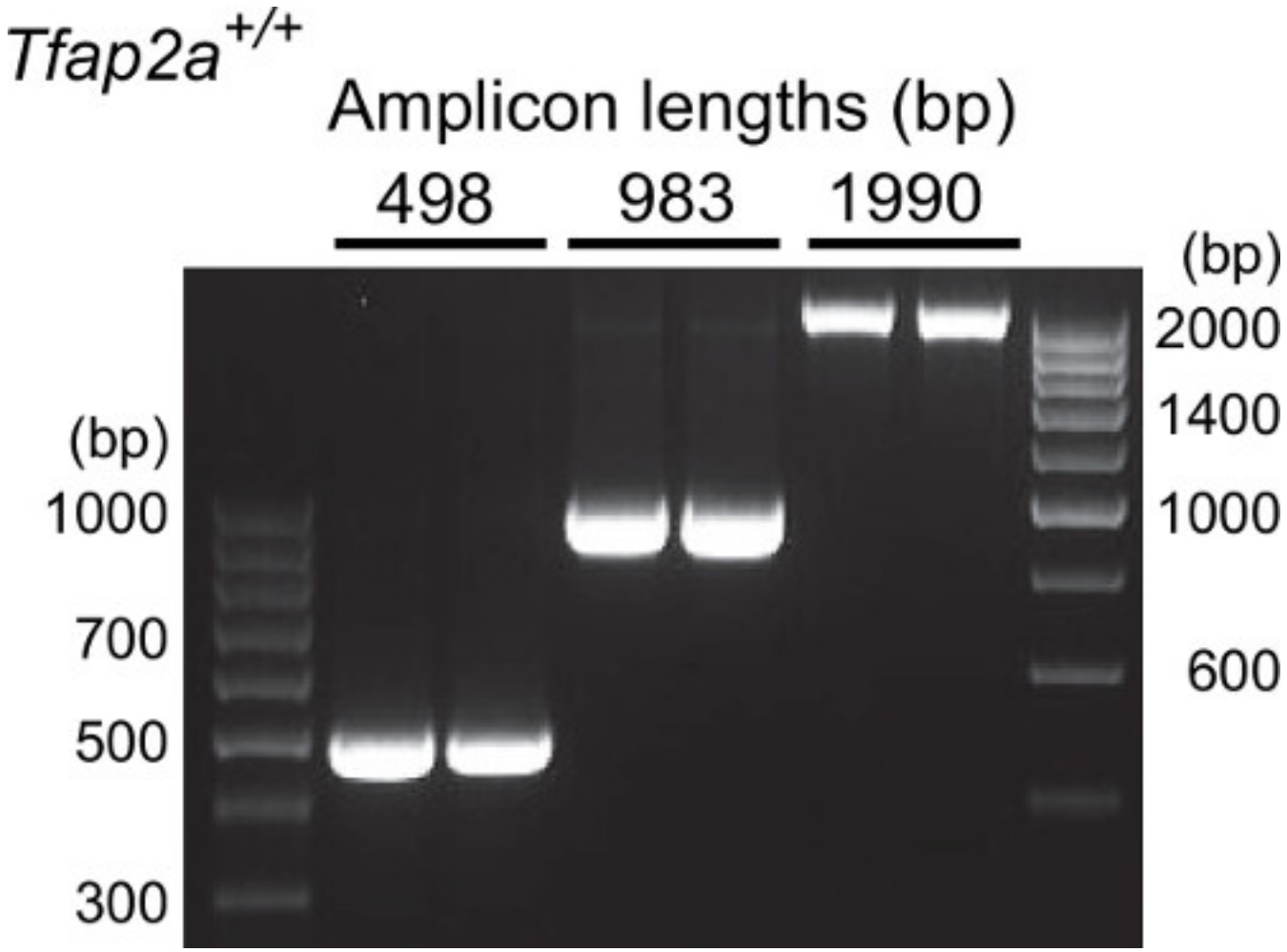

Figure 5. Detection of genomic DNA in the context of variation in length of the PCR amplicon. The *Tfap2a* gene was analyzed with PCR amplicon lengths of 498 bp (left lanes), 983 bp (middle lanes) and 1990 bp (right lanes) in duplicates. The gene was amplified from tails of 3-week-old mice. Molecular-weight size markers in the leftmost and rightmost lanes of the gel represent DNA lengths in steps of 100 and 200 base pairs, respectively. See the **Table of Materials/Equipment** for information about the primers for different amplicons. Please click here to view a larger version of this figure.

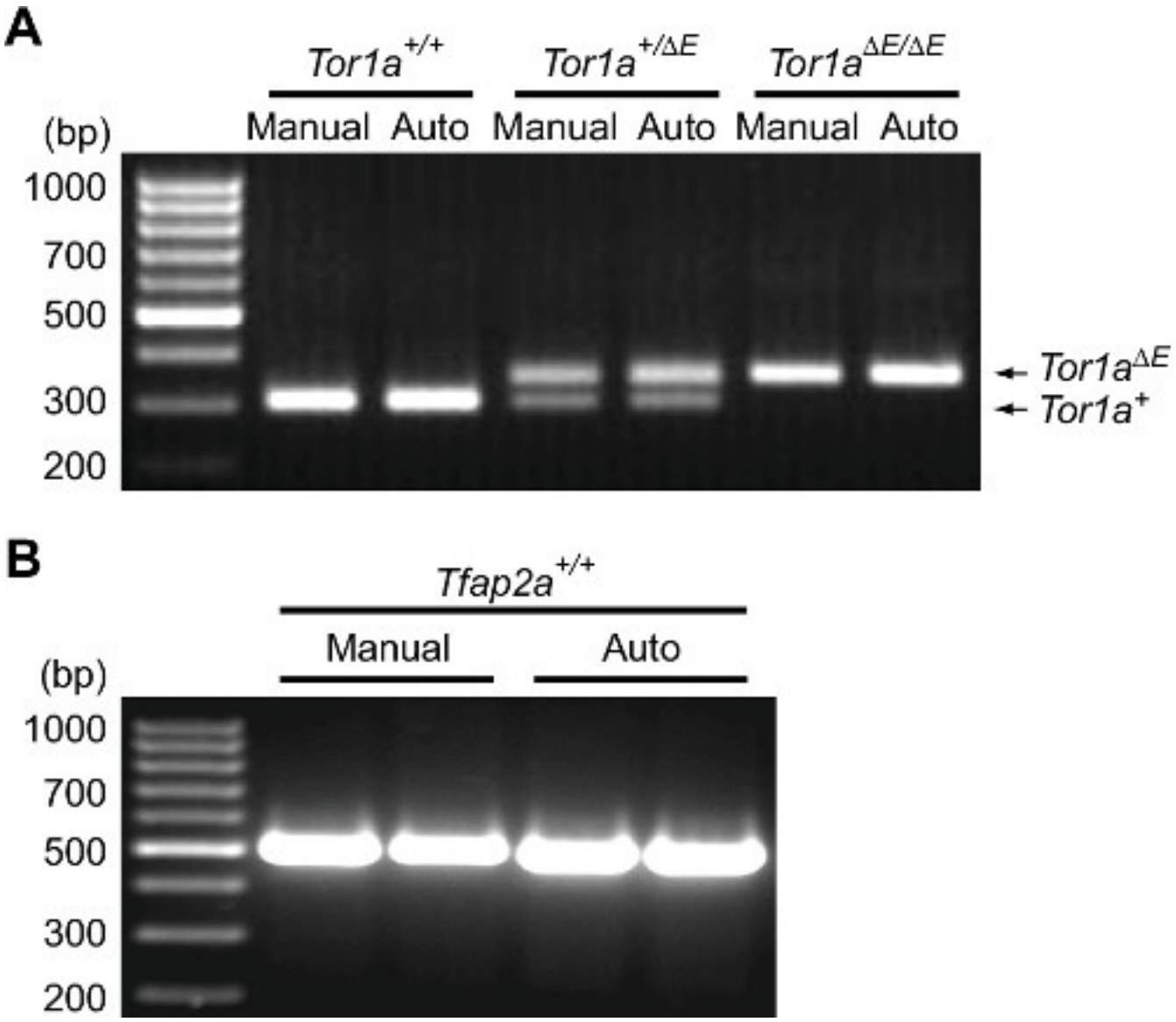

Figure 6. Detection of genomic DNA in the context of variation in DNA extraction method. Outcomes for the manual, single-tube extraction (Manual) and the automated, parallel multi-tube extraction methods (Auto) are compared. The latter method was used throughout this report. Genes were amplified from tails ~4 mm in length, collected from newborns. **(A)** *Tor1a* gene in the newborn pups of ΔE-torsinA knock-in mice. Lanes represent DNAs extracted from wild-type (manual and automated), heterozygous (manual and automated), and homozygous mice (manual and automated) (from left). **(B)** *Tfap2a* gene in 3-week-old wild-type mice. The expected PCR fragment is 498 bp. Please click here to view a larger version of this figure.

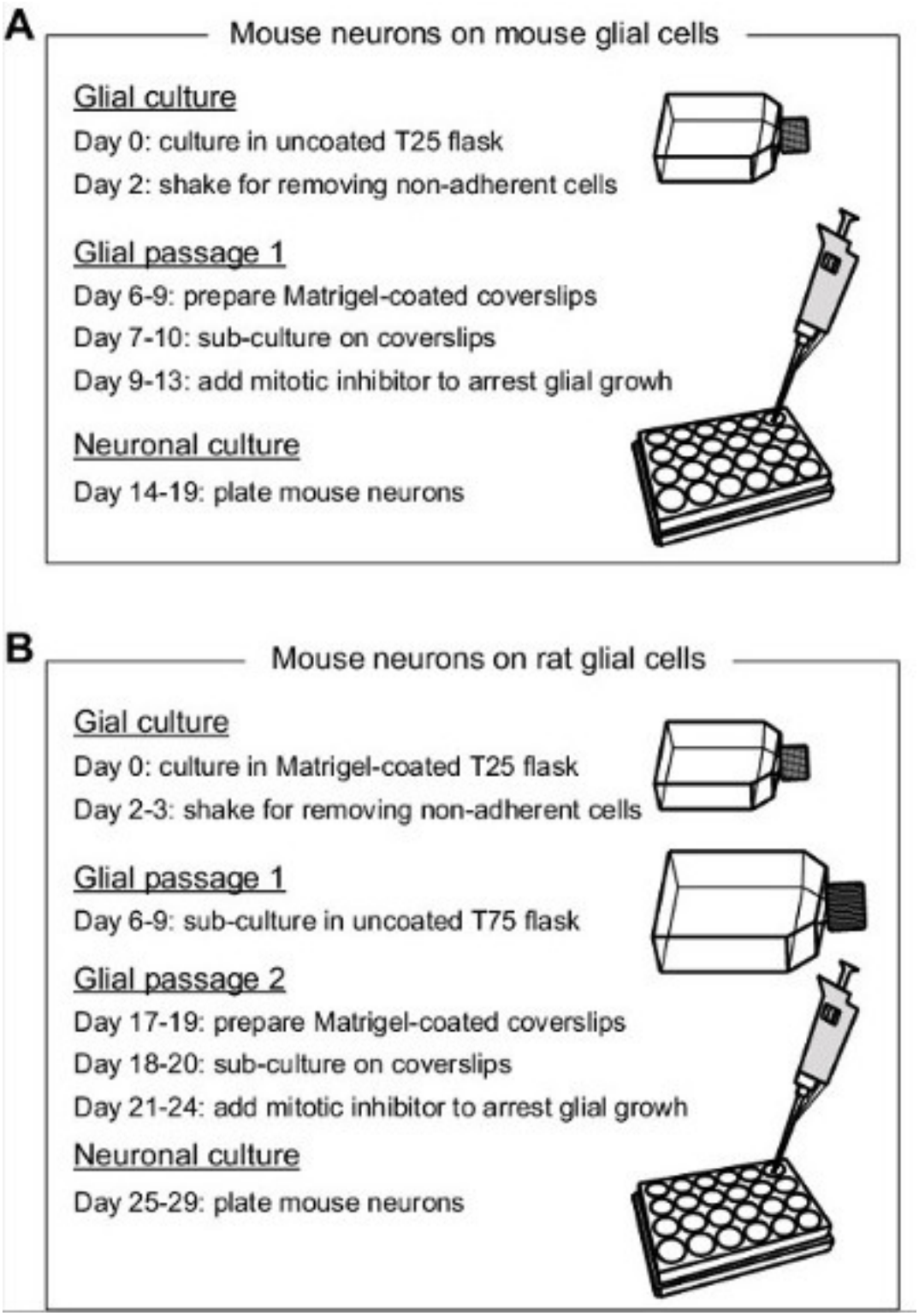

Figure 7. Simplified, schematic illustration of procedures for plating mouse neurons on mouse (A) and rat (B) glial feeder layers. The numbers of days (days *in vitro*) refer to the cumulative days after the glial cells are first plated in culture flasks. They serve only as a rough estimate. For practical details, see the Procedures section. Please click here to view a larger version of this figure.

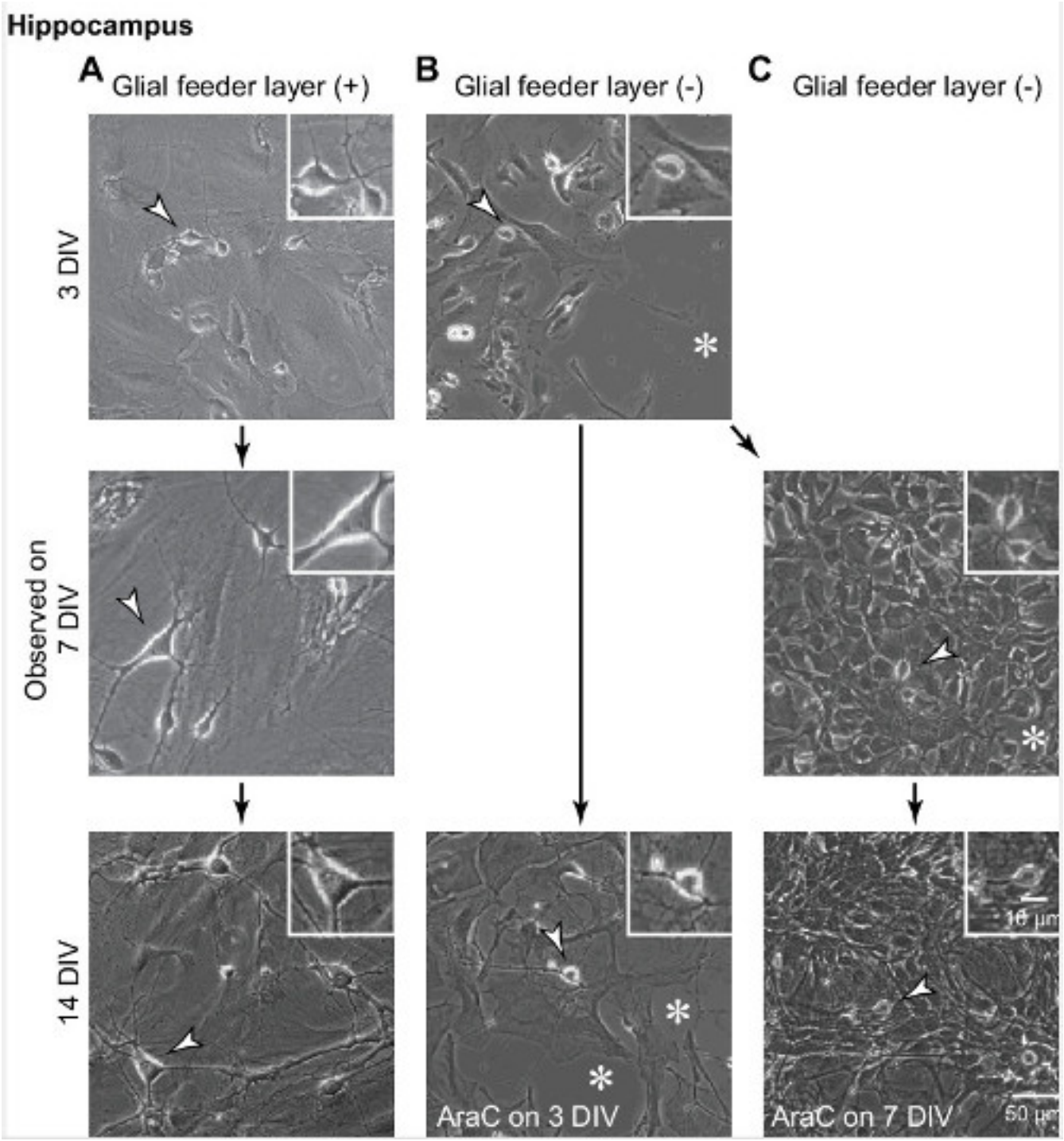

Figure 8. Supportive effect of glial feeder layer on growth of hippocampal neurons in a low-density culture. Neurons were obtained from the CA3-CA1 region of the hippocampus of newborn, wild-type mice. **(A)** Mouse hippocampal cells were plated on coated glass coverslips, which had been pre-seeded with a rat glial feeder layer obtained from the CA3-CA1 region of hippocampus. Neurons were dispersed evenly in a healthy manner. Cultures were observed at 3, 7 and 14 DIV. **(B, C)** Mouse hippocampal cells were plated on coated glass coverslips, which had no pre-established feeder layer. Cultures were observed at 3 DIV (top panel in B) and 7 DIV (middle panel in C) without AraC treatment. In other sets of cultures, the cells were treated with AraC at 3 DIV (bottom panel in B) and 7 DIV (bottom panel in C), and observed at 14 DIV. All images represent the sister cultures obtained from the same pup, whose neurons were plated on the same day. See text for details. For each panel, an example of a neuron is indicated by a white arrowhead and magnified in an inset. Neurons have cell bodies whose perimeter appears bright when viewed by phase-contrast optics, and they also have thick processes. Asterisks indicate areas without glial cells. The cultures were imaged live on an inverted microscope using phase-contrast optics with 20X objective lens (numerical aperture of 0.45) without an intermediate lens (*i.e.,* at 1x). Please click here to view a larger version of this figure.

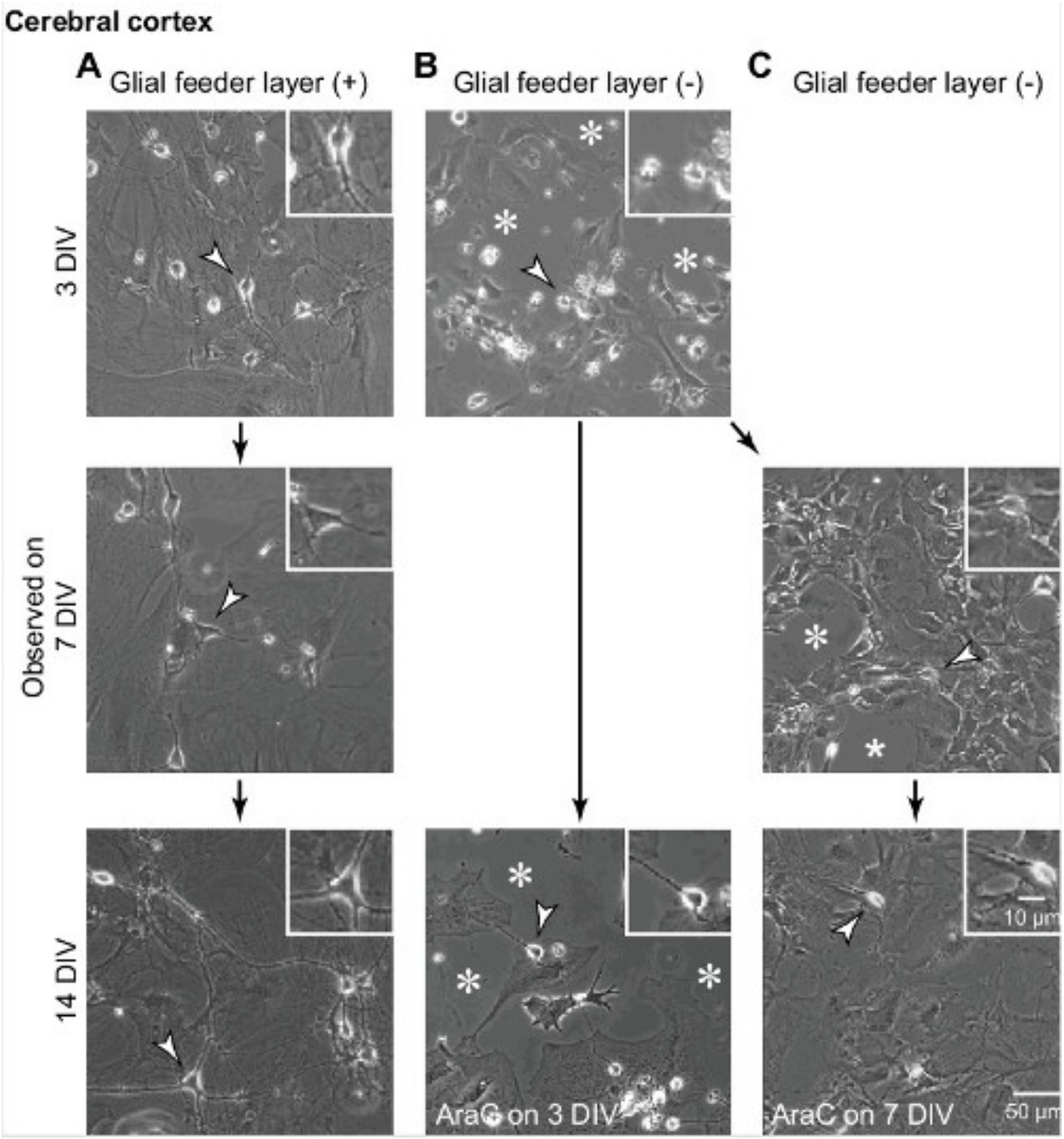

Figure 9. Supportive effect of glial feeder layer on growth of cerebral cortical neurons in a low-density culture. Similar results as in **Figure 8**, but with neurons obtained from the motor region of cerebral cortex. The conditions under labels **A-C** correspond to those in **Figure 8**. Please click here to view a larger version of this figure.

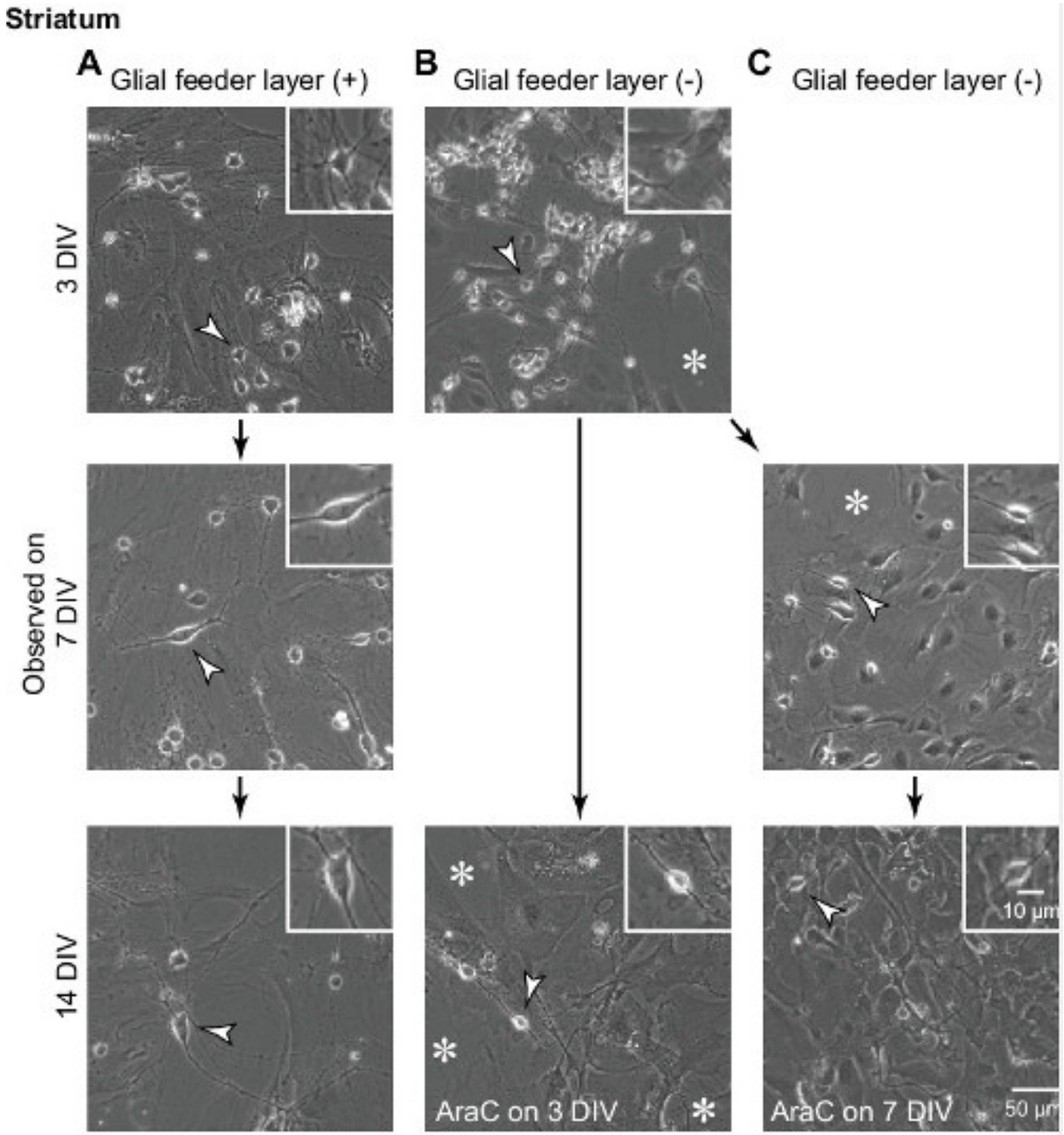

Figure 10. Supportive effect of glial feeder layer on growth of striatal neurons in a low-density culture. Similar results as in **Figures 8** and **9**, but with neurons obtained from the striatum. The conditions under labels **A-C** correspond to those in **Figure 8**. Please click here to view a larger version of this figure.

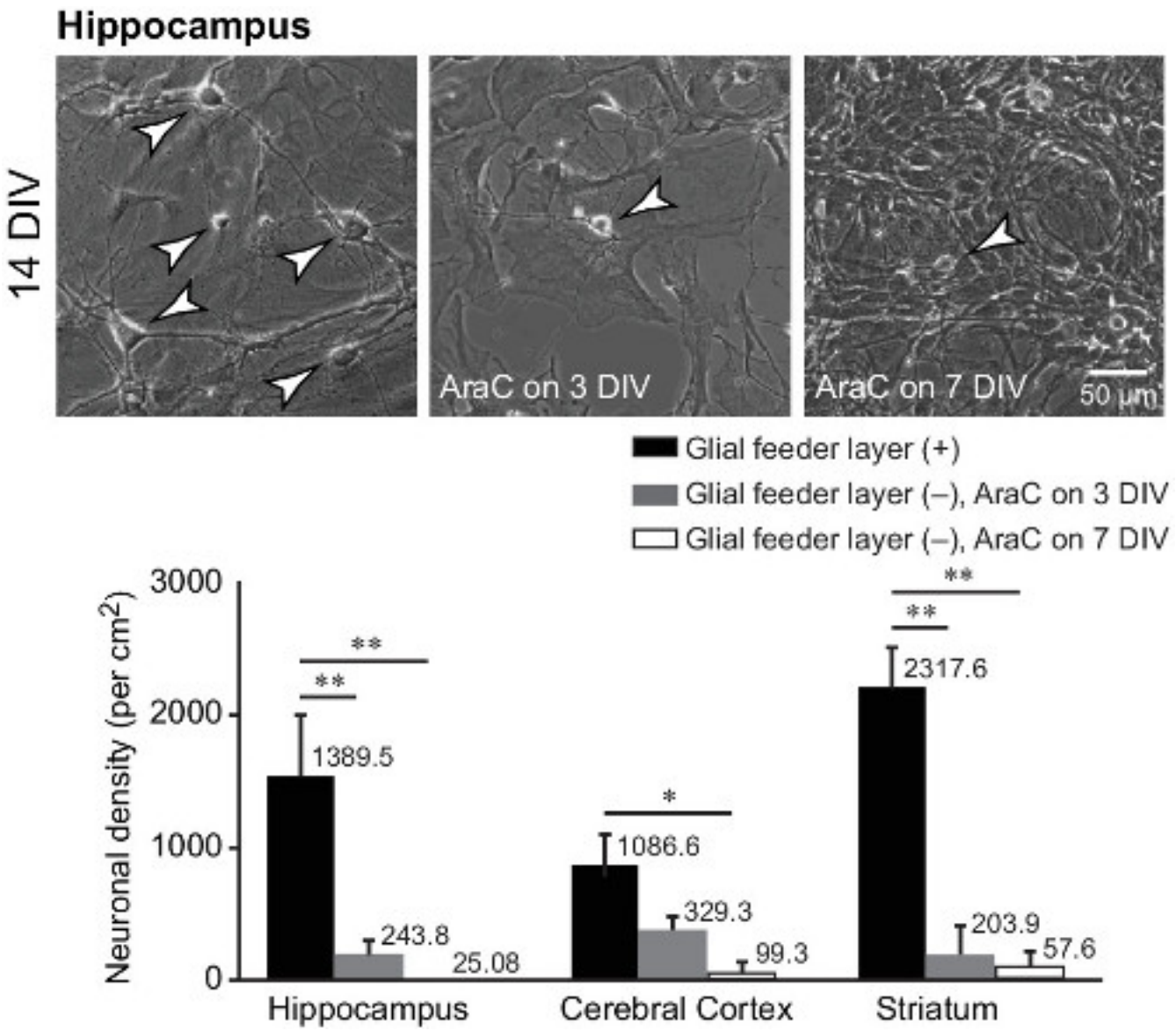

Figure 11. Supportive effect of glial feeder layer on neuronal survival. The number of surviving neurons was counted in the experiments shown in **Figure 8**, using images acquired by phase-contrast microscopy. Images for 14 DIV are shown here again, but with arrowheads pointing to examples of counted neurons. The bar graph shows the number of neurons per image field (449.0 µm x 335.5 µm) (mean ± standard error of the mean, n = 7-24 fields for each culture condition). Asterisks indicate statistically significant differences of 'Glial feeder layer (-), AraC on 3 DIV' and 'Glial feeder layer (-), AraC on 7 DIV' from 'Glial feeder layer (+)' (* $p < 0.05$, ** $p < 0.01$, unpaired Student's *t*-test). The numbers above the bars indicate the neuronal density measured in montages of multiple image fields. Images were acquired using a 20X objective lens. To avoid acquisition bias, all images were acquired along a full vertical strip, from the top to the bottom of a coverslip and passing through the approximate center of the coverslip. Individual images had some overlap (*e.g.,* 1/6 to 1/4 of an image field at the top and bottom). Two methods were used for the analysis. In one, neurons were counted in alternating images to ensure that individual neurons were not counted more than once. The resulting numbers were used to generate the bar graph. In the second method, a single montage was created from the individual images. They were stitched using the Microsoft Image Composite Editor or manually using Photoshop. The montages also excluded multiple counts of the same neurons. The resulting numbers are listed above the bars. In both methods, wide areas at the coverslip periphery that did not contain any cells were excluded. Cells were counted as neurons if they had cell bodies that appeared bright by phase-contrast microscopy, as well as extended cellular processes. Please click here to view a larger version of this figure.

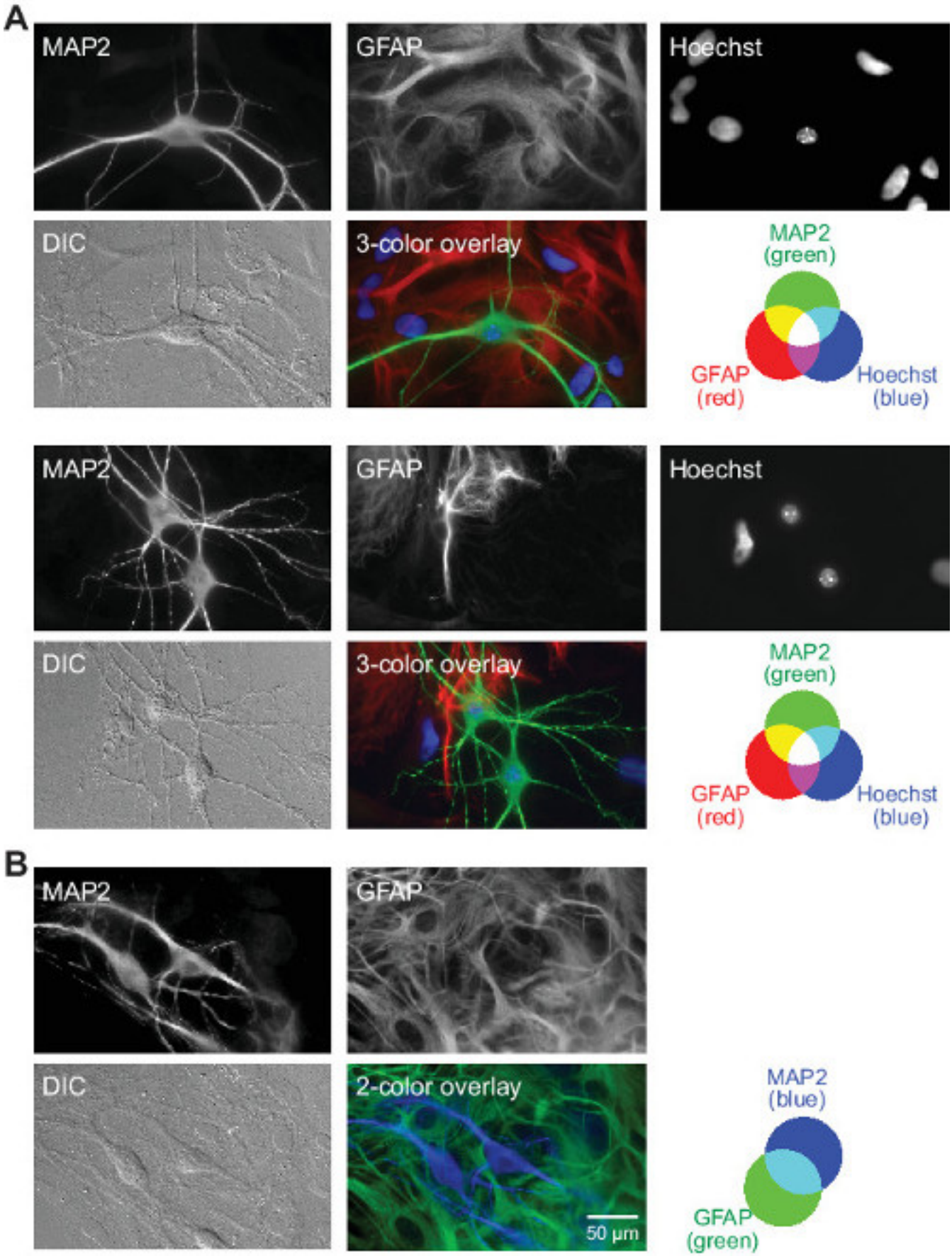

Figure 12. Immunocytochemical identification of cell types in neuronal cultures. The culture condition corresponds to the bottom-left image of **Figure 8A**. Neurons were obtained from the CA3-CA1 region of the hippocampus of wild-type mice, and plated on a glial feeder layer generated from the CA3-CA1 region of hippocampus of wild-type rats. The cultured cells were analyzed by immunocytochemistry for the neuronal marker MAP2, and the astrocytic glial cell marker GFAP. Differential interference contrast (DIC) microscopy was used to reveal the general morphology of the imaged fields, 14-17 days after the neurons were plated on the glial feeder layer. **(A)** Three-color staining,

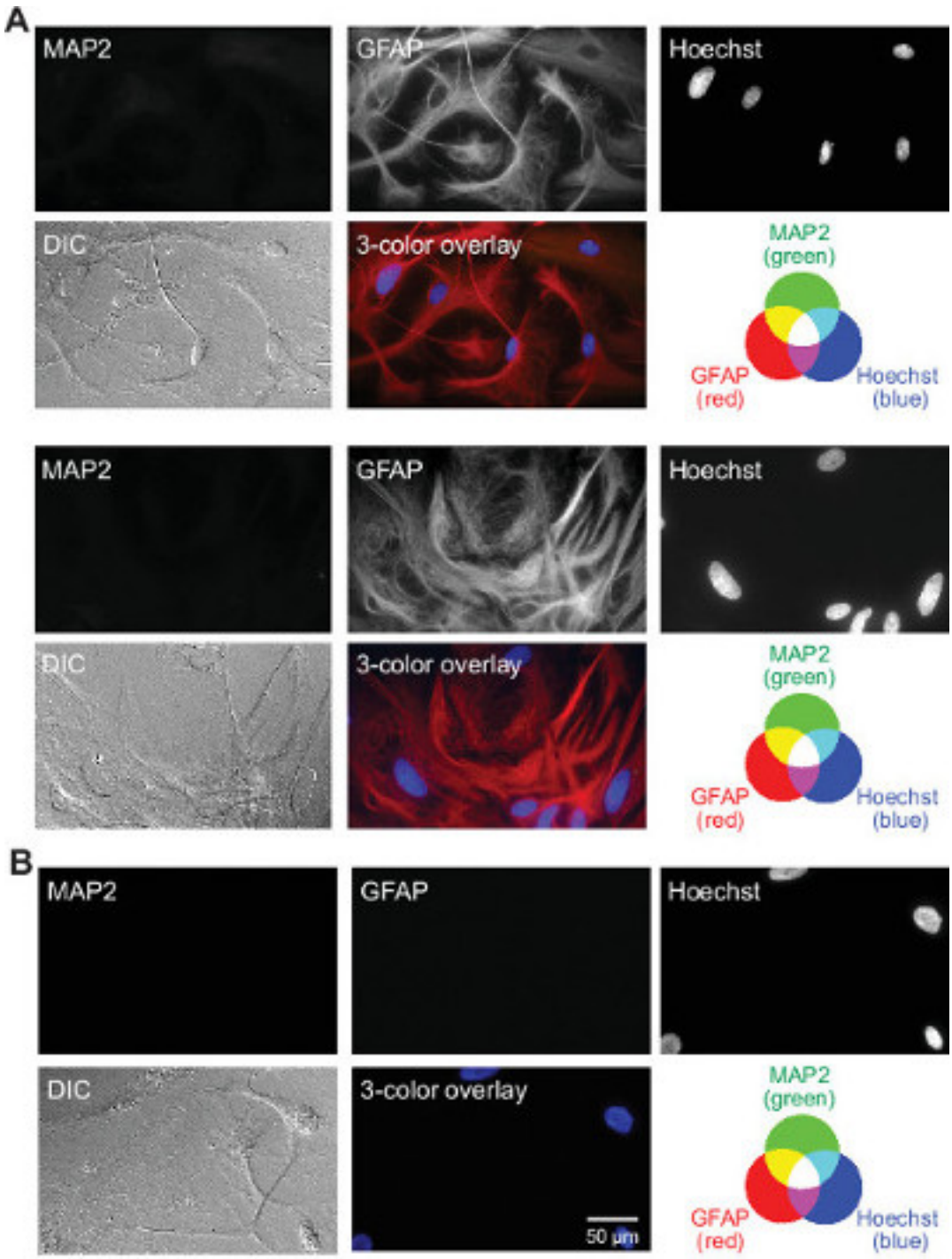

Figure 13. Immunocytochemical identification of cell types in glial feeder layer cultures. Sister cultures of the rat glial feeder layers as in **Figure 12**, but without the plating of mouse neurons. **(A)** Staining using the immunocytochemical procedures described in **Figure 12A**. Two representative image fields are shown. **(B)** Staining of the glial feeder layer using the immunocytochemical procedures described in A, but with the primary antibodies omitted. All MAP2 images in **Figures 12A** and **13A, B** were acquired under the same imaging conditions, and are shown at the same image contrast to allow comparison of intensity. The same procedures were used for GFAP images in **Figures 12A** and **13A**, **B**. The glial feeder layer culture was imaged on the same day as the cultures in **Figure 12**. Thus the glial feeder layers in **Figures 12** and **13** were cultured *in vitro* for the same amount of time. Please click here to view a larger version of this figure.

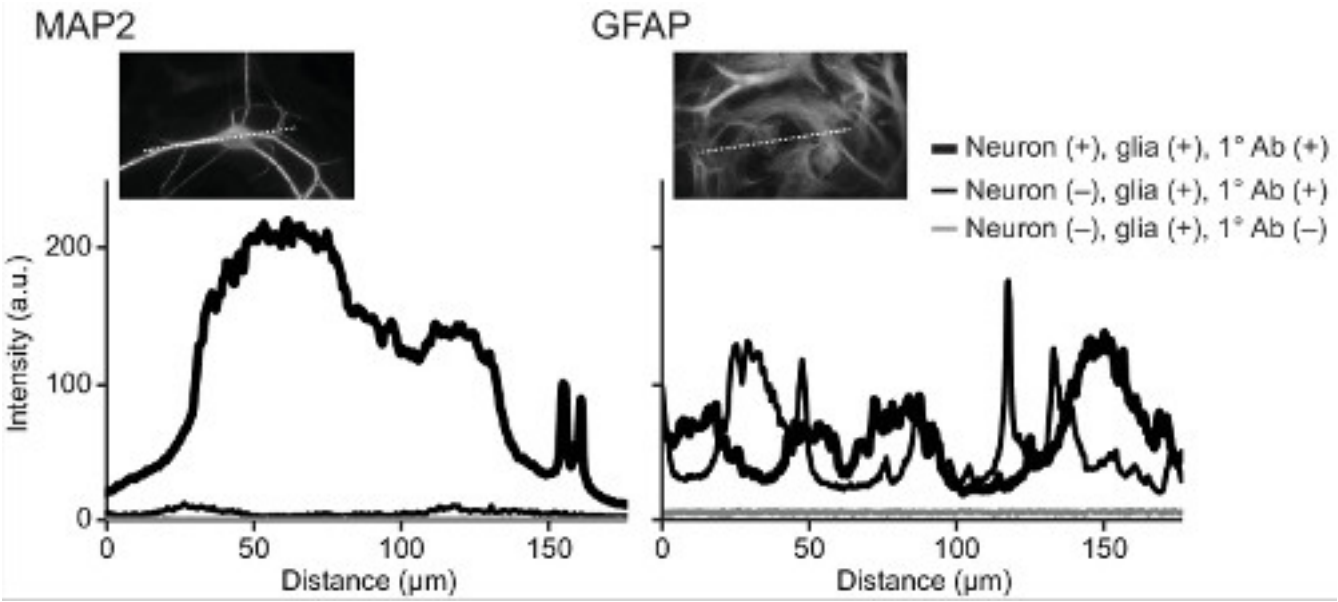

Figure 14. Intensity of immunocytochemical staining. Lines were drawn on the images shown in **Figures 12** and **13**, and the intensity along these was plotted. Insets show images in the top row of **Figure 12A**. The three conditions were: 1) plating of mouse cells (containing neurons) on a rat feeder layer and staining with the primary antibodies (Neuron +, glia +, 1° Ab +), 2) glial feeder layer only (no neuronal plating) and staining with the primary antibodies (Neuron −, glia +, 1° Ab +), and 3) glial feeder layer only (no neuronal plating) and staining without primary antibodies (Neuron −, glia +, 1° Ab −). Neuronal staining (MAP2) was present only when mouse cells were plated (conditions 1 vs. 2), and glial staining (GFAP) was present in both sets of cultures (conditions 1 vs. 2). The immunocytochemical staining was specific to both primary antibodies (conditions 1 vs. 3). Please click here to view a larger version of this figure.

SOLUTIONS
TAE buffer (50x solution)
Tris base, 486 g
Glacial acetic acid, 114.2 ml
0.5 M EDTA, pH 8.0, 200 ml
Add distilled water to bring total volume to 2 L
Make up in a chemical fume hood.
Dilute 50-fold before use.
Hanks' solution
Hanks' Balanced Salts, without calcium chloride, magnesium sulfate and sodium bicarbonate (for 1 L)
$NaHCO_3$, 350 mg (final concentration 4.17 mM)
HEPES, 2.38 g (final concentration, 10 mM)
Adjust to pH 7.4 using 5 M NaOH.
Adjust osmolarity to 310 mOsm using sucrose (Osmolarity tends to ~290 mOsm without any adjustment).
Add distilled water to bring total volume to 1 L
Digestion solution (for trypsin treatment of brain tissue)
NaCl, 800.6 mg (final concentration, 137 mM)
KCl, 37.3 mg (final concentration, 5 mM)
$Na_2HPO_4 \cdot (7H_2O)$, 187.6 mg (final concentration, 7 mM)
HEPES, 595.8 mg (final concentration, 25 mM)
Glucose, 97.3 mg (final concentration, 5.4 mM)
Adjust to pH 7.2 using 5 M NaOH.
Osmolarity tends to ~310 mOsm without any adjustment.
Add distilled water to bring total volume to 100 ml.

Right before usage, add 20 mg of trypsin (final concentration of 10 mg/ml) and 20 µl of DNase (final concentration of 750 units/ml) to 2 ml of digestion solution.
Dissociation solution (for mechanical dissociation of brain tissue)
Hanks' solution
$MgSO_4 \cdot (7H_2O)$, 295.1 mg (final concentration, 11.97 mM)
Adjust osmolarity to 310 mOsm using sucrose.
Total volume is 100 ml.
Right before usage, add 20 µl of DNase (final concentration of 750 units/ml) to 2 ml of dissociation solution.
Plating medium-1 (for mouse glial cells)
Dulbecco's Modified Eagle Medium (DMEM), 449.5 ml
MITO+ Serum Extender, 0.5 ml
FBS, 50 ml
Total volume is 500 ml.
Plating medium-2 (for mouse neurons)
Neurobasal-A, 485 ml
B27, 10 ml
GlutaMAX-I, 5 ml (final concentration, 2 mM)
Total volume is 500 ml.
Plating medium-3 (for rat neurons and glial cells)
Minimum Essential Media (MEM, without phenol red)
Glucose, 2.5 g (final concentration, 27.8 mM)
$NaHCO_3$, 100 mg (final concentration, 2.38 mM)
Transferrin, 50 mg
FBS, 50 ml
GlutaMAX-I, 5 ml (final concentration, 2 mM)
Insulin, 12.5 mg
Total volume is 500 ml.
Growth medium (for rat neurons and glial cells)
MEM (without phenol red)
Glucose, 2.5 g (final concentration, 27.8 mM)
$NaHCO_3$, 100 mg (final concentration, 2.38 mM)
Transferrin, 50 mg
FBS, 25 ml
GlutaMAX-I, 1.25 ml (final concentration, 0.5 mM)
B27 or NS21 {Chen, 2008 #2399}, 10 ml
Cytosine β-D-arabinofuranoside (AraC), 0.56 mg (final concentration, 4 µM)
Total volume is 500 ml.
General comments
Our culture media do not contain antibiotics because they could exert cytotoxic effects on cultured glial cells and neurons (reference 70, 71). This makes it especially important to adhere to sterile procedures in culture-related work.
See the **Table of Reagents** for the detailed sources of chemicals.

Table 1. Solutions

Discussion

The protocol presented here includes procedures for tattooing to label/identify mice, for genotyping mice from tail tips, and for culturing mouse brain neurons at low density. In one round of experiments using 6-8 pups, these procedures typically require ~0.5 hr, ~4 hr and ~2 hr, respectively, at a total of 6-7 hr. This makes it practical for a single experimenter to complete all the procedures necessary from the time of the pups' birth to the plating of neuronal cultures – in less than a single working day (with the exception of prior preparation of glial feeder layers).

Tattooing

Long-term identification of animals is necessary for the purposes of breeding and scientific studies such as analyses of histology, cell function and animal behavior. Tattooing newborn animals is advantageous because it can be carried out rapidly and lasts for much of the animal's life [7,22-25]. Tattooing on the paw pads can be better than toe clipping [23] with respect to preserving testable behaviors, for example in suspension or gripping [22,26], although some studies have not noted such deficiencies (*e.g.,* [25]). There were no instances of mothers rejecting or cannibalizing pups after tattooing. For other methods of long-term identification of animals, see recent reviews [7,23,24].

Genotyping

A critical feature in our protocol is the use of a fast genotyping method. Although similar genotyping methods were described in previous reports (*e.g.,* [27,28]), the system described here has at least two improvements. First, it can tolerate certain variations in the amount of starting tissue, age of animals, and amplicon length. Thus, successful genotyping can be achieved using mice as young as 1 day and as old as 6 months old, and can be carried out using a broad range of primer pairs. Second, this method does not require a stop solution for the DNA extraction step. This eliminates excessive tube handling and pipetting, and allows parallel multi-tube automation of the process with a PCR machine. The number of specimens can be scaled up (*e.g.*, 96 samples) yet processed easily and simultaneously. Also the specimen type is not limited to tail clips; other sample types that could be used include ear punches, toe clippings, whole early embryos, and placenta tissues [2-4,29,30]. Different animal species can also be used. Thus the genotyping procedures are reliable (repeatable with low intra-assay variance) and reproducible (low inter-assay variance between runs or between laboratories), and have the advantage of high scalability.

Note that some caution is required for achieving the expected quality of results. First, during DNA extraction, a large variation in the protocol can degrade the results. For example, a significant reduction in the volume of DNA Extraction Solution (*e.g.,* from 200 to 100 µl in step 2.2) still allows genotyping, but it can reduce the reliability and result in variation in PCR results. Under such conditions, it is recommended to reduce the volume of the DNA extract from 4 to 2 µl, and increase the volume of H_2O from 2 to 4 µl to compensate for the volume change during PCR reactions (step 2.5). Second, at the end of DNA extraction, the solution can be used for PCR immediately without centrifugation in most cases, although the tail will retain its overall structure and will not be completely decomposed. However, the described inversion of the tubes is essential for the purpose of dissociating genomic DNA from the tissue (step 2.4). It is also important to use the top, clear part of the solution, excluding the debris at the bottom of the tube, because inclusion of the latter will lead to inconclusive PCR results. These steps will be effective with minimal time and effort. Equally good results can be obtained by actively vortexing the specimen (in place of the inversions) followed by centrifugation and usage of the supernatant. Third, after the DNA extraction, the DNA can be stored for long-term (*e.g.,* >two weeks). It is recommended to centrifuge the solution using a microcentrifuge (*e.g.,* 3,000-13,000 g at 4 °C for 2 min), transfer the supernatants to new tubes, and store them at -80 °C. When the stored extract is to be used for genotyping, briefly centrifuge the specimen after thawing, and use the supernatant.

Neuronal cultures

Another critical feature of our protocol is the use of a glial feeder layer to establish neuronal cultures at a low plating density. Typically, in primary cultures of mammalian brain neurons, the cells are plated with a relatively high density, on coated coverslips without a glial feeder layer (*e.g.,* [31-39]). When the plating density of neurons is reduced using this method, the initial lack of glial sheet leads to poor neuronal growth and dendritic extension (panels **B**, **C** in **Figures 8-10**), as reported previously [40-42], probably due to poor glial growth [43,44].

Successful, low-density neuronal cultures can be generated by at least three broad types of methods. In one approach, Neurobasal Medium is used as a culture medium. This makes it possible to culture neurons in the absence of a glial feeder layer, and can be used for low-density neuronal cultures [45,46]. In a second approach ('Banker-type' and its modification), glial cells are co-cultured with neurons in the same well but are physically separated from them. In this context the glial cells provide 'trophic support' to neurons without contacting them directly [1,41,42,47-49]. In the third approach, neurons are plated on a pre-established glial feeder layer that supports neuronal growth (*e.g.,* [50-53]) (**Figures 8-10**). Specifically, mouse brain neurons are plated on a glial feeder layer prepared from mice [8,34,54] or rats [41,55,56].

We prefer the last of the three approaches to low-density culture, because the Neurobasal Medium can affect neuronal survival [57], the astrocytic glial cells will be essential in regulating neuronal functions [8,58], and the physical contact between neurons and glial cells may be important. The procedures for culturing the mouse and rat glial cells are similar [59,60], but we have modified them slightly to accommodate for the more rapid *in vitro* growth of rat vs. mouse glial cells. The procedures for the rat cell culture were modified from [61-63]. The use of a glial feeder layer for low-density neuronal cultures makes it necessary to perform rapid genotyping, in order to match the genotype of the feeder layer to that of the neurons within the period between the pups' births and the neonatal deaths or the end of culture window (1-2 postnatal days).

Low-density culture on a glial feeder layer is also an important method when one tries to culture neurons of small nuclei in the brain (*e.g.,* the norepinephrine-releasing locus coeruleus, and the dopamine-releasing substantia nigra). Those nuclei contain only a small number of neurons and would inevitably yield low-density cultures [64-67].

Primary cultures are routinely prepared in our laboratory from the CA3-CA1 region of hippocampus, the motor region of the cerebral cortex and the striatum of mice. The same procedures can be used to prepare neuronal cultures representing other brain regions, for example the whole hippocampus (including the dentate gyrus) and the whole cerebral cortex. Rat neurons from brain regions such as the hippocampus and the locus coeruleus are cultured in similar fashion, using the rat glial feeder layer. These cultured neurons are usually used at 1-4 weeks *in vitro*,

with the exact age of the culture depending on the purpose of the experiment. It is of note that some neurons cultured on a glial feeder layer can survive for more than 10 weeks [34,68].

One potential problem of low-density neuronal cultures is that the neuronal properties can be different from those in high-density cultures or in neurons *in situ*. Comparison of these systems provides an interesting opportunity to study how neuronal development and maturation are affected by multiple factors, such as the neuronal density, the soluble factors secreted from neurons, neuron-to-neuron contact, and glial-neuronal interactions.

In summary, the tattooing-based mouse labeling is long lasting, the genotyping method is rapid, and the culture method allows for plating mouse neurons at low density. The protocol described here can be applied in its entirety to other animal species harboring other genetic mutations. Moreover, individual steps of the protocol can be used for other purposes. Thus the protocol can be used in a wide array of applications based on experimenters' needs.

Disclosures

The author (Zhengmin Huang) is the president of EZ BioResearch LLC that produces reagents described in this article.

Acknowledgements

The authors thank researchers at the University of Iowa, Drs. Luis Tecedor, Ines Martins and Beverly Davidson for instructions and helpful comments regarding striatal cultures, and Drs. Kara Gordon, Nicole Bode and Pedro Gonzalez-Alegre for genotyping assistance and discussions. We also thank Dr. Eric Weyand (Animal Identification and Marking Systems) for helpful comments regarding tattooing, and Dr. Shutaro Katsurabayashi (Fukuoka University) for helpful comments regarding the mouse culture. This work was supported by grants from the American Heart Association, the Department of Defense (Peer Reviewed Medical Research Program award W81XWH-14-1-0301), the Dystonia Medical Research Foundation, the Edward Mallinckrodt, Jr. Foundation, the National Science Foundation, and the Whitehall Foundation (N.C.H.).

References

1. Goslin, K., Asmussen, H., & Banker, G. in *Culturing Nerve Cells.* eds G. Banker & K. Goslin) Ch. 13, 339-370 MIT Press, (1998).
2. Kakazu, Y., Koh, J.Y., Ho, K.W., Gonzalez-Alegre, P., & Harata, N.C. Synaptic vesicle recycling is enhanced by torsinA that harbors the DYT1 dystonia mutation. *Synapse.* **66**, 453-464, doi:10.1002/syn.21534 (2012).
3. Kakazu, Y., Koh, J.Y., Iwabuchi, S., Gonzalez-Alegre, P., & Harata, N.C. Miniature release events of glutamate from hippocampal neurons are influenced by the dystonia-associated protein torsinA. *Synapse.* **66**, 807-822, doi:10.1002/syn.21571 (2012).
4. Iwabuchi, S., Kakazu, Y., Koh, J.Y., & Harata, N.C. Abnormal cytoplasmic calcium dynamics in central neurons of a dystonia mouse model. *Neurosci. Lett.* **548**, 61-66, doi:10.1016/j.neulet.2013.05.047 (2013).
5. Koh, J.Y., Iwabuchi, S., & Harata, N.C. Dystonia-associated protein torsinA is not detectable at the nerve terminals of central neurons. *Neuroscience.* **253C**, 316-329, doi:10.1016/j.neuroscience.2013.08.060 (2013).
6. Iwabuchi, S., Koh, J.Y., Wang, K., Ho, K.W., & Harata, N.C. Minimal change in the cytoplasmic calcium dynamics in striatal GABAergic neurons of a DYT1 dystonia knock-in mouse model. *PLoS One.* **8**, e80793, doi:10.1371/journal.pone.0080793 (2013).
7. Dahlborn, K., Bugnon, P., Nevalainen, T., Raspa, M., Verbost, P., & Spangenberg, E. Report of the Federation of European Laboratory Animal Science Associations Working Group on animal identification. *Lab. Anim.* **47**, 2-11, doi:10.1177/0023677124732903 (2013).
8. Kawano, H. *et al.* Long-term culture of astrocytes attenuates the readily releasable pool of synaptic vesicles. *PLoS One.* **7**, e48034, doi:10.1371/journal.pone.0048034 (2012).
9. Ozelius, L.J. *et al.* The early-onset torsion dystonia gene (*DYT1*) encodes an ATP-binding protein. *Nat. Genet.* **17**, 40-48, doi:10.1038/ng0997-40 (1997).
10. Hanson, P.I., & Whiteheart, S.W. AAA+ proteins: have engine, will work. *Nat. Rev. Mol. Cell. Biol.* **6**, 519-529, doi:10.1038/nrm1684 (2005).
11. White, S.R., & Lauring, B. AAA+ ATPases: achieving diversity of function with conserved machinery. *Traffic.* **8**, 1657-1667, doi:10.1111/j.1600-0854.2007.00642.x (2007).
12. Burdette, A.J., Churchill, P.F., Caldwell, G.A., & Caldwell, K.A. The early-onset torsion dystonia-associated protein, torsinA, displays molecular chaperone activity *in vitro*. *Cell Stress Chaperones.* **15**, 605-617, doi:10.1007/s12192-010-0173-2 (2010).
13. Zhao, C., Brown, R.S., Chase, A.R., Eisele, M.R., & Schlieker, C. Regulation of Torsin ATPases by LAP1 and LULL1. *Proc. Natl. Acad. Sci. U. S. A.* **110**, E1545-1554, doi:10.1073/pnas.1300676110 (2013).
14. Ozelius, L.J., Lubarr, N., & Bressman, S.B. Milestones in dystonia. *Mov. Disord.* **26**, 1106-1126, doi:10.1002/mds.23775 (2011).
15. Albanese, A. *et al.* Phenomenology and classification of dystonia: a consensus update. *Mov. Disord.* **28**, 863-873, doi:10.1002/mds.25475 (2013).
16. Goodchild, R.E., Kim, C.E., & Dauer, W.T. Loss of the dystonia-associated protein torsinA selectively disrupts the neuronal nuclear envelope. *Neuron.* **48**, 923-932, doi:10.1016/j.neuron.2005.11.010 (2005).
17. Dang, M.T. *et al.* Generation and characterization of Dyt1 ΔGAG knock-in mouse as a model for early-onset dystonia. *Exp. Neurol.* **196**, 452-463, doi:10.1016/j.expneurol.2005.08.025 (2005).
18. Tanabe, L.M., Martin, C., & Dauer, W.T. Genetic background modulates the phenotype of a mouse model of DYT1 dystonia. *PLoS One.* **7**, e32245, doi:10.1371/journal.pone.0032245 (2012).
19. Huang, Z., Xu, H., & Sandell, L. Negative regulation of chondrocyte differentiation by transcription factor AP-2α. *J. Bone Miner. Res.* **19**, 245-255, doi:10.1359/jbmr.2004.19.2.245 (2004).
20. Hall, R.D., & Lindholm, E.P. Organization of motor and somatosensory neocortex in the albino rat. *Brain Res.* **66**, 23-38, doi:10.1016/0006-8993(74)90076-6 (1974).

21. Kavalali, E.T., Klingauf, J., & Tsien, R.W. Activity-dependent regulation of synaptic clustering in a hippocampal culture system. *Proc. Natl. Acad. Sci. U. S. A.* **96**, 12893-12900, doi:10.1073/pnas.96.22.12893 (1999).
22. Iwaki, S., Matsuo, A., & Kast, A. Identification of newborn rats by tattooing. *Lab. Anim.* **23**, 361-364, doi:10.1258/002367789780746024 (1989).
23. Wang, L. A primer on rodent identification methods. *Lab. Anim. (NY).* **34**, 64-67, doi:10.1038/laban0405-64 (2005).
24. Deacon, R.M. Housing, husbandry and handling of rodents for behavioral experiments. *Nat. Protoc.* **1**, 936-946, doi:10.1038/nprot.2006.120 (2006).
25. Castelhano-Carlos, M.J., Sousa, N., Ohl, F., & Baumans, V. Identification methods in newborn C57BL/6 mice: a developmental and behavioural evaluation. *Lab. Anim.* **44**, 88-103, doi:10.1258/la.2009.009044 (2010).
26. Schaefer, D.C., Asner, I.N., Seifert, B., Burki, K., & Cinelli, P. Analysis of physiological and behavioural parameters in mice after toe clipping as newborns. *Lab. Anim.* **44**, 7-13, doi:10.1258/la.2009.009020 (2010).
27. Doan, L., & Monuki, E.S. Rapid genotyping of mouse tissue using Sigma's Extract-N-Amp Tissue PCR Kit. *J. Vis. Exp.*, e636, doi:10.3791/636 (2008).
28. Chum, P.Y., Haimes, J.D., Andre, C.P., Kuusisto, P.K., & Kelley, M.L. Genotyping of plant and animal samples without prior DNA purification. *J. Vis. Exp.* e3844, doi:10.3791/3844 (2012).
29. Demeestere, I. *et al.* Follicle-stimulating hormone accelerates mouse oocyte development *in vivo*. *Biol. Reprod.* **87**, 3, 1-11, doi:10.1095/biolreprod.112.099929 (2012).
30. Warner, D.R., Wells, J.P., Greene, R.M., & Pisano, M.M. Gene expression changes in the secondary palate and mandible of Prdm16$^{-/-}$ mice. *Cell Tissue Res.* **351**, 445-452, doi:10.1007/s00441-012-1525-2 (2013).
31. Higgins, D., & Banker, G. in *Culturing Nerve Cells.* eds G. Banker & K. Goslin) Ch. 3, 37-78 MIT Press, (1998).
32. Ahlemeyer, B., & Baumgart-Vogt, E. Optimized protocols for the simultaneous preparation of primary neuronal cultures of the neocortex, hippocampus and cerebellum from individual newborn (P0.5) C57Bl/6J mice. *J. Neurosci. Methods.* **149**, 110-120, doi:10.1016/j.jneumeth.2005.05.022 (2005).
33. Nunez, J. Primary culture of hippocampal neurons from P0 newborn rats. *J. Vis. Exp.* e895, doi:10.3791/895 (2008).
34. Viesselmann, C., Ballweg, J., Lumbard, D., & Dent, E.W. Nucleofection and primary culture of embryonic mouse hippocampal and cortical neurons. *J. Vis. Exp.* e2373, doi:10.3791/2373 (2011).
35. Leach, M.K. *et al.* The culture of primary motor and sensory neurons in defined media on electrospun poly-L-lactide nanofiber scaffolds. *J. Vis. Exp.* e2389, doi:10.3791/2389 (2011).
36. Beaudoin, G.M., 3rd *et al.* Culturing pyramidal neurons from the early postnatal mouse hippocampus and cortex. *Nat. Protoc.* **7**, 1741-1754, doi:10.1038/nprot.2012.099 (2012).
37. Seibenhener, M.L., & Wooten, M.W. Isolation and culture of hippocampal neurons from prenatal mice. *J. Vis. Exp.* e3634, doi:10.3791/3634 (2012).
38. Pacifici, M., & Peruzzi, F. Isolation and culture of rat embryonic neural cells: a quick protocol. *J. Vis. Exp.* e3965, doi:10.3791/3965 (2012).
39. Tischbirek, C.H. *et al.* Use-dependent inhibition of synaptic transmission by the secretion of intravesicularly accumulated antipsychotic drugs. *Neuron.* **74**, 830-844, doi:10.1016/j.neuron.2012.04.019 (2012).
40. Nakanishi, K., Nakanishi, M., & Kukita, F. Dual intracellular recording of neocortical neurons in a neuron-glia co-culture system. *Brain Res. Brain Res. Protoc.* **4**, 105-114, doi:10.1016/S1385-299X(99)00003-3 (1999).
41. Kaech, S., & Banker, G. Culturing hippocampal neurons. *Nat. Protoc.* **1**, 2406-2415, doi:10.1038/nprot.2006.356 (2006).
42. Kaech, S., Huang, C.F., & Banker, G. General considerations for live imaging of developing hippocampal neurons in culture. *Cold Spring Harb. Protoc.* **2012**, 312-318, doi:10.1101/pdb.ip068221 (2012).
43. Song, H., Stevens, C.F., & Gage, F.H. Astroglia induce neurogenesis from adult neural stem cells. *Nature.* **417**, 39-44, doi:10.1038/417039a (2002).
44. Tang, X. *et al.* Astroglial cells regulate the developmental timeline of human neurons differentiated from induced pluripotent stem cells. *Stem Cell Res.* **11**, 743-757, doi:10.1016/j.scr.2013.05.002 (2013).
45. Ivkovic, S., & Ehrlich, M.E. Expression of the striatal DARPP-32/ARPP-21 phenotype in GABAergic neurons requires neurotrophins *in vivo* and *in vitro*. *J. Neurosci.* **19**, 5409-5419 (1999).
46. Kaneko, A., & Sankai, Y. Long-term culture of rat hippocampal neurons at low density in serum-free medium: combination of the sandwich culture technique with the three-dimensional nanofibrous hydrogel PuraMatrix. *PLoS One.* **9**, e102703, doi:10.1371/journal.pone.0102703 (2014).
47. Wang, X.F., & Cynader, M.S. Effects of astrocytes on neuronal attachment and survival shown in a serum-free co-culture system. *Brain Res. Brain Res. Protoc.* **4**, 209-216, doi:10.1016/S1385-299X(99)00019-7 (1999).
48. Fath, T., Ke, Y.D., Gunning, P., Gotz, J., & Ittner, L.M. Primary support cultures of hippocampal and substantia nigra neurons. *Nat. Protoc.* **4**, 78-85, doi:10.1038/nprot.2008.199 (2009).
49. Shimizu, S., Abt, A., & Meucci, O. Bilaminar co-culture of primary rat cortical neurons and glia. *J. Vis. Exp.* e3257, doi:10.3791/3257 (2011).
50. Mennerick, S., Que, J., Benz, A., & Zorumski, C.F. Passive and synaptic properties of hippocampal neurons grown in microcultures and in mass cultures. *J. Neurophysiol.* **73**, 320-332 (1995).
51. Chen, G., Harata, N.C., & Tsien, R.W. Paired-pulse depression of unitary quantal amplitude at single hippocampal synapses. *Proc. Natl. Acad. Sci. U. S. A.* **101**, 1063-1068, doi:10.1073/pnas.0307149101 (2004).
52. Albuquerque, C., Joseph, D.J., Choudhury, P., & MacDermott, A.B. Dissection, plating, and maintenance of dorsal horn neuron cultures. *Cold Spring Harb. Protoc.* **2009**, pdb prot5274, doi:10.1101/pdb.prot5274 (2009).
53. Xu, H.P., Gou, L., & Dong, H.W. Study glial cell heterogeneity influence on axon growth using a new coculture method. *J. Vis. Exp.* e2111, doi:10.3791/2111 (2010).
54. Daniel, J.A., Galbraith, S., Iacovitti, L., Abdipranoto, A., & Vissel, B. Functional heterogeneity at dopamine release sites. *J. Neurosci.* **29**, 14670-14680, doi:10.1523/JNEUROSCI.1349-09.2009 (2009).
55. Calakos, N., Schoch, S., Sudhof, T.C., & Malenka, R.C. Multiple roles for the active zone protein RIM1α in late stages of neurotransmitter release. *Neuron.* **42**, 889-896, doi:10.1016/j.neuron.2004.05.014 (2004).
56. Garcia-Junco-Clemente, P. *et al.* Cysteine string protein-α prevents activity-dependent degeneration in GABAergic synapses. *J. Neurosci.* **30**, 7377-7391, doi:10.1523/JNEUROSCI.0924-10.2010 (2010).
57. Hogins, J., Crawford, D.C., Zorumski, C.F., & Mennerick, S. Excitotoxicity triggered by Neurobasal culture medium. *PLoS One.* **6**, e25633, doi:10.1371/journal.pone.0025633 (2011).

58. Panatier, A., Vallee, J., Haber, M., Murai, K.K., Lacaille, J.C., & Robitaille, R. Astrocytes are endogenous regulators of basal transmission at central synapses. *Cell.* **146**, 785-798, doi:10.1016/j.cell.2011.07.022 (2011).
59. Noble, M., & Mayer-Proschel, M. in *Culturing Nerve Cells.* eds G. Banker & K. Goslin) Ch. 18, 499-543 MIT Press, (1998).
60. Ahlemeyer, B., Kehr, K., Richter, E., Hirz, M., Baumgart-Vogt, E., & Herden, C. Phenotype, differentiation, and function differ in rat and mouse neocortical astrocytes cultured under the same conditions. *J. Neurosci. Methods.* **212**, 156-164, doi:10.1016/j.jneumeth.2012.09.016 (2013).
61. Malgaroli, A., & Tsien, R.W. Glutamate-induced long-term potentiation of the frequency of miniature synaptic currents in cultured hippocampal neurons. *Nature.* **357**, 134-139, doi:10.1038/357134a0 (1992).
62. Ryan, T.A., Reuter, H., Wendland, B., Schweizer, F.E., Tsien, R.W., & Smith, S.J. The kinetics of synaptic vesicle recycling measured at single presynaptic boutons. *Neuron.* **11**, 713-724, doi:10.1016/0896-6273(93)90081-2 (1993).
63. Harata, N.C., Choi, S., Pyle, J.L., Aravanis, A.M., & Tsien, R.W. Frequency-dependent kinetics and prevalence of kiss-and-run and reuse at hippocampal synapses studied with novel quenching methods. *Neuron.* **49**, 243-256, doi:10.1016/j.neuron.2005.12.018 (2006).
64. Yamamoto, M., Steinbusch, H.W., & Jessell, T.M. Differentiated properties of identified serotonin neurons in dissociated cultures of embryonic rat brain stem. *J. Cell Biol.* **91**, 142-152, doi:10.1083/jcb.91.1.142 (1981).
65. Nakajima, Y., & Masuko, S. A technique for culturing brain nuclei from postnatal rats. *Neurosci. Res.* **26**, 195-203, doi:10.1016/S0168-0102(96)01101-7 (1996).
66. Arttamangkul, S., Torrecilla, M., Kobayashi, K., Okano, H., & Williams, J.T. Separation of μ-opioid receptor desensitization and internalization: endogenous receptors in primary neuronal cultures. *J. Neurosci.* **26**, 4118-4125, doi:10.1523/JNEUROSCI.0303-06.2006 (2006).
67. O'Farrell, C.A., Martin, K.L., Hutton, M., Delatycki, M.B., Cookson, M.R., & Lockhart, P.J. Mutant torsinA interacts with tyrosine hydroxylase in cultured cells. *Neuroscience.* **164**, 1127-1137, doi:10.1016/j.neuroscience.2009.09.017 (2009).
68. Jiang, M., Deng, L., & Chen, G. High Ca^{2+}-phosphate transfection efficiency enables single neuron gene analysis. *Gene Ther.* **11**, 1303-1311, doi:10.1038/sj.gt.3302305 (2004).
69. Chen, Y., Stevens, B., Chang, J., Milbrandt, J., Barres, B.A., & Hell, J.W. NS21: re-defined and modified supplement B27 for neuronal cultures. *J. Neurosci. Methods.* **171**, 239-247, doi:10.1016/j.jneumeth.2008.03.013 (2008).
70. Robert, F., & Hevor, T.K. Abnormal organelles in cultured astrocytes are largely enhanced by streptomycin and intensively by gentamicin. *Neuroscience.* **144**, 191-197, doi:10.1016/j.neuroscience.2006.08.059 (2007).
71. Robert, F., Cloix, J.F., & Hevor, T. Ultrastructural characterization of rat neurons in primary culture. *Neuroscience.* **200**, 248-260, doi:10.1016/j.neuroscience.2011.10.002 (2012).

Materials List for:

Rapid Genotyping of Animals Followed by Establishing Primary Cultures of Brain Neurons

Jin-Young Koh*[1,2], Sadahiro Iwabuchi*[1], Zhengmin Huang[3], N. Charles Harata[1]

[1]Department of Molecular Physiology & Biophysics, University of Iowa Carver College of Medicine

[2]Department of Psychiatry, University of Iowa Carver College of Medicine

[3]EZ BioResearch LLC

*These authors contributed equally

Correspondence to: N. Charles Harata at charles-harata@uiowa.edu

URL: http://www.jove.com/video/51879
DOI: doi:10.3791/51879

Materials

Name	Company	Catalog Number	Comments
REAGENTS - tattooing			
Machine Cleanser	Animal Identification and Marking Systems, Inc.	NMCR3	This is used to clean the needles and the holder after tattooing.
Machine Drying Agent	Animal Identification and Marking Systems, Inc.	NDAR4	This is used to dry the needles and holder after cleaning.
Neonate Tattoo Black Pigment	Animal Identification and Marking Systems, Inc.	NBP01	
Skin Prep Applicator	Animal Identification and Marking Systems, Inc.	NSPA1	Q-tip.
Skin Prep solution	Animal Identification and Marking Systems, Inc.	NSP01	This reagent delivers a thin layer of oil that enhances the efficiency of tattooing and prevents tattoo fading, by (information from vendor): 1) preventing non-tattooed skin from being stained temporarily, thereby allowing the quality of a paw pad tattoo to be easily evaluated before the pup is returned to its home cage – the stained skin surface can be confused with the tattooed skin, 2) reducing skin damage during tattooing – softening the skin and lubricating the needle will help the needle penetrate the skin without causing skin damage, and 3) preventing molecular oxygen from entering the skin, thereby reducing inflammatory responses to reactive oxygen species that can be generated.
REAGENTS - genotyping			
EZ Fast Tissue/Tail PCR Genotyping Kit (Strip Tube Format)	EZ BioResearch LLC	G2001-100	
2X PCR Ready Mix II	EZ BioResearch LLC	G2001-100	A red, loading dye for electrophoresis is included in the 2X PCR Ready Mix solution.
Tissue Lysis Solution A	EZ BioResearch LLC	G2001-100	Prepare DNA Extraction Solution by mixing 20 µl of Tissue Lysis Solution A and 180 µl of Tissue Lysis Solution B per specimen.

Tissue Lysis Solution B	EZ BioResearch LLC	G2001-100	Prepare DNA Extraction Solution by mixing 20 µl of Tissue Lysis Solution A and 180 µl of Tissue Lysis Solution B per specimen.
Acetic acid, glacial	VWR	BDH 3092	
Agarose optimized grade, molecular biology grade	rpi	A20090-500	We use 2% agarose gels in TAE buffer containing the SYBR Safe DNA gel stain (diluted 10,000-fold) or ethidium bromide (0.5 µg/ml gel volume).
Ethidium bromide	Sigma-Aldrich	E7637-1G	
Ethylenediamine tetraacetic acid, disodium salt dihydrate (EDTA)	Fisher	BP120-500	
Filtered Pipet Tips, Aerosol-Free, 0.1-10 µl	Dot Scientific Inc	UG104-96RS	Use pipette tips that are sterile and free of DNA, RNase and DNase. For all steps involving DNA, use filtered pipette tips to avoid cross-contamination.
Filtered Pipet Tips, Premium Fit Filter Tips, 0.5-20 µl	Dot Scientific Inc	UG2020-RS	Use pipette tips that are sterile and free of DNA, RNase and DNase. For all steps involving DNA, use filtered pipette tips to avoid cross-contamination.
Filtered Pipet Tips, Premium Fit Filter Tips, 1-200 µl	Dot Scientific Inc	UG2812-RS	Use pipette tips that are sterile and free of DNA, RNase and DNase. For all steps involving DNA, use filtered pipette tips to avoid cross-contamination.
Molecular weight marker, EZ DNA Even Ladders 100 bp	EZ BioResearch LLC	L1001	We use either of these three molecular weight markers.
Molecular weight marker, EZ DNA Even Ladders 1000 bp	EZ BioResearch LLC	L1010	
Molecular weight marker, TrackIt, 100 bp DNA Ladder	GIBCO-Invitrogen	10488-058	
PCR tubes, 8-tube strips with individually attached dome top caps, natural, 0.2 ml	USA Scientific	1402-2900	Use tubes that are sterile and free of DNA, RNase and DNase. An 8-tube strip is easy to handle and to group the specimens than individual tubes.
PCR tubes, Ultraflux Individual	rpi	145660	Use tubes that are sterile and free of DNA, RNase and DNase.
Seal-Rite 0.5 ml microcentrifuge tube, natural	USA Scientific	1605-0000	Use tubes that are sterile and free of DNA, RNase and DNase.
SYBR Safe DNA gel stain * 10,000x concentration in DMSO	GIBCO-Invitrogen	S33102	
Tris base	rpi	T60040-1000	
Primers for amplifying Tor1a gene in ΔE-torsinA knock-in mice			5'-AGT CTG TGG CTG GCT CTC CC-3' (forward) and 5'-CCT CAG GCT GCT CAC AAC CAC-3' (reverse) (reference 18). These primers were used at a final concentration of 1.0 ng/µl (~0.16 µM) (reference 2).
Primers for amplifying Tfap2a gene in wild-type mice			5'-GAA AGG TGT AGG CAG AAG TTT GTC AGG GC-3' (forward), 5'-CGT GTG GCT GTT GGG GTT GTT GCT GAG GTA-3' (reverse) for the 498-bp amplicon, 5'-CAC CCT ATC AGG GGA GGA CAA CTT TCG-3' (forward), 5'-AGA

			CAC TCG GGC TTT GGA GAT CAT TC-3' (reverse) for the 983-bp amplicon, and 5'-CAC CCT ATC AGG GGA GGA CAA CTT TCG-3' (forward), 5'-ACA GTG TAG TAA GGC AAA GCA AGG AG-3' (reverse) for the 1990-bp amplicon. These primers are used at 0.5 µM.
REAGENTS - cell culture			
5-Fluoro-2′-deoxyuridine	Sigma-Aldrich	F0503-100MG	See comments section of uridine for more information.
B-27 supplement	GIBCO-Invitrogen	17504-044	
Cell Culture Dishes 35 x 10 mm Dishes, Tissue Culture-treated	BD falcon	353001	
Cell Culture Flasks, T25, Tissue Culture-treated, Canted-neck, plug-seal cap, 25 cm^2 Growth Area, 70 ml	BD falcon	353082	
Cell Culture Flasks, T75, Tissue Culture-treated, Canted-neck, vented cap, 75 cm^2 Growth Area, 250 ml	BD falcon	353136	
Conical Tube, polypropylene, 15 ml	BD falcon	352095	
Countess (cell number counter) chamber slides	GIBCO-Invitrogen	C10312	
Cytosine β-D-Arabinofuranoside hydrochloride (Ara-C hydrochloride)	Sigma-Aldrich	C6645-100mg	
D-(+)-Glucose (Dextrose) anhydrous, SigmaUltra, 99.5% (GC)	Sigma-Aldrich	G7528-250G	
Dish, Petri glass 100 x 15 mm	Pyrex	3160-101	
Distilled water	GIBCO-Invitrogen	15230-147	
DNase Type II	Sigma-Aldrich	D4527-200KU	Stock solution is prepared at 1,500 units/20 µl = 75,000 units/ml in distilled water.
Dulbecco's Modified Eagle Medium (DMEM), high glucose, GlutaMAX, pyruvate	GIBCO-Invitrogen	10569-010, 500 ml	
Fast PES Filter Unit, 250 ml, 50 mm diameter membrane, 0.2 µm Pore Size	Nalgene	568-0020	
Fast PES Filter Unit, 500 ml, 90 mm diameter membrane, 0.2 µm Pore Size	Nalgene	569-0020	
Fetal bovine serum (FBS)	GIBCO-Invitrogen	26140-079	
Glass coverslip, 12 mm Round, thickness 0.09–0.12 mm, No. 0	Carolina	633017	
GlutaMAX-I	GIBCO-Invitrogen	35050-061	
Hanks' Balanced Salts	Sigma-Aldrich	H2387-10X	
HEPES, ≥99.5% (titration)	Sigma-Aldrich	H3375-250G	
Hydrochloric acid, 37%, A.C.S reagent	Sigma-Aldrich	258148-100 ML	
Insulin	Sigma-Aldrich	I5500-250 mg	

Magnesium sulfate heptahydrate, $MgSO_4$•($7H_2O$), BioUltra, ≥99.5% (Fluka)	Sigma-Aldrich	63138-250G	
Matrigel Basement Membrane Matrix solution, Phenol Red-Free	BD Biosciences	356237	This is the coating material for coverslips and flasks. 1) To prepare it, thaw the Matrigel Basement Membrane Matrix solution on ice, which usually takes ~1 day. Using a pre-cooled pipette, aliquot the thawed solution into pre-cooled T25 flasks on ice, and store the flasks at -20 °C. To prepare the working Matrigel solution, thaw the aliquotted Matrigel in a flask on ice, dilute 50-fold by adding pre-cooled MEM solution and keep the diluted solution at 4 °C. It is important to pre-cool all cultureware and media that come into contact with Matrigel, except during and after the coating of coverslips, to prevent it from prematurely forming a gel. 2) To coat the glass coverslips or culture flasks with Matrigel, apply the Matrigel solution to the surface. Before plating cells, it is important to completely dry up the surface. For this purpose, it might be helpful to aspirate Matrigel during the cellular centrifugation immediately before plating the cells and to allow enough time for drying.
Minimum Essential Medium (MEM)	GIBCO-Invitrogen	51200-038	
MITO+ Serum Extender, 5 ml	BD Biosciences	355006	
Multiwell Plates, Tissue Culture-treated 24-well plate	BD falcon	353047	
Multiwell Plates, Tissue Culture-treated 6-well plate	BD falcon	353046	
Neurobasal-A Medium (1X), liquid	GIBCO-Invitrogen	10888-022	
Nitric Acid	VWR	bdh 3044	
NS (Neuronal Supplement) 21	prepared in the lab		Source: reference 69
Pasteur pipets, 5 ¾”	Fisher	13-678-6A	Use this cotton-plugged 5 ¾” Pasteur pipette for cellular trituration. Fire-polish the tip beforehand to smooth the cut surface and to reduce the internal diameter to 50-80% of the original. Too small a tip will disrupt the cells and reduce cell viability, but too large a tip will decrease the efficiency of trituration.
Pasteur pipets, 9”	Fisher	13-678-6B	
Potassium chloride (KCl), SigmaUltra, ≥99.0%	Sigma-Aldrich	P9333-500G	
Serological pipet, 2 ml	BD falcon	357507	
Serological pipet, 5 ml	BD falcon	357543	
Serological pipet, 10 ml	BD falcon	357551	
Serological pipet, 25 ml	BD falcon	357525	
Serological pipet, 50 ml	BD falcon	357550	

Sodium bicarbonate (NaHCO3, Sodium hydrogen carbonate), SigmaUltra, ≥99.5%	Sigma-Aldrich	S6297-250G	
Sodium chloride (NaCl), SigmaUltra, ≥99.5%	Sigma-Aldrich	S7653-250G	
Sodium hydroxide (NaOH), pellets, 99.998% trace metals basis	Sigma-Aldrich	480878-250G	
Sodium phosphate dibasic heptahydrate (Na_2HPO_4•($7H_2O$)), ≥99.99%, Aldrich	Sigma-Aldrich	431478-250G	
Sucrose, SigmaUltra, ≥99.5% (GC)	Sigma-Aldrich	S7903-250G	
Syringe filter, sterile, 0.2 µm	Corning	431219	
Syringe, 3 ml	BD falcon	309585	
Transferrin, Holo, bovine plasma	Calbiochem	616420	
Trypan Blue stain, 0.4%	GIBCO-Invitrogen	T10282	This is used for counting live/ dead cells. Renew an old trypan blue solution if it is re-used many times (*e.g.* several times a week for several weeks), because it will form precipitates and result in erroneous readouts of cellular density.
Trypsin, type XI	Sigma-Aldrich	T1005-5G	
Trypsin-EDTA solution, 0.25%	GIBCO-Invitrogen	25200-056	
Uridine	Sigma-Aldrich	U3003-5G	Stock solution is prepared at 50-mg 5-fluoro-2'-deoxyuridine and 125 mg uridine in 25 ml DMEM (8.12 and 20.48 mM, respectively).
REAGENTS - immunocytochemistry			
Antibody, rabbit polyclonal anti-MAP2	Merck Millipore	AB5622	
Antibody, mouse monoclonal anti-GFAP cocktail	Merck Millipore	NE1015	
EQUIPMENT - tattooing			
AIMS	Animal Identification and Marking Systems, Inc.	NEO–9	This Neonate Rodent Tattooing System is an electric system that works by rapidly moving 1- or 3-point tattoo needles vertically into the skin. Activate the tattoo machine once for approximately 0.5 sec, while the tattoo needle tips are kept perpendicular to the skin surface. We prefer three-needle tattooing to maximize the tattooed area, but one-needle tattooing is effective on narrower areas, *e.g.* the toes, or if fine mechanical control is necessary, *e.g.* when numbers are tattooed. Two rounds of tattooing at the slowest speed (setting "1" out of 3 steps) are typically sufficient to produce a visible and long-lasting tattoo of the paw pads.
EQUIPMENT - genotyping			
Electrophoresis system, horizontal, Wide Mini–Sub Cell GT	BIO–RAD	170–4405	Typical electrophoresis parameters are electrical field strength at 6 V/ cm and 25 min duration for a 10 cm gel.

FluorChem 8800	ProteinSimple	FluorChem 8800	
PCR, MJ Mini Thermal Cycler	BIO-RAD	PTC-1148EDU	Our PCR reactions for the Tor1a gene in ΔE-torsinA knock-in mice are as follows: 1 cycle of denaturation at 94 °C for 3 min, 35 cycles of denaturation at 94 °C for 30 sec, annealing at 58 °C for 30 sec, extension at 72 °C for 2 min. This is followed by final extension at 72 °C for 10 min, and holding at 4 °C.
Power supply, PowerPac Basic	BIO-RAD	164-5050	
EQUIPMENT - cell culture			
Automated cell counter, Countess	GIBCO-Invitrogen	C10310	This automated cell counter separately measures the densities of live and dead cells (non stained and stained by trypan blue, respectively). It is important to know the optimal range of density measurements: the counter that we use has the highest accuracy in the range from 1 x 10^5 to 4 x 10^6 cells/ml. If the measured cell density values fall outside the recommended range, adjust the resuspension volume appropriately.
Biological Safety Cabinet, Class II, Type A2	NUAIRE	NU-425-400	This hood is used for all cell culture procedures, except for brain dissection.
CO_2 Incubator, AutoFlow, Humidity Control Water Jacket	NUAIRE	NU-4850	
Horizontal Clean Bench	NUAIRE	NU-201-330	This clean bench is used for brain dissection (steps 3.1.1 and 3.1.2 of "Brain Dissection and Cellular Dissociation)".
Orbit LS Low Speed Shaker	Labnet	S2030-LS-B	
SORVALL RC-6 Plus Superspeed Centrifuge	Fisher	46910 (centrifuge)/46922 (rotor)	